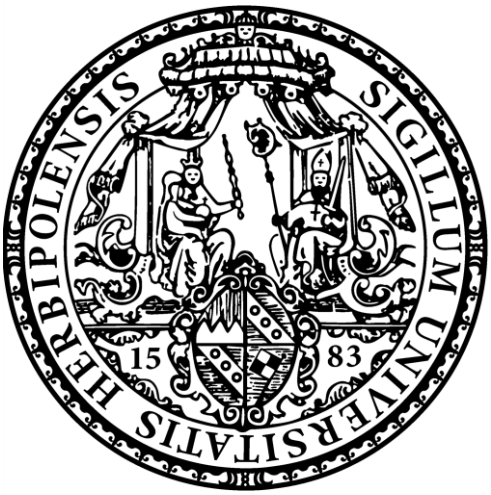

Functional analysis of *DROSHA* and *SIX1* mutations in kidney development and Wilms tumor

Funktionelle Analysen von *DROSHA* und *SIX1* Mutationen in der Nierenentwicklung und dem Wilms Tumor

Doctoral thesis for a doctoral degree
at the Graduate School of Life Sciences,
Julius-Maximilians-Universität Würzburg,
Section Biomedicine

submitted by

Philip Kruber

from

Greven

Würzburg 2018

Submitted on: ……..……..

Office stamp

Members of the Thesis Committee:

Chairperson: **Prof. Dr. Alexander Buchberger**

Primary Supervisor: **Prof. Dr. Manfred Gessler**

Supervisor (Second): **Prof. Dr. Ricardo Benavente**

Supervisor (Third): **Prof. Dr. Svenja Meierjohann**

Date of Public Defence: ……..

Date of Receipt of Certificates: ……

Nothing in life is to be feared, it is only to be understood.
Now is the time to understand more, so that we may fear less.

Marie Curie

Index

1 Summary

1.1 Summary (English)

Wilms tumor (WT) is the most common kidney cancer in childhood. It is a genetically heterogeneous tumor and several genetic alterations have been identified in WT patients. Recurrent mutations were found in the homeo-domain of *SIX1* and *SIX2* in high proliferative tumors (18.1% of the blastemal-type tumors) as well as in the microprocessor genes *DROSHA* and *DGCR8* (18.2% of the blastemal-type tumors), indicating a critical role of the *SIX-SALL* pathway and aberrant miRNA processing in WT formation. Underlined by the fact that a significant overlap between mutations in *DROSHA* and *SIX1* was found, indicating a synergistic effect.

To characterize the *in vivo* role of *DROSHA* and *SIX* mutations during kidney development and their oncogenic potential, I analyzed mouse lines with either a targeted deletion of *Drosha* or an inducible expression of human *DROSHA* or *SIX1* carrying a tumor-specific E1147K or Q177R mutation, respectively.

The *DROSHA* mutation E1147K was predicted to act in a dominant negative manner. Six2-cre mediated deletion of *Drosha* in nephron progenitors led to a lethal phenotype with apoptotic loss of progenitor cells and early termination of nephrogenesis. Mosaic deletions via Wt1-cre^{ERT2} resulted in a milder phenotype with viable offspring that developed proteinuria after 2-4 weeks, but no evidence of tumor formation. Activation of the *DROSHA-E1147K* transgene via Six2-cre, on the other hand, induced a more severe phenotype with apoptosis of progenitor cells, proteinuria and glomerular sclerosis. The severely growth-retarded mice died within the first two months. This strong phenotype was consistent with the predicted dominant-negative effect of *DROSHA-E1147K*.

Analysis of the *SIX1-Q177R* mutation suggested that the mutation leads to a shift in DNA binding specificity instead of a complete loss of DNA binding. This may end up in subtle changes of the gene regulatory capacity of SIX1. Six2-cre mediated activation of *SIX1-Q177R* lead to a viable phenotype with no alterations or shortened life span. Yet a global activation of *SIX1-Q177R* mediated by Zp3-cre resulted in bilateral hydronephrosis and juvenile death of the mice.

To mimic the synergistic effect of *DROSHA* and *SIX1* mutations, I generated compound mutants in two combinations: A homozygous deletion of *Drosha* combined with an activation of *SIX1-Q177R* and a compound mutant with activation of *DROSHA-E1147K* and *SIX1-Q177R*. Each mouse model variant displayed new phenotypical alterations. Mice with Six2-cre mediated homozygous deletion of *Drosha* and activation of *SIX1-Q177R* were not viable, yet heterozygous deletion of *Drosha* and activation of *SIX1-Q177R* led to hydronephrosis, proteinuria and an early death around stage P28. Combined

activation of *DROSHA-E1147K* and *SIX1-Q177R* under Six2-cre resulted in proteinuria, glomerulosclerosis and lesions inside the kidney. These mice also suffered from juvenile death. Both mouse models could confirm the predicted synergistic effect.

While these results underscore the importance of a viable self-renewing progenitor pool for kidney development, there was no evidence of tumor formation. This suggests that either additional alterations in mitogenic or antiapoptotic pathways are needed for malignant transformation, or premature loss of a susceptible target cell population and early lethality prevent WT formation.

1.2 Zusammenfassung (Deutsch)

Der Wilms Tumor ist der am häufigsten auftretende Nierentumor im Kindesalter. Er ist genetisch heterogen und bisher wurden bereits verschiedene genetische Mutationen in Wilms Tumor Patienten gefunden. Es konnten wiederkehrende Mutationen in der Homeo-Domäne der Gene *SIX1* und *SIX2* und in den Genen des Mikroprozessorkomplexes *DROSHA* und *DGCR8* gefunden werden. Die Ergebnisse weisen darauf hin, dass einerseits die gestörte Prozessierung von miRNAs und andererseits der *SIX-SALL* Signalweg eine wichtige Rolle im Entstehungsprozess des Wilms Tumors spielen. Des Weiteren konnte die Analyse der blastem-reichen Tumore einen möglichen synergetischen Effekt zwischen *DROSHA* und *SIX1* aufzeigen.

Um die Bedeutung von *DROSHA* und *SIX* Mutationen für die Nierenentwicklung und für die Tumorgenese *in vivo* zu untersuchen, wurden in dieser Arbeit Mausmodelle mit konditioneller Deletion von *DROSHA* oder induzierbarer Expression der *DROSHA* Mutation E1147K bzw. der *SIX1* Mutation Q177R analysiert.

Es wurde vermutet, dass die E1147K Mutation einen dominant-negativen Effekt besitzt. Six2-cre vermittelte Deletion von *DROSHA* in Nierenvorläuferzellen führte zu einem letalen Phänotyp, der sich durch Apoptose von Vorläuferzellen und vorzeitigen Abbruch der Nephrogenese auszeichnete. Mosaik-Deletion mittels Wt1-cre^{ERT2} führte zu einem deutlich milderen Phänotyp. Die Nachkommen waren lebensfähig, entwickelten aber innerhalb der ersten 2-4 Wochen eine Proteinurie. Bei beiden, so erzeugten, Mauslinien konnten keine Tumorbildung feststellen werden. Aktivierung des *DROSHA-E1147K* Transgenes durch Six2-cre brachte einen deutlich gravierenderen Phänotyp hervor. Dieser zeichnete sich durch Apoptose von Vorläuferzellen, sowie Proteinurie und Glomerulosklerose aus. Die im Wachstum stark retardierten Mäuse starben innerhalb der ersten zwei Monate nach der Geburt. Dieser Phänotyp unterstreicht den vermuteten dominant-negativen Effekt von *DROSHA-E1147K* auch *in vivo*.

Analysen der Q177R Mutation konnten zeigen, dass diese Mutation in der Homeo-Domäne des *SIX1* Genes wahrscheinlich nicht zu einem kompletten Verlust der Fähigkeit, DNA zu binden, führt, sondern eher eine leichte Verschiebung der DNA Bindespezifität als Folge hat. Das könnte eine subtile Veränderung in der Fähigkeit von *SIX1* Gene zu regulieren bedeuten. Six2-cre vermittelte Aktivierung des *SIX1-Q177R* Transgenes hatte jedoch keinen sichtbaren Effekt für den Phänotyp der Mäuse. Dennoch hatte eine globale Aktivierung des Transgenes durch Zp3-cre bilaterale Hydronephrose und einen frühzeitigen Tod der Mäuse zur Folge.

Summary

Um den bereits vermuteten Synergieeffekt zwischen *DROSHA-E1147K* und *SIX1-Q177R* zu untersuchen, wurden zwei neue Mausgenotypen erzeugt. Einerseits wurde eine Mauslinie mit dem *SIX1-Q177R* Transgen und der *Drosha* Deletion, andererseits eine Mauslinie, die sowohl das *SIX1-Q177R* Transgen, als auch das *DROSHA-E1147K* Transgen besitzt, verpaart. Beide Mauslinien entwickelten jeweils neue Phänotypen. Mäuse mit Six2-cre vermittelter, homozygoter Deletion von *Drosha* und gleichzeitiger Aktvierung von *SIX1-Q177R* waren nicht lebensfähig, während Mäuse mit heterozygoter Deletion von *Drosha* und gleichzeitiger Aktvierung von *SIX1-Q177R* sehr wohl lebensfähig waren. Diese Mäuse entwickelten wiederum Hydronephrose, sowie Proteinurie und verstarben innerhalb des ersten Lebensmonats. Kombinierte Aktivierung von *DROSHA-E1147K* und *SIX1-Q177R* mittels Six2-cre führte ebenfalls zu Proteinurie. Jedoch litten die Mäuse nicht an Hydronephrose, sondern an Glomerulosklerose und Zystenbildung. Ebenfalls starben die Mäuse einen frühzeitigen Tod. Beide Mausmodelle konnten, durch die Ausprägung neuer Phänotypen, den vermuteten Synergieeffekt beweisen.

Die Ergebnisse dieser Arbeit zeigen deutlich, wie wichtig ein lebensfähiger Zellpool an selbst-erneuernden Vorläuferzellen für die Nierenentwicklung ist. Dennoch konnten keine Anzeichen für eine Tumorbildung gefunden werden. Das lässt vermuten, dass weitere genetische Veränderungen z.B. in mitogenen oder anti-apoptotischen Signalwegen von Nöten sind, um eine maligne Transformation zu gewährleisten. Natürlich könnte auch der frühzeitige Verlust der verantwortlichen Zellpopulation und das frühe Absterben der Embryos ein Hindernis für die Wilms Tumorbildung sein.

2 Introduction

To understand the developmental mechanisms that lead to the formation of Wilms tumor, it is essential to understand the process of kidney development in embryos. Therefore, this introduction is structured as followed: Firstly, an insight into the kidney, its function and the embryonal nephrogenesis is given. Afterwards, the Wilms tumor and the Wilms tumor screens, which were performed simultaneously by Wegert et al. (2015) and Walz et al. (2015), are summarized. Finally, an overview of the two most promising oncogenes, which were proposed by the screens, and their possible connection, is presented.

2.1 The Kidney

The bilateral kidneys are not only a simple disposer of waste, they are the central organs of homeostasis in mammals (Figure 1 A). The human kidney is able to filter 180 liters of primary urine per day. Apart from filtering metabolic waste, the kidney also adjusts water, salt and pH levels to keep the homeostasis of tissue fluids at an equilibrium. Furthermore, the kidney regulates blood pressure via the renin-angiotensin-aldosterone system, calcium and phosphate levels by the activation of vitamin D and finally erythropoiesis through the production of erythropoietin (McMahon 2016).

2.1.1 Function and organization of the kidney

The functional element of the kidney is the nephron (Figure 1 B). The mouse kidney has 12,000 to 16,000 nephrons per kidney, while the human kidney can have 200,000 to 1.8 million of these complexly patterned nephrons which are compartmentalized in various specialized subunits (Hughson et al. 2003; Short et al. 2014).

The actual renal filtration happens inside the renal corpuscle at the proximal extent of the nephron (Figure 1 C) (Scott and Quaggin 2015). At this proximal extent afferent vasculature forms the glomerulus, which is basically a tangle of punctured blood vessels. To maintain integrity and permeability of the vasculature, mesangial cells are located closely opposed to the vascular endothelium (McMahon 2016). Fluid can pass from the glomerular capillaries into the interstitial space of the Bowman's capsule. The capillaries are lined with podocytes that are located on top of the glomerular basement membrane, which builds a surprisingly thick and highly specialized filtering barrier that prevents serum solutes of molecular weight over 15 kDa like serum albumin from passing into the nephron (Miner 2011; Suh and Miner 2013).

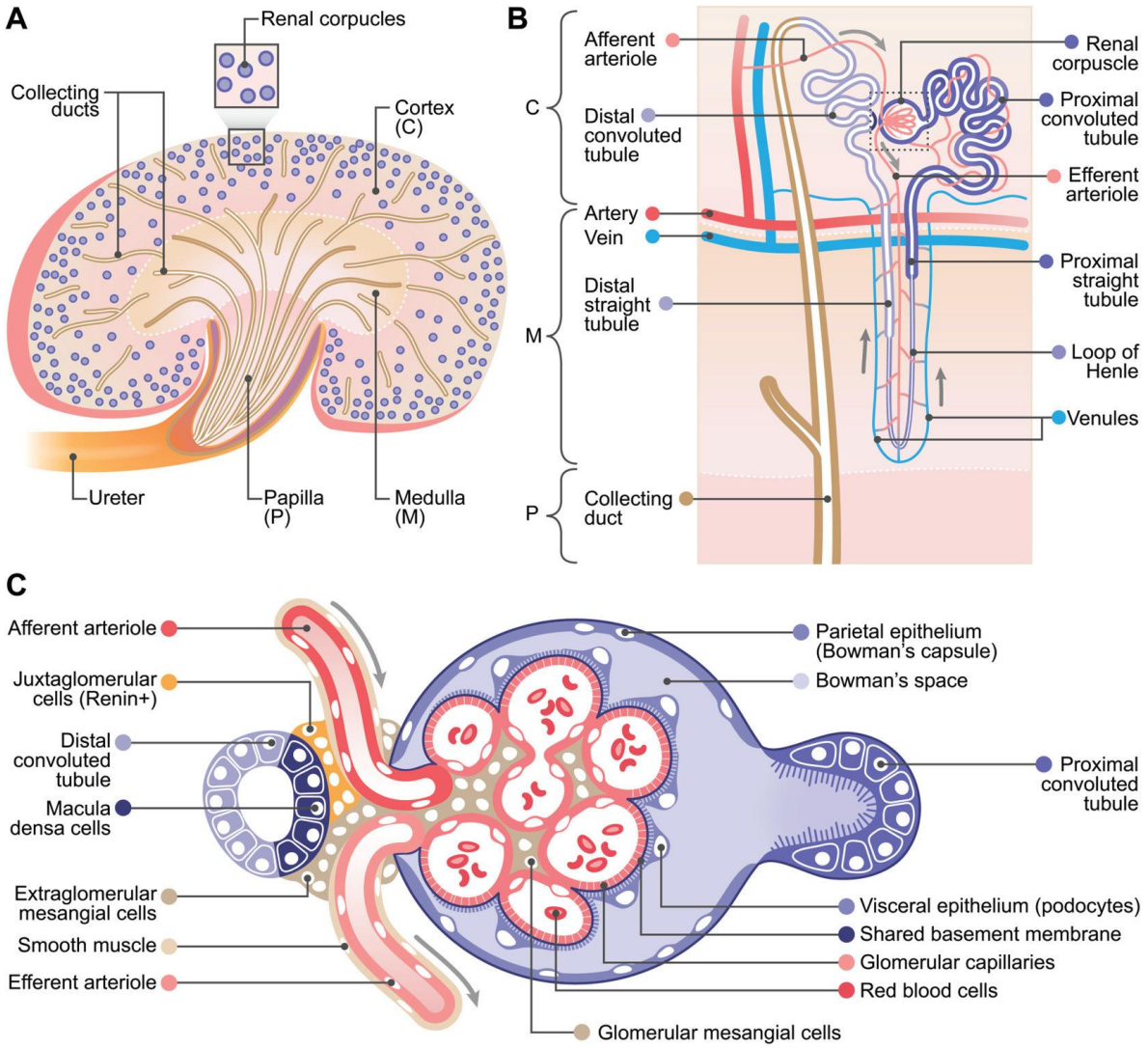

Figure 1: Schematic overview of the adult mouse metanephric kidney

(**A**) Overview of the adult kidney on the basis of specific regional organization. (**B**) Composition of the nephron. (**C**) Structure of the renal corpuscle and related structures (dashed box in B). Illustration from (McMahon 2016) with permission of Elsevier.

While the renal corpuscle and the segments of the proximal tubule (S1 and S2) are located in the outer cortex of the kidney (Figure 1 B, bracket C), the final segment of the proximal tubule (S3) is located in the outer medullary region (Figure 1 B, bracket M) (McMahon 2016). The proximal tubule epithelial membrane is covered with various membrane-embedded channels and transporters. Their main function is the reuptake of important small molecules like glucose, amino acids and minerals.

The proximal tubule extends with the loop of Henle far into the medulla before looping back and becoming the distal tubule segment inside the renal cortex (Figure 1 B). The main function of the loop of Henle is regulation of urine concentration, while the distal tubule segment returns sodium and calcium into the blood stream. The return of sodium and calcium ions is mediated by aldosterone and

parathyroid hormones and plays an important part in water uptake as well as for pH balance (Subramanya and Ellison 2014).

Finally, the distal tubule is connected to the collecting duct (Figure 1 B). The collecting duct originates from the ureter and forms a ramified epithelial network throughout the kidney. This collecting duct system channels the urine from the kidney through the ureter to the bladder. The renal papilla acts as the exit point for the tubular network out of the kidney parenchyma and the water permeable medullary collecting duct helps to retain water (Al-Awqati and Gao 2011; Pearce et al. 2015).

In close relation to each glomerulus lies another important and specialized part of the distal tubule, the macula densa (Bell, Lapointe, and Peti-Peterdi 2003). It is located at the point of entry of the afferent arterioles and the exit of the efferent arterioles (Figure 1 C). The macula densa is responsible for reducing fluid flow into the glomerulus depending on the salt levels in the distal tubule. By this mechanism the filtration rate is controlled and kept at an optimal level. Additionally, the macula densa interacts with juxtaglomerular cells, which surround the glomerular arterioles, thereby regulating the systemic blood pressure with the help of renin secretion and indirectly through renin's catalytic influence on the angiotensinogen system (Bell, Lapointe, and Peti-Peterdi 2003).

2.1.2 Nephrogenesis in mice

The intermediate mesoderm gives rise to the metanephric kidney in chronologically and regionally distinct processes (Taguchi et al. 2014; Takasato and Little 2015). At embryonic day 8.75 (E8.75) the paired nephric ducts occur at the level of rostral somites and extend in the posterior direction while inducing mesonephric tubular structures alongside them (Figure 2 A). When it reaches the hind limb level at stage E10.5 each nephric duct interacts with the metanephric mesenchyme cells and the dynamic process of kidney development begins (Combes, Davies, and Little 2015; Costantini and Kopan 2010; Little and McMahon 2012):

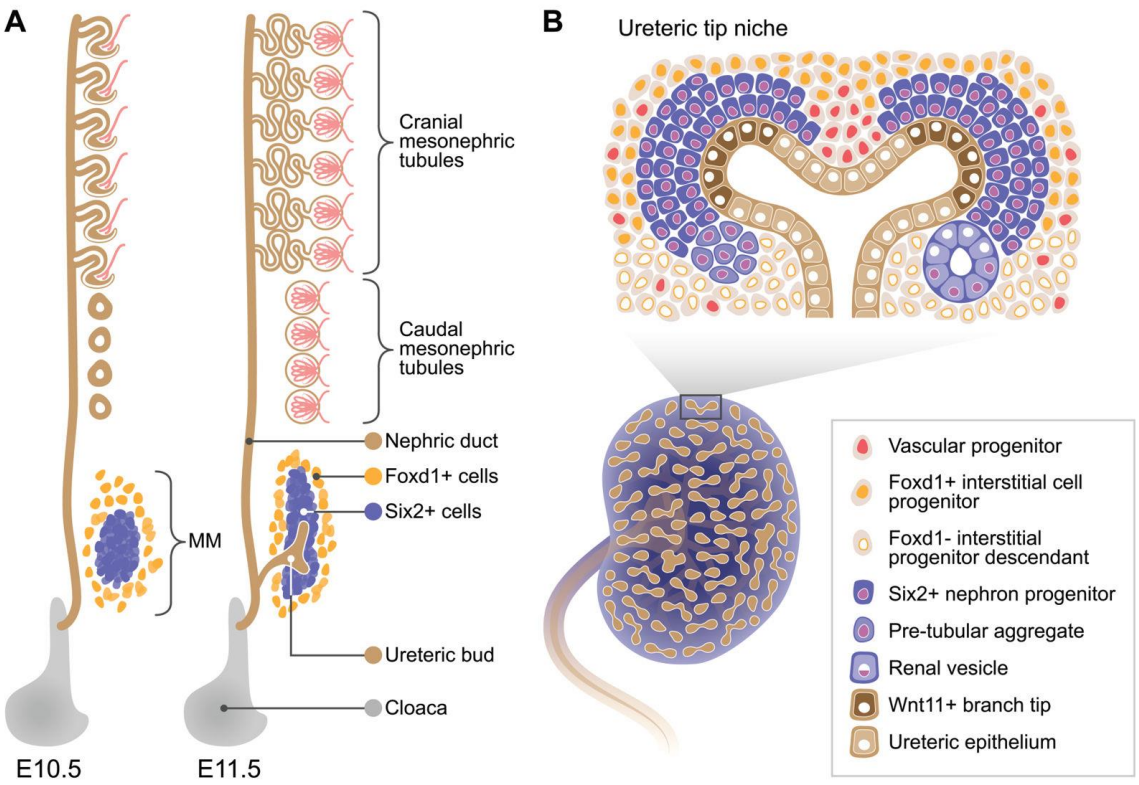

Figure 2: Schematic overview of mouse kidney development

(**A**) Illustration of the mesonephric and metanephric kidney anlage before (E10.5) and after (E11.5) UB infiltration into the MM. (**B**) Cellular composition of the collecting duct (duct tip *Wnt11* positive), the nephron (*Six2* positive), interstitial (*Foxd1* positive) and the vascular progenitors within ureteric tip niche. Illustration from (McMahon 2016) with permission of Elsevier.

Induced by signals from the mesenchymal cells the ureteric bud, a single, bilateral ductal outgrowth, grows into the medial positioned metanephric mesenchyme. This ingrowth leads to a condensation of mesenchymal cells around the tip and branching of the ureteric bud (Figure 2 A). At stage E11.5 the branched ureteric bud forms a T-like structure. The branching of the ureteric bud proceeds until day 2 after birth (P2) and the ureteric bud derived epithelium will have undergone 12 generations of branching until this point. By the end of this process this ongoing branching has formed the complete urine collecting duct system (Short et al. 2014). While the cap mesenchymal cells induce ingrowth and branching, the branch tips of the ureteric bud on their part signal expansion and differentiation of the cap mesenchyme (Figure 2 A, Figure 3 A). For each branching incident a subgroup of mesenchymal cells condensates into the pretubular aggregate, a tight cluster right under the branch tip. The pretubular aggregate develops into the renal vesicle, the most primitive stage of the nephron development. Each renal vesicle will form a mature nephron. Half of all nephrons are formed in the first two days after the branching stops at stage P2-4 (Short et al. 2014). The final number of nephrons is limited to the size of the progenitor cell pool and can vary in different mouse strains (Cebrian et al. 2014). Within 24 to 36 hours the renal vesicle first develops into the comma-shaped body and then

into the S-shaped body (Figure 3 A). The distal part of the S-shaped body connects to the collecting duct and forms a luminal connection, which will be essential for fluid flow throughout the kidney (Kao et al. 2012). At the proximal part of the S-shaped body the glomerular cleft is formed (Figure 3 A). After cleft formation the renal corpuscle assembly starts with endothelial cell migration into the cleft accompanied by podocyte specification in the proximal epithelium. The other segments of the nephron are derived from the remaining part of the S-shaped body. The nephron related vascular network is formed by vasculogenesis and angiogenesis while the development of the renal tubule epithelium proceeds. In addition, interstitial cell types arrange around tubules and vasculature, and neurons extend into the kidney to stimulate differentiated target sites. Ultimately the number of nephrons surpasses the number of ureteric branches. In mice multiple nephrons can attach to a single branch, while in the human kidney nephrons can also attach to one another, generating a cascade of nephrons.

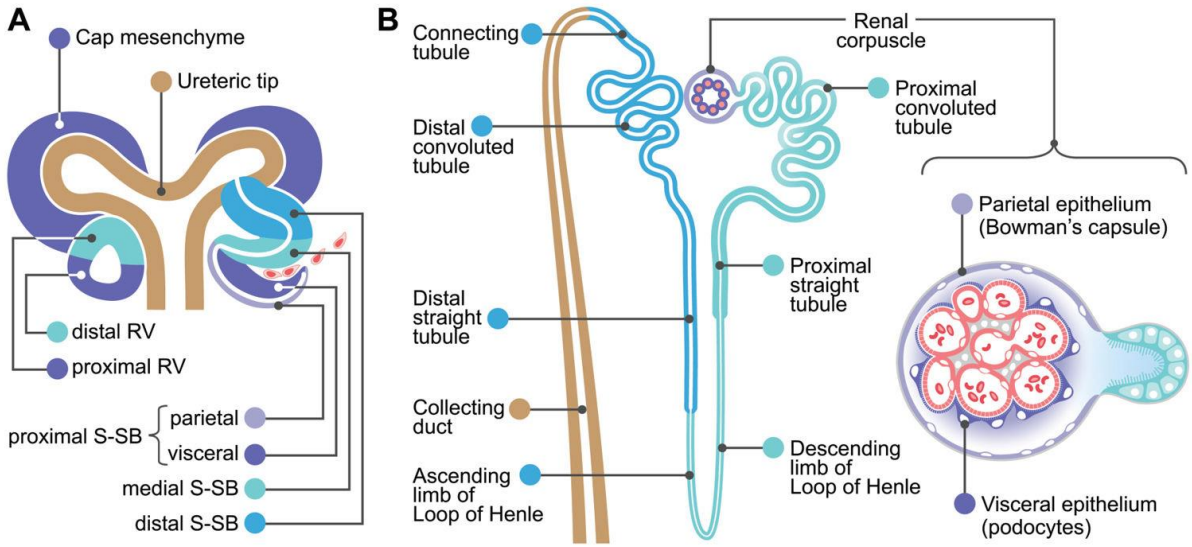

Figure 3: Schematic overview of nephron patterning process

(**A**) Transition from renal vesicle to patterned S-shape body. (**B**) Hypothetical map of different cell fates from progenitor cells in S-shaped bodies to sub-domains of the matured nephron. Illustration from (McMahon 2016) with permission of Elsevier.

So far, it is not fully understood at what time point the first functional nephrons are completed in the kidneys of mice, but filtering seems to start around E16.5 (McMahon 2016). Since nephron development is a continual process of ureteric tip branching, condensation and differentiation of progenitor cells into renal vesicles and further into matured nephrons, different stages of maturated nephrons can be seen over the whole prenatal and postnatal kidney development until the full kidney function is established around stage P7.

Nonetheless, the underlying cellular dynamics of embryonal nephron morphogenesis are still not fully understood. The transition from renal vesicles to S-shaped bodies goes along with growth and excessive epithelial restructuring (Figure 3 A) (McMahon 2016). A disturbed proliferation may lead to

failure in distal elongation, but since there are no 3D studies of the different transition stages from renal vesicle to S-shaped bodies, it is still unclear which molecular and cellular processes are the central driving forces (Georgas et al. 2009). However, after the connection between the distal S-shaped body and the ureteric epithelium is settled, one can find clear molecular heterogeneity present along the proximal-distal axis of the nascent nephron (Georgas et al. 2009). Interestingly, fate mapping studies could identify a structural coherence between defined gene expression domains of the S-shaped body and the adult nephron composition (Figure 3 B) (Barker et al. 2012; Harding et al. 2011).

2.1.3 The progenitor cell pool

As mentioned in the previous chapter, all functional subunits of the nephron are derived from a progenitor cell pool that is established before the initial ureteric bud outgrowth happens at stage E10.5 (Kobayashi et al. 2008). This progenitor cell pool originates from *Six2* positive progenitor cells that are self-renewing and multipotent. Studies have shown that the absence of *Six2* leads to a premature differentiation of all progenitor cells in the direction of renal vesicle at stage E12.5, which shows the importance of *Six2* expression for maintenance of progenitor cell fate (Kobayashi et al. 2008; Self et al. 2006). Apart from *Six2* more transcription factors have been found that are either involved in specification or maintenance of the *Six2* progenitor cell pool: *Six1*, *Hox11* paralogs (*Hoxa11*, *Hoxc11* and *Hoxd11*), *Pax2*, *Wt1* and *Sall1* (Little and McMahon 2012; O'Brien and McMahon 2013).

Since *Cited1* is solely expressed in the undifferentiated nephron progenitors, it has become the standard marker for correct identification of the nephron progenitor compartment (Boyle et al. 2008). In contrast, *Six2* is expressed in regions of epithelializing nephron precursors, although only for a limited time span, while *Cited1* expression is limited exclusively to uncommitted nephron progenitors (Mugford et al. 2009; Park et al. 2012). Remarkably, *Cited1* expression is not mandatory for kidney development even with its nephron progenitor specificity (Boyle et al. 2007). The progenitor niche is not as homogenous as expected. Depending on *Six2* expression levels and proliferation rates, the progenitor cell pool is divided into different subsets of cell pools (Short et al. 2014). It is still to be shown, if these subsets have different roles in the developmental program of the kidney (Short et al. 2014).

In mice the ratio of nephron progenitors to tip niche declines over the time of embryogenesis and then sharply drops at birth (Short et al. 2014). At stage P3-4 all nephron progenitors are gone and the number of nephrons gained throughout nephrogenesis by this point is the final number of nephrons for the whole life span of the mouse. In the human kidney nephrogenesis is completed in week 36, which implies that the sharp drop in nephron progenitors to tip niche ratio is not necessarily an event triggered by birth (Hinchliffe et al. 1991).

As could be seen, nephrogenesis is a sophisticated interaction between various signal pathways and their genetic factors which are responsible for complex tissue differentiation processes. A disturbance of this balance can have a severe outcome. As example, an early decline in progenitor cells can lead to agenesis or reduction of kidney volume. On the other hand, a transition of undifferentiated cells into the juvenile kidneys can give rise to tumorous diseases.

2.2 Wilms Tumor

Wilms tumor, also known as the nephroblastoma, is the most common solid cancer in childhood. It was first described in 1899 by the surgeon Max Wilms (1867-1918). Wilms already identified the nephroblastoma as a tumor identity that derives from the mesodermal layer and realized that its different tissue types originate from undifferentiated progenitor cells. These facts led him to the conclusion that the cause of the nephroblastoma must be a developmental defect in embryogenesis (Coppes-Zantinga and Coppes 1999).

2.2.1 Epidemiology

Wilms tumor is the most frequent kidney tumor in childhood. WT has an incidence of 1 of 10,000 in the USA and Europe (Wegert et al. 2015). The incidence rates are considerably lower in Asia (Breslow et al. 1993). The majority of Wilms tumors are sporadic (98-99%) and unilateral (90-95%). Bilateral tumors are far less common (5-10%) and affect mostly younger children with a high familiar disease risk (Huff 1998). Unilateral cases are diagnosed at a mean age of 44 months and bilateral cases around 31 months (Horner et al. 2009).

2.2.2 Pathogenesis

Since Wilms tumor presents itself most of the time as painless and asymptotic, the majority of WT are diagnosed because of abdominal swellings. In fewer cases, WT is recognized during to a routine check-up. 20-30% of cases presenting signs and symptoms including abdominal pain, malaise and either microscopic or macroscopic hematuria (Davidoff 2012). In 25% of the affected children, associated hypertension is diagnosed. The hypertension might be an effect caused by increased renin activity. Other symptoms can include: urinary tract infections, varicocele, fever, anemia or, if the patient has lung metastases, dyspnea or tachypnea can occur. The methods of choice for diagnosis are abdominal sonography and/or magnetic resonance imaging. Tumor specific markers in blood or urine are not known so far. Tumor biopsy is only recommended for children under 6 months or over 16 years and only if the imaging techniques do not give a definitive diagnosis (Babyn et al. 1995).

2.2.3 Histology

Wilms tumor develops from undifferentiated tissue that still shows mitotic activity. The origin of WT are metanephric progenitors that can differentiate into different tissue types such as epithelial, stromal or blastemal tissue. Accordingly, the Wilms tumor can consist all of these tissue types. If a tumor contains all three of these components, the tumor is classified as a triphasic tumor (Figure 4). Depending on the prevalent tissue type (>65%), the tumor is characterized as epithelial-, stromal- or blastemal-type.

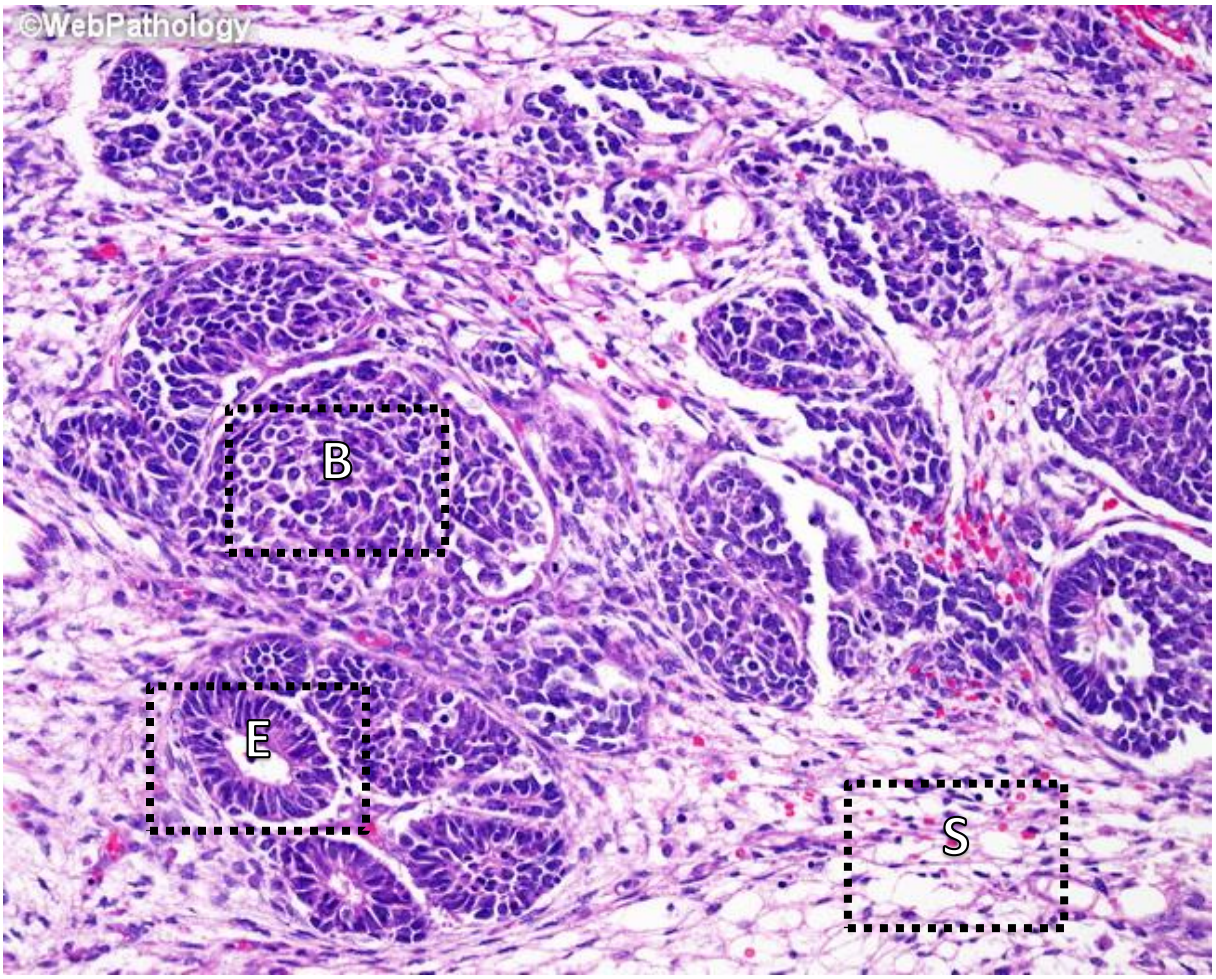

Figure 4: Histology of the Wilms tumor

An example of the typical triphasic histological appearance of the Wilms tumor with blastemal (B), stromal (S) and epithelial (E) components. (www.webpathology.com *25.09.17*)

A correct histological classification is of high prognostic value. Tumors may be classified as having low, intermediate or high risk (Vujanic et al. 2002). Since chemotherapy has an impact on the histological type of the tumor, it is important to know if the tumor was removed before or after chemotherapy. The classification guidelines are as followed:

Table 1: Classification of Wilms tumor on the basis of histological subtypes (Vujanic et al. 2002)

GRADE	PREOPERATIVE CHEMOTHERAPY	PRIMARY SURGERY
LOW RISK	cystic partial differentiated entirely necrotic	cystic partial differentiated
INTERMEDIATE MALIGNANCY	epithelial stromal-type mixed-type regressive focal anaplasia	epithelial stromal-, blastemal-type mixed-type regressive focal anaplasia
HIGH MALIGNANCY	blastemal-type diffuse anaplasia	diffuse anaplasia

Beside the histological classification, a tumor staging depending on local expansion, affection of lymph nodes and status of metastases is done:

Table 2: Staging of Wilms tumors (Vujanic et al. 2002)

STAGE	CRITERIA
I	limited to kidney, renal capsule intact, complete resection
II	extent beyond kidney, penetrates renal capsule, complete resection
III	incomplete resection, positive lymph nodes, no distant metastases
IV	distant metastases (lung, liver, bone, brain etc.), positive lymph nodes outside abdominopelvic region
V	bilateral renal tumor at diagnosis

In the majority of cases the Wilms tumor appears in a sporadic manner, yet rare cases of familial predisposition (1-2%) are known (Matsunaga 1981). The inheritance is autosomal dominant, but incomplete penetrance seems to be prevalent. In the past, only three genes *WT1*, *CTNNB1* and *WTX* have been known as reoccurring mutations (Ruteshouser, Robinson, and Huff 2008). One third of the Wilms tumor cases showed one of these mutations. *WT1* and *WTX* mutations occur with comparable frequency and *CTNNB1* displays synergistic effects with *WT1*. Still, the etiology of the Wilms tumor seems to be as complex as it is heterogeneous and two thirds of the tumor cases have an unknown genetic background (Ruteshouser, Robinson, and Huff 2008). New studies, including the recent Wilms tumor screens, have started to reveal the possible genetic composition of WT by discovering more

reoccurring mutations regarding, for example, the microprocessor complex and the *SIX-SALL* pathway (Wegert et al. 2015; Walz et al. 2015).

2.2.4 Therapy

There are two different guidelines to treat the Wilms tumor: In Europe and other countries patients are treated according to the Société International d'Oncologie Pédiatrique (SIOP) protocol, while in North America patients are treated according to the Children's Oncology Group (COG) protocol. The COG protocol favors primary surgery followed by chemotherapy and/or radiotherapy, while based on the SIOP protocol patients are treated with preoperative chemotherapy followed up by surgery and personalized postoperative chemotherapy and/or radiotherapy (Dome et al. 2013; Vujanic and Sandstedt 2010). A diverse histological appearance with different contributions of blastemal, stromal and epithelial tissue is characteristic for the Wilms tumor and different treatment protocols can influence the contribution of each tissue type. 35% of primarily resected tumors (COG) are categorized as blastemal-types, while the blastemal-type contribution drops to 9.5% for tumors treated with preoperative chemotherapy (SIOP) (Weirich et al. 2001). The blastemal contribution in primarily resected tumors is not of prognostic significance, but interestingly for patients who are treated with preoperative chemotherapy the apparently chemotherapy-resistant remaining viable blastema is associated with a poor prognosis and reduced relapse-free survival (58.4% in contrast to 86.7%) (Weirich et al. 2004). Diffuse anaplasia and the associated *TP53* mutation have a comparably unfavorable outcome (Lahoti et al. 1996). This comparison highlights the importance of understanding the underlying genetic basis of remaining blastema and identifying related biomarkers for new therapeutic approaches.

2.2.5 Prognosis

The overall therapeutic cure of the Wilms tumor is satisfactory. Since the early 20th century, the survival rate has hugely increased from 10% to 90%, due to improved surgery methods and a risk-related therapy with chemotherapy and radiotherapy (Sonn and Shortliffe 2008). Nevertheless, the survival rate still depends mainly on the histology and stage of the tumor. The relapse-free two year survival rate of a patients with a high risk, bilateral or metastatic Wilms tumor drops below 50%. In general, patients suffer from a relapse within the first two years after primary diagnosis in 10-15% of cases. Follow up examinations on a regular basis with the given diagnostic imaging techniques are crucial for early relapse recognition. The normal therapeutic strategy of treating a relapse consists of chemotherapy, radiotherapy and surgery. As already pointed out, the overall survival rate of patients suffering from Wilms tumors is satisfactory, but there are still downsides of the therapeutic measures. For example the chemotherapeutic agent Doxorubicin can have a toxic effect on heart muscle cells, which has a negative impact on heart function and can lead to heart failure (Levitt, Hamard, and

Demignon 2012). Also, radiotherapy in childhood, especially in the spinal region, affects growth and organ function, but more importantly it is the main cause for the elevated risk of suffering from a second malignant neoplasm (Levitt, Hamard, and Demignon 2012; Taylor et al. 2008; Wright, Green, and Daw 2009). Furthermore, radiotherapy can lead to endocrine defects like precocious puberty, hypogonadism (primary or central), altered fertility and/or sexual function, low BMI, the metabolic syndrome and hypothalamic obesity (Rose et al. 2016). These long-term effects demonstrate how important it is to find the right balance of chemotherapy and radiotherapy for each patient and to keep the burden on young patients as minimal as possible. Therefore, definite classification and deep understanding of the genetic basis of chemo-resistant blastemal remnants in WT is mandatory to find the right therapeutic strategy.

2.2.6 Mouse model of the Wilms tumor

The heterogeneity regarding genetic background and histological appearance made it difficult to establish a model system for Wilms tumor. Valuable results in reproduction of the triphasic characteristics of the Wilms tumor *in vivo* were achieved by transplantation of xenografts originated from humans into mice (Houghton et al. 2007; Yeger et al. 1985). It were Hu and colleagues (2011) who established the first mouse model that could recapitulate a subset of human WT. They engineered mice that maintain mosaic ablation of *Wt1* and biallelic upregulation of *Igf2* by ubiquitous expression of tamoxifen-inducible cre-recombinase. In 2016, the same group used nephron progenitor specific cre-recombinase under the *Six2* or *Cited1* promotor to introduce the same *Wt1* ablation and biallelic *Igf2* expression in mice. Furthermore, they engineered a new mouse model with a *Cnntb1* mutation that is known to stabilize β-catenin (Huang et al. 2016). While the *Wt1* ablation together with biallelic *Igf2* expression again resulted in the typical triphasic tumor appearance, the mice with the *Cnntb1* mutation developed tumors with predominant epithelial histology and a gene expression profile not characteristic for early renal mesenchyme. Targeting either of these alterations to stromal progenitors did not result in tumor formation. These results demonstrated that committed nephron progenitors are the origin of WT. Furthermore, it could be shown that committed stromal progenitors were less susceptible to tumorigenic growth and stromal-type tumors arise from mesenchymal cells before commitment to a stromal linage (Huang et al. 2016).

2.3 Wilms Tumor screens

To gain a more detailed genetic insight into Wilms tumor and especially the remaining persistent blastema of chemotherapy treated patients, Wegert et al. (2015) analyzed a large cohort of blastemal-type Wilms tumors by exome sequencing. The results were validated by a replication cohort. The study revealed several possible oncogenic driver genes for Wilms tumor. Recurrent mutations were found in the homeo-domain of *SIX1* and *SIX2* in highly proliferative tumors (18.1% of the blastemal-type

tumors), in the microprocessor genes *DROSHA* and *DGCR8* (18.2% of the blastemal-type tumors) and in *DICER* and *DIS3L2*, which are both involved in miRNA processing as well. Alteration could also be found in the genes *IGF2*, *MYCN* and *TP53*. Especially alteration in *TP53* has a severe negative impact on patient outcome. Interestingly, the study found an overlap between mutations in *DROSHA* and *SIX1*, which was significant ($p < 10^{-6}$), and may be a strong hint for a synergistic effect (Wegert et al. 2015). The findings of Wegert et al. (2015) were further validated by a parallel study done by Walz et al. (2015) that found the same *SIX* and *DROSHA* mutations in blastemal-type WT.

2.4 The SIX gene family

The members of the SIX family are homologs of genes that are well known in the fruit fly *Drosophila melanogaster*, namely *Drosophila sine oculis* (*So*), *Optix* and *Dsix4*. As the name suggests *So* loss leads to a deficiency of the compound eye in the fly, while *Optix* expression in other than retinal tissue causes eye formation in this tissue. *Dsix4* is important for the development of mesoderm derivatives such as somatic muscles, somatic cells of the gonad and fat tissue (Kumar 2009). In vertebrates the SIX family splits up into three groups: *Six1*/*Six2* are homologs of *So*, *Six3*/*Six6* of *Optix* and *Six4*/*Six5* of *Dsix4*. Characteristic for the SIX family members are the Six-type homeodomain (HD, 60 aa) and the Six-domain (SD, 110-115 aa). The SIX family members can be found in different species throughout the vertebrates up to higher mammals (Kumar 2009; Kawakami et al. 2000).

From all the mentioned SIX family members, the most profoundly studied over the last two decades has been *Six1*. Various studies could show its involvement in the development of tissues in respective organs such as the auditory system, the kidney, muscles, sensory organs and craniofacial structures (Wu et al. 2015). Also, *Six1* contribution to tumorigenesis has been the topic of many studies. *Six1* is known for playing a role in breast cancer, ovarian cancer, cervical cancer, hepatocellular carcinoma, rhabdomyosarcoma, Wilms tumor and colorectal cancer (Wu et al. 2015).

2.4.1 *Six1* in kidney development

As already pointed out in chapter 2.1.2, the outgrowth of the UB into the metanephric mesenchyme is the initial start point of nephrogenesis. This outgrowth seems to be indirectly regulated and controlled by SIX1 and its co-factor EYA1 (Costantini 2006). Knockout of *Eya1* leads to renal agenesis (Xu et al. 1999), but it is known that EYA1 alone cannot affect transcription due to its inability to enter the nucleus. The entrance of EYA1 into the nucleus is only possible if mediated by SIX protein family members (Ohto et al. 1999). This leads to the conclusion that SIX1 has an indirect effect on UB outgrowth and that kidney development depends on the interaction of SIX1 and EYA1 (Xu et al. 2003). Consequently, *Six1* knockout at early stages of kidney development can lead to failure of UB invasion, followed by apoptosis of the metanephric mesenchyme. In *Six1* deficient mice, expression levels of

Pax2, *Six2* and *Sall1* in the metanephric mesenchyme are downregulated. All three genes are critical factors in early kidney development and especially SALL1 is known to be a direct downstream target of SIX1 (Bouchard et al. 2002; Nishinakamura et al. 2001; Chai et al. 2006). The interactions with SALL1 and EYA1 indicate that SIX1 is a critical factor for kidney development. *Six1* mutations that affect these interactions may play an important role in developmental disorders.

2.4.2 *SIX1* in tumor development

Six1 is involved in different types of cancer including breast cancer, ovarian/ cervical carcinoma, colorectal cancer and hepatocellular carcinoma (Wu et al. 2015). An overview of the regulatory network of *SIX1* in tumorigenesis is shown in Figure 5.

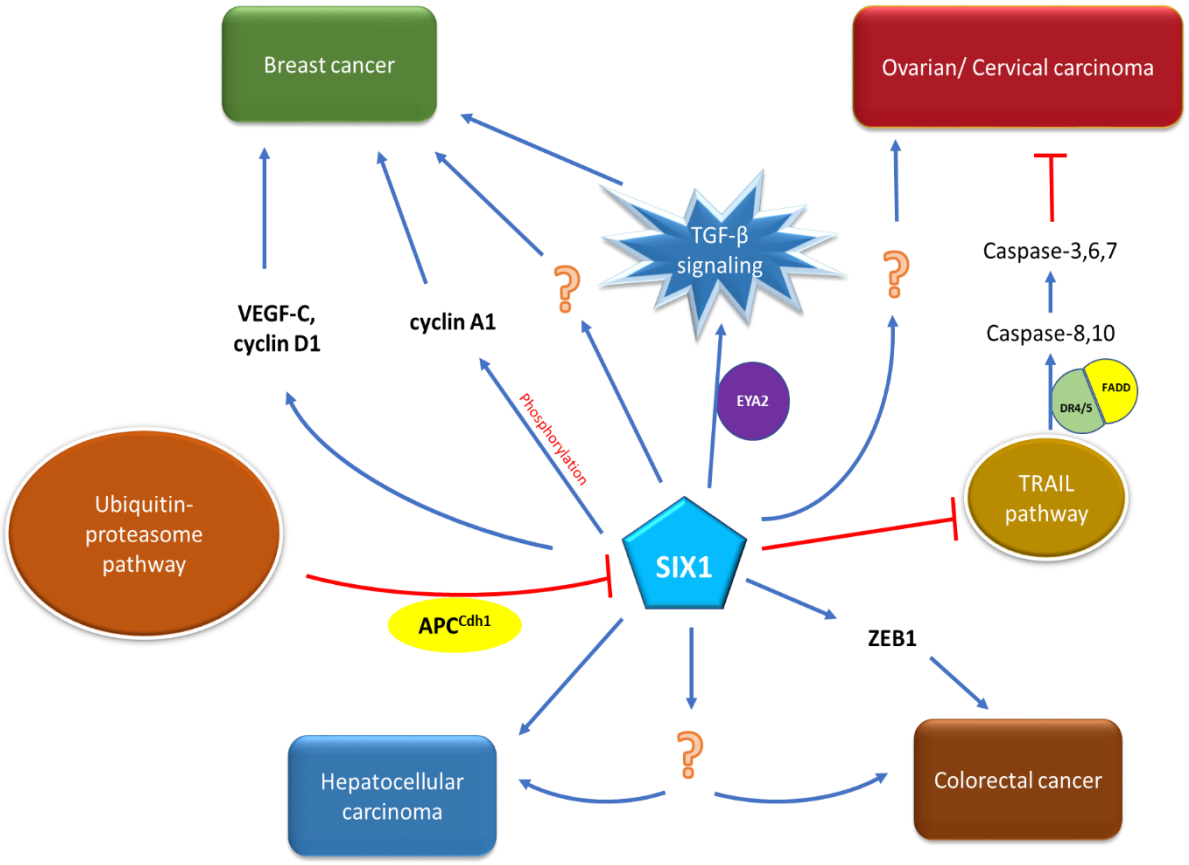

Figure 5: SIX1 in tumorigenesis

Mechanisms and pathways of positive and negative regulation of Six1 in different cancer types. (Illustration based on (Wu et al. 2015))

In 1998 *SIX1* was for the first time reported to be overexpressed in a high number of mammary carcinomas and a correlation between metastatic breast cancer was predicted (Ford et al. 1998). That *SIX1* has a function in metastatic regulation was also predicted by a study of rhabdomyosarcoma (Yu et al. 2004). It has been shown that SIX1 overexpression can abolish the G2 cell cycle checkpoint, which is induced by DNA damage (Ford et al. 1998). To date, many studies could prove the correlation

between *SIX1* mutations and breast cancer (Micalizzi et al. 2009; Radisky 2009; Reichenberger et al. 2005). Especially, the direct activation of c*yclin A1* transcription by SIX1 is a critical factor, due to c*yclin A1* involvement in cell proliferation, cell survival, DNA repair and angiogenesis (Coletta et al. 2004). Thereby, SIX1 overexpression promotes breast cancer cell proliferation and tumorigenesis. Apart from *cyclin A1*, SIX1 regulates other genes that are known for their pro-tumorigenic properties, for example *cyclin D1*, *c-Myc* and *Ezrin* (Yu et al. 2006) and SIX1 overexpression induces tumor growth and metastasis in breast cancer due to increased TGF-β signaling (Micalizzi et al. 2009; Micalizzi et al. 2010). Furthermore, recent studies could show that SIX1 also plays a role in the induction of lymphangiogenesis and distant metastasis in breast cancer by upregulation of lymphangiogenic factor VEGF-C (Wang et al. 2012).

Apart from its prominent role in breast cancer, *SIX1* also is involved in hepatocellular carcinoma (HCC), ovarian and cervical cancer. In HCC, *SIX1* is associated with tumor recurrence and metastasis (Ng et al. 2006). Thus, *SIX1* mRNA could be found in 85% of liver tumor tissue, while almost completely absent in nontumor tissue, and also the SIX1 protein could only be detected in tumor tissue. A recent study identified 52 possible target genes of SIX1 in HCC, but whether these targets are involved in the development or metastasis of HCC is still not confirmed (Ng et al. 2010). For ovarian and cervical cancer SIX1 is a proposed biomarker because of its high expression in both tumor types (Behbakht et al. 2007; Wan et al. 2008). In comparison with a normal ovary, SIX1 is overexpressed in 50% of early and 63% of late stage ovarian carcinomas, can promote cell proliferation and prevent tumor necrosis (Behbakht et al. 2007).

2.4.3 *SIX1* and Wilms tumor

SIX1 protein expression has been proposed as a candidate marker for blastema in WT. From all candidates (SIX1, CITED1 and CD65) SIX1 shows the highest detection specificity for postchemotherapy WT blastema (Sehic, Ciornei, and Gisselsson 2014; Sehic et al. 2012). SIX1 detection may help to successfully identify and quantify blastemal elements after preoperative chemotherapy and surgery and by that helps to determine correct histopathological risk stratification.

In the analyzed blastemal-type Wilms tumor cohort (2.3), the somatic hotspot mutation which occurred with the highest frequency (10%, 6 of 58 cases) was an A to G transition in exon 1 of the *SIX1* gene (Wegert et al. 2015). This mutation leads to a substitution from glutamine to arginine at position 177 (Q177R) that affects the homeo-domain of the SIX1 protein. Further screening of a larger unselected cohort of Wilms tumors (n=529) could detect 17 cases of mostly heterozygous *SIX1 Q177R* mutations. Furthermore, 6 cases with the same Q177R mutation were found in the *SIX2* gene, which is highly homologous to *SIX1* and a downstream target of SIX1 in embryonic kidney development. Also, one truncation mutation of *SALL1* was found. *SALL1* is also activated by SIX1, leading to the conclusion

that the whole pathway downstream of SIX1 plays an important role for tumorigenesis in WT. Since the mutations were somatic and sequencing of cDNA showed an equal expression of wild type and mutant allele, Wegert et al. (2015) suggest a dominant effect.

Wegert et al. predicted that the Q177R mutation leads to an altered DNA binding ability of SIX1 because crystal structure analysis had shown that the exchanged residue is placed in the major groove of the bound DNA. A change in promotor activation of downstream targets of SIX1/2, as well as SALL1, could not be detected by luciferase assay (Wegert et al. 2015). The conclusion of the results achieved in the Wilms tumor screen and further analysis of the Q177R mutation suggest that the mutation leads to a shift in DNA binding specificity instead of a complete loss of DNA binding. This may end up in subtle changes to the gene regulatory capacity of SIX1.

2.5 The microprocessor protein DROSHA

The ribonuclease III enzyme DROSHA together with its partner, the double-stranded RNA binding protein DGCR8, form the microprocessor complex. The microprocessor organizes the essential nuclear processing step of miRNAs biogenesis.

2.5.1 miRNA biogenesis

Mammalian miRNAs are embedded in long primary miRNAs, which can be located within exons or introns. After transcription by the RNA polymerase II, pri-miRNAs are processed within the nucleus and then further in the cytoplasm to become mature miRNAs. For the processing inside the nucleus, DROSHA and DGCR8 form together the microprocessor complex which converts the pri-miRNA into precursor miRNA. After the export of the pre-miRNA out of the nucleus by EXPORTIN5, the pre-miRNA can by further processed by the DICER, an RNase III enzyme, into mature miRNA (Figure 6).

In detail, it has been shown that DROSHA is able to form two different kind of complexes. The smaller of the two complexes consists of DROSHA and its partner DGCR8, which together build the minimal catalytically active complex *in vitro* that directs cleavage and thereby the processing of pri-miRNAs to pre-miRNAs (Gregory et al. 2004; Landthaler, Yalcin, and Tuschl 2004). Alternatively, DROSHA and DGCR8 together can interact with further RNA-binding proteins like RNA helicases, heterogeneous nuclear ribonucleoproteins (hnRNPs) and proteins that regulate activity of DROSHA/ DGCR8, which forms a larger complex (Siomi and Siomi 2010). DROSHA/ DGCR8 are both essential for processing of pri-miRNA: DGCR8 braces the pri-miRNA at the hairpin and recognizes the distance between the double-stranded RNA and single-stranded RNA junction (Han et al. 2006). With its endonuclease activity, DROSHA is able to cleave the pri-miRNA exactly 11 bp away from this junction (Han et al. 2004). After exportation by EXPORTIN5, the so called dicing of the pre-miRNA by DICER gives rise to the 22 nt long mature miRNA duplex. In mammals this dicing step is supported by the interaction of

DICER with two partner proteins, the TAR (transactivating response), RNA-binding protein (TRBP) and protein activator of the interferon induced protein kinase (PACT), which are not necessary for DICER activity, but play a role in defining the cleavage site and recruiting the RNA-induced silencing complex (RISC) (Fukunaga et al. 2012). Either the 5p arm or the 3p arm of the miRNA duplex has the preference to bind to one of the multiple Argonaute proteins (AGO) (Peters and Meister 2007). The miRNA functions as a guide to target specific mRNAs and can result in degradation or translation inhibition of the transcripts reliant on the complementarity of miRNA and mRNA (Huntzinger and Izaurralde 2011). Apart from this canonical production of miRNAs there are different non-canonical pathways that are able to produce functional miRNAs. One example is the generation of mature miRNAs by spliceosome activity (mirtrons) (Yang and Lai 2011).

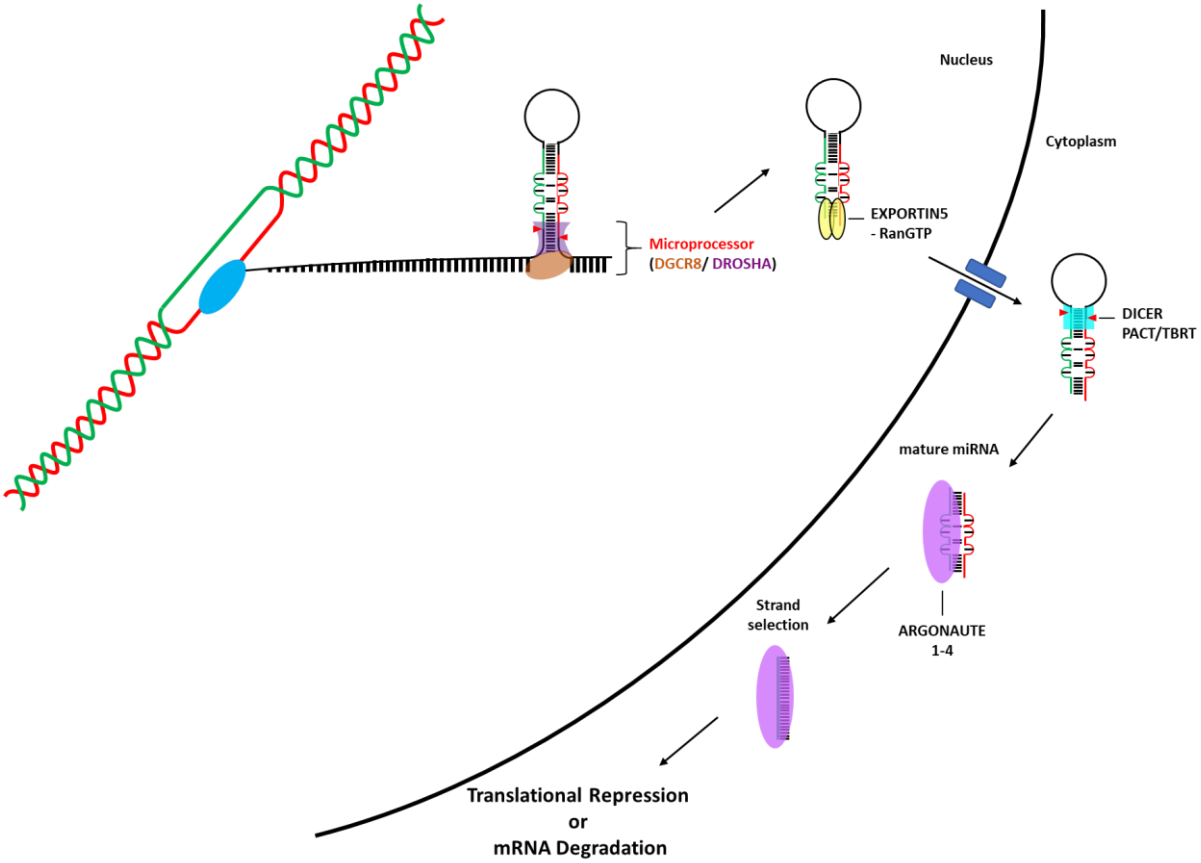

Figure 6: miRNA biogenesis

Long pri-mRNAs are transcribed by RNA polymerase II and are afterwards processed by the microprocessor complex containing DROSHA and DGCR8. The cleavage by DROSHA and DGCR8 leads to 2 nt 3' overhangs that are recognized by EXPORTIN5-RanGTP and allows transport out of the nucleus into the cytoplasm. In the cytoplasm DICER cuts at the stem loop and creates an RNA duplex. Out of this duplex only one strand is preferentially used and able to bind to Ago, which acts as a guide to the targeted mRNA for translational repression or degradation. (Illustration based on (Macias, Cordiner, and Caceres 2013))

2.5.2 *DROSHA* and Wilms tumor

Mutations regarding the microprocessor complex and especially *DROSHA* and *DGCR8* were the second most prevalent somatic mutations found by the exome sequencing screen of blastemal-type Wilms tumors (Wegert et al. 2015). Five *DROSHA* mutations could be identified, four affected one of the metal binding amino acids inside the RNase IIIb domain. The RNase IIIb domain is critical for catalytic activity of DROSHA (Gan et al. 2006). All mutations led to an amino acid transition from glutamic acid to lysine at aa 1147 (n=3) or 1222 (n=1). The last mutation D973H affected the catalytic center of the RNase IIIa domain. Further screening of Wilms tumor cases (n=363) revealed 13 additional tumors with the *DROSHA* E1147K mutation. The identified mutations were heterozygous in tumor DNA and cDNA for all cases. Furthermore, multiple biopsies (up to six) of different tumors (n=8) were screened and all displayed heterozygous mutations (Wegert et al. 2015). This suggests a possible dominant effect of heterozygous *DROSHA* mutations.

The hotspot mutations in *DGCR8* either affected the RNA binding domain with a charge reversal amino acid alteration at amino acid 518 (E518K), resulting in an early protein truncation behind amino acid 81, or exhibited a nonsense mutation (E213X). Since the E518K alteration was most prevalent (4 out of 6 tumors), 719 additional cases were screened for this mutation. An additional 20 tumors positive for the E518K alteration were identified. Overall, the cumulative incidence of the E518K mutation was 3.2%. In contrast to *DROSHA*, most of the *DGCR8* mutations were homozygous, which might be an indication for recessive activity (Wegert et al. 2015).

2.6 Possible Synergistic effect of *DROSHA* and *SIX1*

The results of exome sequencing cohort showed significant overlap between *DROSHA* and *SIX1* mutations. Of 45 cases, seven displayed a double mutant tumor). In contrast a combination of *DGCR8* and *SIX1* mutation only occurred once (Figure 7). One can assume that a possible functional and synergistic link might only exists between *DROSHA* and *SIX1* (Wegert et al. 2015).

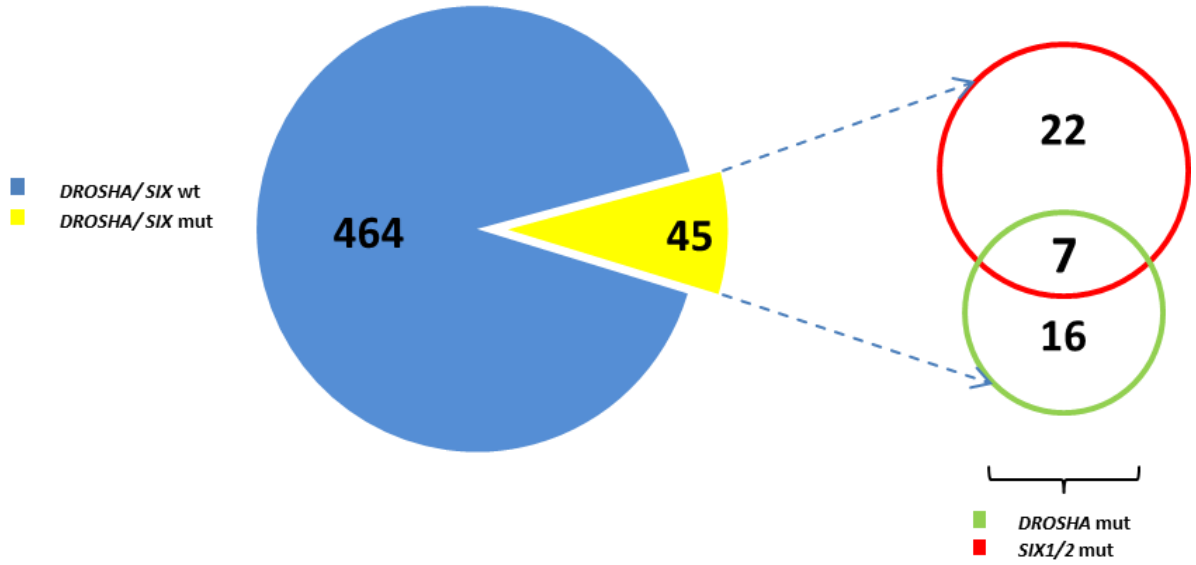

Figure 7: Overlapping mutations between *SIX1/2* and *DROSHA*
X^2 test: $p < 10^{-6}$

The possible synergistic effect and because *SIX* and *DROSHA* alterations were the most prevalent of all found mutations, the aim of this study was the establishment of *DROSHA E1147K* and *SIX1 Q177R* mutant mice to understand the influence of these genes on kidney development and to find out if one of these mutations is sufficient to induce WT. Furthermore, after establishment and analysis of both mouse models, compound mutants were bred to investigate the possible synergistic effects of both mutations and its importance regarding WT.

3 Material

3.1 Equipment

Table 3: Equipment used

Equipment	Company
HM 340E Rotary Microtome	Thermo Scientific, USA
Mastercylcer ep realplex	Eppendorf, Germany
NanoDrop ND-1000 Spektrophotometer	PeqLab, USA
Nikon Eclipse TS100 with Intenslight C-HGFI	Nikon, Japan
Nucleofector™ II/2b Device	Lonza, USA
Zeiss Axioskop	Zeiss, Germany

3.2 Chemicals and disposables

All disposals were either purchased from Sarstedt (Germany) or Eppendorf (Germany). All chemicals not included in Table 4 were ordered from ROTH (Germany) or Sigma-Aldrich (Germany). All enzymes used for cloning were purchased from NEB (USA). Oligonucleotides listed in 9.1 were synthesized by Sigma-Aldrich (Germany).

Table 4: Chemicals used

Chemicals/ Disposables	Company
Aprotinin	Sigma-Aldrich, Germany
Beta-mercaptoethanol	Sigma-Aldrich, Germany
CHIR99021	Axon, Netherlands
DIG RNA Labeling Mix	Roche, Switzerland
DMEM	Sigma-Aldrich, Germany
Fetal calf serum (FCS)	Sigma-Aldrich, Germany
His-taq polymerase	self-made
Kaiser's glycerol gelatine	Merck, Germany
Leukemia inhibitory factor (LIF)	self-made
Leupeptin	Sigma-Aldrich, Germany
Metafecten Pro	Biotex, Germany
Parafilm® M	Sigma-Aldrich, Germany
Penicillin/Streptomycin 100x	PAA, Germany

Pepstatin	Sigma-Aldrich, Germany
peqGOLD TriFast™	Peqlab, Germany
Proteinase K	Roche, Switzerland
QuadriPERM Box	Heraeus, Germany
RNAse A	Thermo Scientific, USA
Roti®-Histokitt	ROTH, Germany
SuperfrostTM plus slides	Thermo Scientific, USA
SybrGreen	Sigma-Aldrich, Germany

3.3 Buffers

All *in situ* buffers used before hybridization with the RNA probe were prepared with DEPC water or treated with DEPC.

Table 5: Buffers used

Buffer	Components
Standard buffers	
PBS	150 mM NaCl, 2.7 mM KCl, 8 mM Na_2HPO_4, 1.8 mM KH_2PO_4
TE	10 mM Tris pH 8.0, 1 mM EDTA
DNA buffers	
Base buffer 50x	1.25 M NaOH, 10 mM EDTA.
Cell lysis buffer	100 mM Tris pH 8.5, 5 mM EDTA pH 8.0, 0.5 % SDS, 200 mM NaCl
DNA loading dye 10x	50 % glycerol, 15 % ficoll, 10 mM EDTA pH 8.0
Neutral buffer 50x	2 M Tris-Base pH 5
PCR buffer 10x	200 mM Tris pH 8.8, 100 mM $(NH_4)_2SO_4$, 100 mM KCl, 20 mM $MgSO_4$, 1 % TritonX-100, 1 % BSA-acetylated
SB 20x	200 mM NaOH pH 8.0 with boric acid
TAE 50x	50 mM EDTA, 2 M Tris acetate pH 8
Protein buffers	
Blotting buffer	25 mM Tris pH 8.3, 150 mM Glycine, 10 % Methanol
Detection buffer	100 mM Tris pH 8.0, 250 mM luminol, 90 mM coumaric acid, 0.01 % H_2O_2
Protein loading buffer 2x	100 mM Tris pH 6.8, 4 % SDS, 0.25 % Bromophenol blue, 25 % glycerol, 200 mM DTT

RIPA buffer	50 mM Tris pH 8.0, 1 % Nonidet P40, 0.5 % Sodium deoxycholate, 0.1 % SDS, 150 mM NaCl, 1 mM EDTA. *Fresh before use:* 1 µg/ ml Aprotinin, Leupeptin, Pepstatin mix, 50 µg/ ml PMSF
SDS running buffer	25 mM Tris pH 8.3, 192 mM glycine, 1 % SDS
***in situ* buffers**	
Hybridization solution	50 % Formamide deionized, 1.3 x SSC pH 5, 5 mM EDTA, 0.5 % CHAPS, 100 µg/ ml Heparin, 0.2 % Tween-20
MABT	100 mM maleic acid, 150 mM NaCl, 1 % Tween-20, pH 7.5
MOPS 20x	200 mM MOPS, 50 mM NaAc, 10 mM EDTA
NTE (RNase Buffer)	0.5 NaCl, 10 mM Tris-HCl pH 7.0, 5 mM EDTA
NTMT	10 mM NaCl, 50 mM $MgCl_2$, 100 mM Tris-HCl pH 9.5, 0.1 % Tween-20
PFA 4 %	1x PBS, 4 % PFA. Adjust pH to 7.0
Proteinase K buffer	20 mM Tris pH 7.5, 1 mM EDTA
SSC 20x	3 M NaCl, 0.3 M Na citrate x 2 H_2O, citric acid pH 5
TBST	140 mM NaCl, 2.7 mM KCl, 25 mM Tris-HCl pH 7.5, 0.1 % Tween-20
Tris/ Glycine buffer	0.1 M Tris, 0.1 glycine

3.4 Kits

Table 6: Kits used

Name	**Company**
Gel extraction kit	Omega Bio-Tek, USA
Maxblock™ Autofluorescence Reducing Reagent Kit	Dianova, Germany
Nucleofector™ Kit for Mouse Embryonic Stem Cells (mES)	Lonza, USA
Plasmid midi kit	Omega Bio-Tek, USA
Plasmid mini kit	Omega Bio-Tek, USA
RevertAid Reverse Transcriptase	Thermo Scientific, USA

3.5 Antibodies

Table 7: Antibodies used

Name	Species	#	Company
Primary Antibodies			
α-cCasp3 (Asp175)	rabbit	9579	Cell Signaling, Netherlands
α-Digoxigenin-AP,FAB fragments	sheep	11093274910	Roche, Switzerland
α-Flag-M2	mouse	H9658	Sigma-Aldrich, Germany
α-GFP (AA246)	goat	ABIN100085	Antibodies online, USA
α-Ki-67	rabbit	ab16667	Abcam, UK
α-Nephrin	mouse	AF3159	R&D Systems, USA
α-WT1 (13B5)	mouse		Mundlos et al. (1993)
Secondary Antibodies			Invitrogen, USA
Alexa 594-α-goat	donkey	A-11058	Thermo Scientific, USA
Alexa 594-α-mouse	donkey	R37115	Thermo Scientific, USA
Alexa 594-α-rabbit	donkey	R37119	Thermo Scientific, USA
Alexa488-α-goat	donkey	A-11055	Thermo Scientific, USA

3.6 Plasmids

The plasmids were cloned by Anja Winkler (AG Gessler, EBCh, Wuerzburg). Afterwards, the constructs were verified by Sanger sequencing.

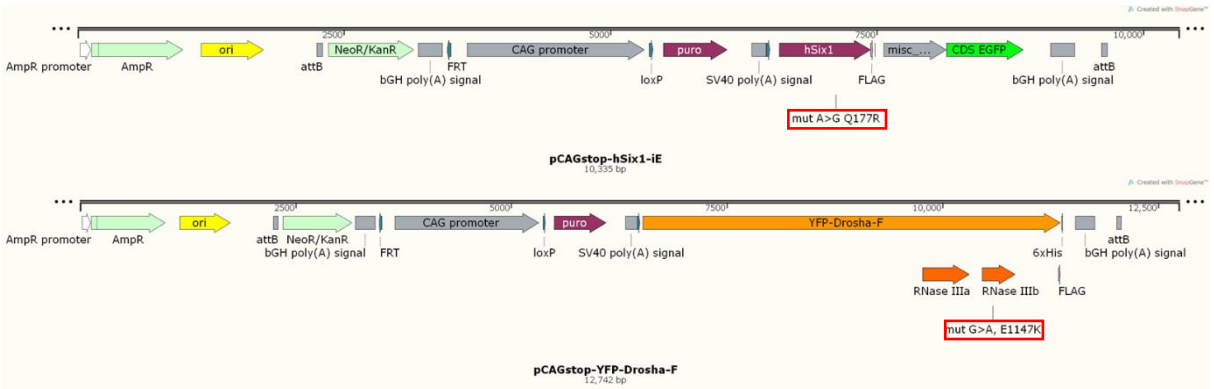

Figure 8: Plasmid constructs for integration into ES cells via RMCE

Both mutation sites (DROSHA-E1147K and SIX1-Q177R) are indicated with red boxes for the corresponding construct.

3.7 Cell lines

IDG3.2-R26.10-3 (I3) murine ES cells, (Hitz, Wurst, and Kuhn 2007).

NSNL neomycin resistant feeder cells, (Hitz, Wurst, and Kuhn 2007).

3.8 Mouse lines

All experiments on animals were carried out in accordance with national and institutional guidelines (TierSchG).

The Wt1-cre^{ERT2} (Wt1$^{tm2(cre/ERT2)Wtp}$) and the Six2-cre (*Tg(Six2-EGFP/cre)1Amc/J*) breeder pairs as well as the floxed Droshat^{m1Litt} mouse line were obtained from C. Englert (FLI Jena) and V. Taylor (Basel University) respectively. The inducible DROSHA-E1147K and SIX1-Q177R alleles were generated via recombinase mediated cassette exchange (4.9) in IDG3.2-R26.10-3 ES cells by Anja Winkler (SIX1-Q177R) and myself (DROSHA-E1147K). The injection of the ES cells into C57BL/6 blastocysts was performed by M. R. Bösl (Center for Experimental Molecular Medicine, Wuerzburg University Hospital, 97078 Würzburg) (4.9.4).

3.9 Software

Table 8: Software used

Name	Version	Source
Fiji (ImageJ)	1.5J	OpenSource, NIH, USA
Leica Application Suite	4.1	Leica, Germany
Mastercylcer realplex	2.2	Eppendorf, Germany
Nikon NIS-Elements AR	3.2	Nikon, Japan
SnapGene™	1.1.3	GSL Biotech, USA

4 Methods

4.1 DNA isolation

4.1.1 Rapid DNA isolation from tissue or cells

For a quick and simple isolation of DNA from tissue or cells the Base/ Neutral method is used. Especially for mouse genotyping, it is the method of choice. Tissue or cells are placed in a reaction tube and 50 µl of 1x Base solution is added. The sample is incubated on a heater for 30 min at 95°C. The sample is cooled down to RT and 50 µl of Neutral solution is added. Solution volume can vary with the size of the tissue sample or cell pellet, but the proportion of Base and Neutral solution always stays 1:1.

4.1.2 DNA isolation from cells

The use of cell lysis buffer is another quick method to gain high concentrations of DNA from cells. The cell pellet (1-5 x10^6 cells) is resuspended in 700 µl of cell lysis buffer with 7 µl Proteinase K (10µg/ ml) and incubated at 55°C overnight. On the next day, 1 ml of isopropanol is added and the sample is centrifuged at maximal speed for 5 min. The supernatant is discarded, the pellet is washed with 70 % ethanol. After another centrifugation step, the pellet is dried and resuspended in 100 µl TE buffer. For maximal yield the sample is incubated for 15 min at 60°C and stored at -20°C. The concentration of isolated DNA is estimated through absorbance using a Nanodrop spectrometer.

4.2 RNA isolation

For isolation of RNA from tissue or cells peqGOLD TriFast™ is used. Tissue is homogenized and cell pellets are resuspended in TriFast™. RNA is isolated according to manufacturer's protocol. The concentration of isolated RNA is measured through absorbance using a Nanodrop spectrometer.

4.3 Reverse transcription

For first strand cDNA synthesis for quantitative realtime PCR the Thermo Scientific RevertAid Reverse Transcriptase kit is used. All working steps are performed as recommended by the manufacturer.

4.4 Cloning

All cloning is done by using standard molecular methods and Sanger sequencing for construct verification.

4.5 Cell culture

IDG3.2-R26.10-3 (I3) murine ES cells are cultured at 37°C and 5 % CO_2 in DMEM (high glucose with glutamine and sodium pyruvate) supplemented with 15% heat inactivated FCS, 1 MHEPES, 1% non-essential amino acids, 100 mM beta-mercaptoethanol, penicillin/ streptomycin (100 U/ ml / 100 µg/

ml) and leukemia-inhibitory factor (LIF) (1000 U/ ml) on porcine skin gelatine (0.1 % in PBS) coated cell culture dishes. It is essential to change the medium every day.

To maintain pluripotency, ES cells are grown either on coated cell culture dishes in the presence of LIF or on inactivated neo-resistant feeder cells. Ideally, pluripotent ES cell colonies should appear as round to ovoid clusters with defined margins on top of the feeder cells. In this work, ES cells are cultured on neo-resistant and mitomycin-C treated feeder cells (inactivated NSNL). These embryonic feeder cells are derived from E13-E14 mouse embryos harboring the *neo* gene. NSNL feeder cells are cultured at 37°C and 5% CO_2 in DMEM supplemented with 10 % heat inactivated FCS, 1% non-essential amino acids and penicillin/ streptomycin (100 U/ ml / 100 µg/ ml). Feeder cells grow on normal cell culture dishes and can be treated according to common cell culture protocols. For the use as feeder cells for ES cell growth, the feeder cells need to be mitotically inactivated. Therefore, a confluent dish is washed with PBS and treated with mitomycin C (10 µg/ ml) containing DMEM for at least 2 hours (up to 6 h). Afterwards, the cell dish is washed with PBS for three times and either used directly or frozen in the described medium including 10% DMSO at -80°C for later use.

4.6 PCR Analysis

For analysis of DNA a standard PCR reaction is used. PCR products are analyzed by SB agarose gel electrophoresis.

Standard-PCR reaction

2 µl	10x PCR buffer
0.2 µl	dNTPs 100 mM
0.2 µl	His-tag 15 U/ µl
0.5 µl	5’ primer 10 pmol
0.5 µl	3’ primer 10 pmol
16 µl	H_2O
1 µl	DNA

Standard-PCR program

95°C	3 min	Initial denaturation
95°C	30 sec	Denaturation ┐
55°C*	30 sec	Annealing |- 35 cycles
72°C*	45 sec	Elongation ┘
72°C	5 min	Final elongation
16°C	∞	End

* Annealing temperature is depending on primer combination and elongation time can vary depending on the size of the desired product.

4.7 Quantitative realtime PCR

For quantitative realtime PCR, 2 µg of RNA are reverse transcribed into first strand cDNA and diluted 1:10 for the qRT-PCR reaction. The annealing temperature of the PCR is set to 60°C and SybrGreen (1:2000 in H_2O/ 0.5 % DMSO) is used for quantification. To verify the PCR products melting curve analysis and SB agarose gel electrophoresis are used. For expression level normalization the housekeeping gene HPRT is used. All measurements are done as technical duplicates or triplicates.

qRT-PCR reaction

2.5 µl	10x PCR buffer
1.5 µl	Ethylenglycol
0.25 µl	dNTPs 100 mM
0.75 µl	SybrGreen
0.25 µl	His-tag 15 U/ µl
0.75 µl	5' primer 10 pmol
0.75 µl	3' primer 10 pmol
13.25 µl	H_2O
5 µl	cDNA template

qRT-PCR program

95°C	3 min	Initial denaturation
95°C	15 sec	Denaturation ┐
60°C	10 sec	Annealing |- 40 cycles
72°C	20 sec	Elongation ┘
55-60°C	10 min	Melting curve (+4°C/ min)
16°C	∞	End

4.8 Two-tailed RT-qPCR

In this study the two-tailed RT-qPCR is used to measure miRNA expression of tissue samples derived from mouse embryos. This method was established by Androvic et al. (2017).

The two-tailed RT primer secondary structures are predicted with the help of the UNAfold web server (http://unafold.rna.albandy.edu/) (Markham and Zuker 2008). Two-tailed RT primers as well as qPCR primers are designed according to the target miRNA and synthesized by Sigma-Aldrich, Germany.

The total RNA is extracted from samples with peqGOLD TriFast™ and according to manufacturer's protocol. 10 ng of total RNA is put into 10 µl reaction volume and the reaction is performed with the Thermo Scientific RevertAid Reverse Transcriptase kit as follows:

cDNA synthesis reaction:

x µl	10 ng total RNA
1 µl	1 µM two-tailed RT primer mix
ad to 12 µl with DEPC- H_2O	
4 µl	5x RT buffer
0.5 µl	40 U/ µl Ribolock RNase Inhibitor
2 µl	dNTPs 10 mM
1 µl	200 U/ µl ReverseTranscriptase
0.5 µl	DEPC- H_2O
20 µl reaction volume	

The reaction is incubated for 45 min at 25°C and inactivated for 5 min at 70°C. Afterwards, the 20 µl reaction mix is 10x diluted with 180 µl of H_2O. The subsequent qPCR is performed with 20 µl reaction mix and 5 µl cDNA template according to the following setup:

qRT-PCR program

95°C	30 sec	
95°C	5 sec	┐
60°C	15 sec	┘ 45 cycles
95°C	5 sec	
55-60°C	10 min	Melting curve
16°C	∞	End

4.9 Recombinase mediated cassette exchange

With the help of site specific recombination, the recombinase mediated cassette exchange (RMCE) enables the exchange of the preexisting gene cassette for an analogous cassette carrying the gene of interest (GOI) in mammalian cells. In this study the RMCE method is used to generate murine ES cells that harbor a cre-recombinase inducible loxP-stop-loxP (LSL) cassette followed by either a SIX1-Q177R-IRES-eGFP or a YFP-DROSHA-E1147K-Flag fusion (3.6). The protocol used in this study is based on the publication of Hitz et al. (2007).

The donor vector with the GOI can be integrated into ES cells that contain the acceptor site within the *Rosa26* locus. For later selection the donor vector contains a promotor-less hygromycin resistance coding region and poly A site. Both GOI and the hygromycin coding region are flanked by attB recognition sites. The *Rosa26* acceptor allele (R26.10) contains a pair of attP recognition sites that flank a hygromycin B resistance region and a poly A site. The C31 integrase can now mediate the recombination between the pairs of attB and attP sites. The catalyzed exchange destroys the attB and

attP sites, it addresses, and converts them in attR and attL sites. This leads to an exchange of the hygro-pA with the neo-pA-GOI site now flanked by the attR and attL sites (Figure 9).

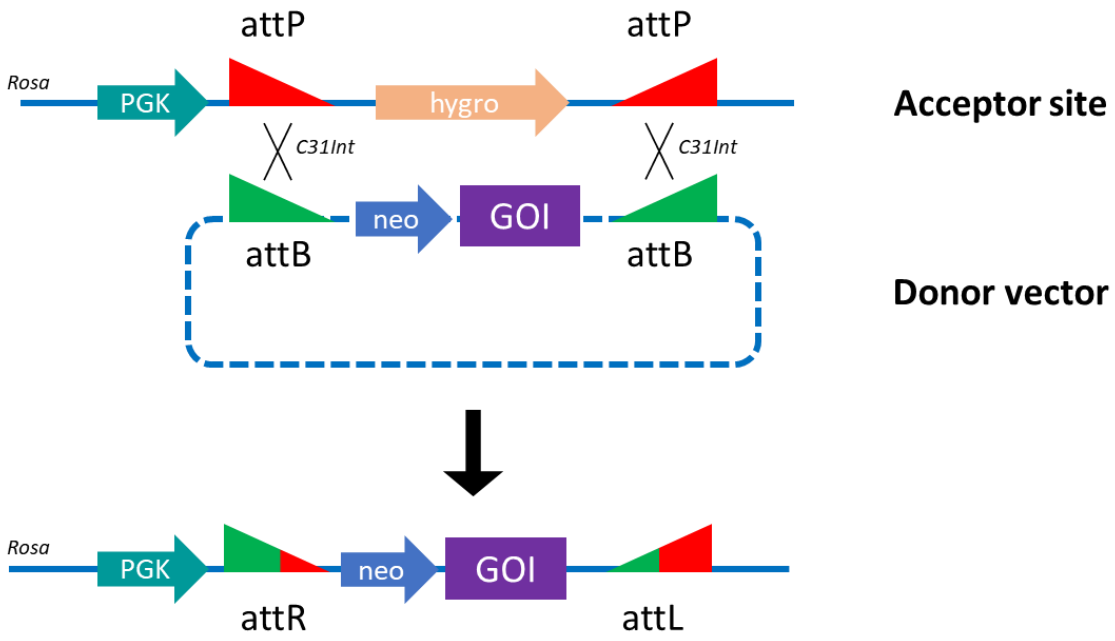

Figure 9: Scheme for C31Integrase mediated RMCE

The attR and attL sites are not further recognized by the C311 integrase. For induction of the described exchange, R26.10 ES cells are cotransfected with the donor vector and the expression vector of the C31 integrase. Since the hygro-pA site is exchanged by the neo-pA-site, neo resistant ES cell colonies are selected, expanded and analysed via PCR and Western blot for the expression of the GOI. In this study the IDG3.2-R26.10-3 (I3) murine ES cells are used for RMCE (3.7).

4.9.1 Vector precipitation

The donor vector (pCAG-LSL-YFP-DROSHA-E1147K-F respectively pCAG-LSL-SIX1-Q177R-IRES-eGFP) and the pCAG-C31Int-bpA vector are put in the precipitation reaction with the ratio 1:1 or 13:7. 1/10 volume of 3 M NaAc pH 5.2 and 2 volumes of 100 % ethanol are added to the DNA mix. After an incubation at -20°C for 20 min, the sample is centrifuged and the pellet washed 2 times with 70 % ethanol. Afterwards, work is continued under the laminar flow hood and with sterile reagents. The dry pellet is resuspended in 10 µl ddH_2O and incubated for 15 min, followed by gentle mixing via pipetting. The DNA is incubated another 15 min and then used either directly for transfection or stored at -20°C.

4.9.2 Transfection of murine ES cells

For murine ES cell transfection the Nucleofector™ Kit for Mouse Embryonic Stem Cells and Nucleofector™ II/2b Device are used. The murine ES cells are counted and 2x 10^6 cells are centrifuged

at 900 rpm for 3 min. The pellet is resuspended in 90 µl of Nucleofector solution and combined with the 10 µl vector-DNA mix (4.9.1). The combined solution of ES cells and vector-DNA is transferred into a Lonza-mESC-cuvette and electroporated in the Nucleofector™ II/2b Device (program Ax024). After electroporation, pre-warmed ES cell medium (4.5) is added and the cell suspension is transferred to a 10 cm cell culture plate coated with neo resistant feeder cells. The medium is changed every day. From the second day after electroporation, 400 µg/ ml G418, an analog of neomycin, is added to the medium to select correctly recombined cell colonies. After picking and expanding surviving ES cell colonies, analysis for correct integration is done via PCR.

4.9.3 RMCE control of transfected ES cells via nested PCR

To check for successful recombinase mediated cassette exchange and correct integration of the GOI into the acceptor site, the picked cell colonies are expanded and a fraction is lysed for DNA extraction (4.1.2). The DNA is analyzed via nested PCR, which minimizes non-specific products. For nested PCRs two sets of primers are used in two successive PCR runs. The second run amplifies a secondary target within the product of the first run. Therefore, the product of the first run is diluted 1:100 and 1 µl is used for the second PCR reaction.

The correct integration into the *Rosa26* locus is checked with the two primer pairs *PGK-forw/ neo-rev* and *PGK-forw/Neotest1* for 5' integration and two primer pairs *bGHpA-for/ R523* and *hes1KO2-bgh/ R523* for 3' integration. Furthermore, the landing site is checked with the two primer pairs *FRTneo2/R523* and *FRTneo2/ Rosa-rev* and the two primer pairs *FRTneo2/hygro5'out* and *PGK-forw/ hygro5'out*, which should not amplify a product, if the *Rosa26* locus is correctly targeted. The RMCE method holds the possibility to integrate the GOI in the wrong direction. To analyze the direction of the GOI, the two primer pairs *reverse/ neo-rev* and *T3-69/ Neotest1* are used. If the GOI is integrated in the right direction, no product should be amplified. Remaining plasmid is controlled with the two primer pairs *reverse/ neoA* and *T3-69/ Neotest1*. Additionally, construct specific PCRs are done for GFP (*GFP-real-for/ GFP-real-rev*), FLAG tag (*Flag-tag-for/ reverse*) and the human transgenes SIX1-Q177R (*hSIX1-f/ hSIX1-r*) or DROSHA-E1147K (*hDrosha-for1/ hDrosha-rev1*). The integrated constructs with annotated primers are shown in Figure 10. All used primers are listed in Table 10.

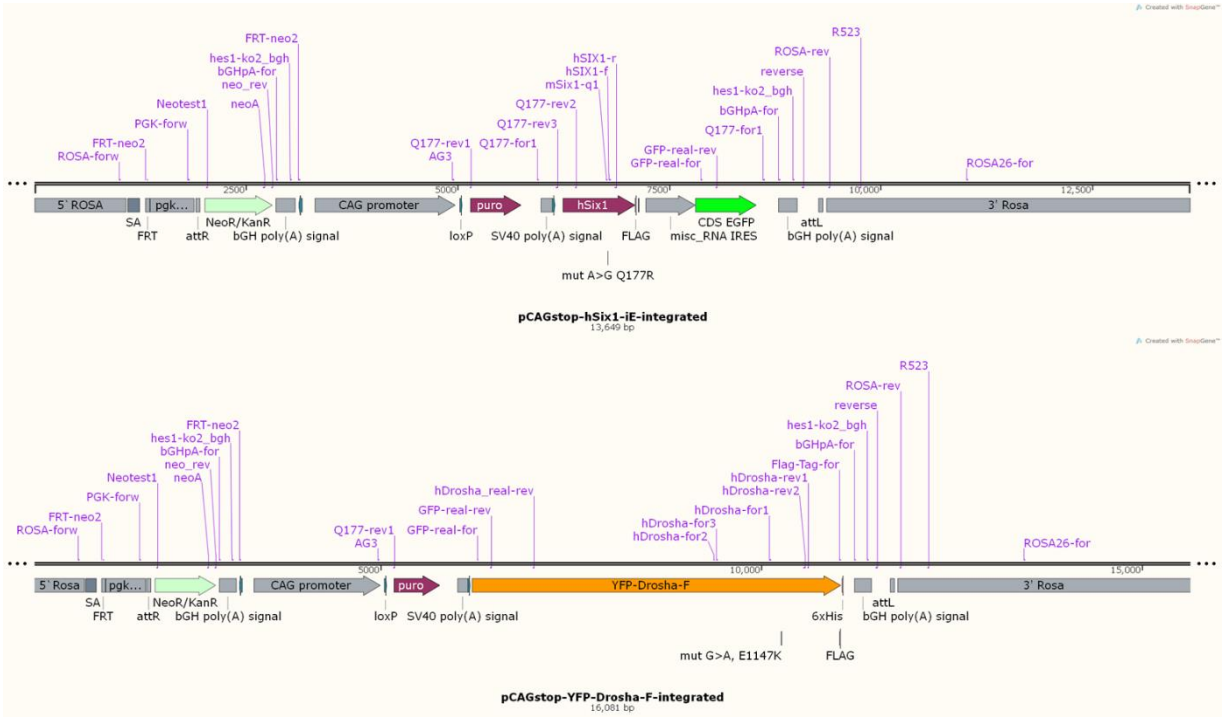

Figure 10: Maps of constructs successfully integrated into the *Rosa26* locus
Primers used to control correct integration via RMCE are indicated in purple.

4.9.4 Implantation of mES-cells into mice

Correctly targeted ES cells are injected into C57BL/6 blastocysts and implanted into foster mothers. Resulting chimeras are bred to C57BL/6 mice and offspring are tested for germline transmission. The injection and implantation were carried out by Michael Bösl at ZEMM, Würzburg.

4.10 Mouse genotyping

Cre transgenes were genotyped by PCR using the primer pairs *mCitrine-3'out* and *ROSA26-creER* for Six2-cre, *Wt1-creERT2-for* and *Wt1-creERT2-TG* for WT1-creERT2 and *mCitrine-3'out* and *SM22-3'-cre* for Zp3-cre. Deletion of *Drosha* was controlled with the primers *mDrosha-flox1* and *mDrosha-flox2* and *mDrosha-flox4* to amplify the wild type (300 bp) , lox-P site insertion (350 bp) and the deleted (510 bp) allele. The SIX1-Q177R and the DROSHA-E1147K line were tested with primers *R26F2*, *Rosa-rev* and *TK1* to amplify wild type (240 bp) and transgene (542 bp) fragments. Cre-mediated activation in SIX1-Q177R mice was documented with the primers *AG3*, *Q177-rev2* and *Q177-for1* to amplify the inactive (221 bp) or activated (333) allele. Activation for DROSHA-E1147K mice was controlled with the primers *AG3*, *GFP-real-rev* and *Q177-for1* to amplify the inactive (492 bp) or activated (362) allele. All used primers are listed in Table 10.

4.11 Preparation of mouse embryos and tissue

For preparation of mouse embryos or organs for further analysis like hematoxylin/ eosin staining, *in situ* hybridization or whole organ immunofluorescence the mice are mated overnight and the female mice are controlled for the vaginal plug the following day, which is stated as embryonal stage 0.5 (E0.5). In the presented work, whole embryos or organs between stage E11.5 - E18.5 were extracted. If the mice are born, the day of birth is marked as first day post birth (P1) and ongoing.

The pregnant mice or the adult mice were sacrificed. Afterwards, the mouse embryos or organs were dissected and washed in PBS. Next the tissue is fixed with 4 % PFA/ PBS. For organs that are dissected later than stage P14, the PBS and 4 % PFA/ PBS solutions are applied via syringe into the left ventricle of the heart to achieve maximal perfusion of the organ and to minimize the autofluorescence caused by erythrocytes. After fixation the embryos/ organs are washed with PBS (2x) and 0.9 % NaCl for 10 min each and dehydrated with an ascending isopropanol series (30 %, 50 %, 70 %, 85 %, 95 %, and 2x 100 %) for 30 min to 2 h each depending on the size of the fixated embryos/ organs. Subsequent to the dehydration, the embryos/ organs are incubated with isopropanol : chloroform (1:1) and transferred to the intermediate medium chloroform. For embedding, the embryos/ organs are incubated in chloroform : paraffin (1:1) in an open vessel for as long as the chloroform needs to evaporate. To make sure the embryos/ organs are properly infused, the paraffin solution is changed for three times. Afterwards, the embryos/ organs are embedded into paraffin blocks and kept at 4°C. 5 µm sections are cut with a microtome, stretched on a 42°C water bath and transferred to Superfrost™ plus slides. The slides are dried for 30 min at 42°C and can be stored afterwards again at 4°C. If used for *in situ* hybridization, all used solutions are prepared RNase free.

4.12 Hematoxylin and eosin staining

The widely used method for histological analysis of tissue samples is the hematoxylin and eosin staining (HE staining). The oxidation product of hematoxylin hemalum colors the nuclei of cells blue and the counterstaining with aqueous eosin colors eosinophilic structures like the cytoplasm and protein deposition in different shades of red, pink and orange.

The slides are deparaffinized with xylol 10 min (2x) and then hydrated with an descending ethanol series from >99 % (2x 3 min) to 50 % (every concentration is incubated for 3 min) ending in ddH_2O for 3 min. After hydration, the slides are stained in hemalum for 5-10 min and rinsed with ddH_2O. The slides are now placed under flowing tap water for 10 min and are rinsed again with ddH_2O. Subsequently, the slides are counterstained with eosin (0.1 %, aqueous) for 5-10 min. The slides are washed with ddH_2O for 3 min, followed by ascending ethanol series from 96 % to 100 % (5 min) and

finally the intermediate medium xylol (2 times for 5min). Next, the slides are embedded with the ready to use embedding medium Roti®-Histokitt.

4.13 *in situ* hybridization

The *in situ* hybridization is a sophisticated and established method to analyze timing and localization of gene expression patterns on tissue sections. Single strand RNA probes that are complementary to cellular mRNA are labeled by the integration of Digoxigenin labeled UTP through *in vitro* transcription. These Digoxigenin labeled UTP can be detected via immunohistochemical alkaline phosphatase linked antibodies and a subsequent color reaction.

Preserving RNA is a difficult task due to the presence of RNase enzymes on glassware, in reagents and on laboratory personnel and clothes. RNase is able to rapidly destroy RNA in the cell or the RNA probe itself. The use of sterile techniques, gloves, and solutions to prevent RNase contamination of the probes or tissue RNA is mandatory.

4.13.1 Preparation of Digoxigenin-labeled RNA probes

RNA probes of approximately 800 bases length exhibit the highest sensitivity and specificity, but the length of the probes can range from 250 to 1,500 bases. For correct preparation of antisense *in situ* RNA probes, the sequence or gene of interest has to be integrated into a plasmid vector with RNA polymerase binding sites such as T3, T7 or SP6 promotors. 10 µg of plasmid DNA is linearized with a suitable restriction enzyme to produce a 5' end with either a 5'-overlap or a blunt end and afterwards purified with Phenol and Chloroform : Isoamyl ethanol (24:1). The DNA precipitation is done with 1/10 volume 3 M NaOAc and 2.5 volume 100 % ethanol at -20°C and subsequently washed with 70 % ethanol. The DNA pellet is resuspended in 20 µl DEPC-H_2O. For the *in vitro* transcription 2 µg of linearized plasmid DNA is used:

2 µg	linearized plasmid DNA
2 µl	10x transcription buffer
2 µl	Digoxigenin-labeling mix
0.8 µl	RNase inhibitor
1.2 µl	RNA polymerase
ad to 20 µl	DEPC-H_2O

The transcription reaction is incubated for 2 h at 37°C. Afterwards, 1 µl of DNAseI is added and the reaction is incubated for another 15 min at 37°C. A formaldehyde agarose gel with 2 µl of the transcription reaction is run for integrity control of the RNA probe. The RNA is precipitated with 7 µl 7.5 M NH_4OAc and 75 µl >99 % ethanol either at -80°C for 30 min or -20°C overnight and after that washed with 70 % ethanol. The pellet is resuspended in 100 µl DEPC-H_2O and diluted with 500-900 µl of hybridization mix (1:5 - 1:10) depending on the thickness of the band shown by the formaldehyde agarose gel. The ready to use probe can be stored at -20°C.

4.13.2 *in situ* staining of paraffin slides

5 µm sections of designated tissue are transferred to Superfrost™ plus slides and placed for 30 min at 68°C in the incubator to melt the paraffin. After melting, the remaining paraffin is removed by a 2 times 10 min washing step with chloroform. Rehydration is achieved with a descending alcohol series, starting with two times 5 min of >99 % Ethanol (95 %, 90 %, 80 %, 70 %, 50 %, 30 %) and ending with two times 5 min PBS. The slides are now fixed again with 4 % PFA/ PBS and washed with PBS twice for 5 min. Then the slides are treated with 10 µg/ ml Proteinase K for 10 min and after a 5 min washing step with PBS again fixed with 4 % PFA for 30 min. Further washing with two times 5 min PBS, two times 5 min 2x SSC and two times 15 min Tris/ Glycine buffer is carried out. The slides are placed into Heraeus QuadriPERM boxes. Then 60 µl of denaturized RNA-probe (1:100 diluted in hybridization mix) is pipetted on the tissue carrying side of the slides and they are covered with Parafilm® M. Hybridization takes place at 70°C overnight. The following day, the slides are washed three times with 5x SSC for 20 min and afterwards with preheated 0.5x SSC/ 20 % Formamide at 60°C for 40 min. The 0.5x SSC/ 20 % Formamide is changed and cooled down to 37°C for 15 min. Next, the slides are incubated for 15 min at 37°C in NTE, 30 min in 10 µg/ ml RNase A/ NTE and 15 min NTE. All three incubation steps are done at 37°C, followed by a 30 min washing step with 0.5x SSC/ 20 % Formamide at 60°C and an additional step at RT with 2x SSC for 30 min. The slides are now blocked for 1 h with MABT/ 1 % blocking reagent at RT. The α-Digoxigenin-AP is diluted 1:5000 in MABT/ 1 % blocking reagent, pipetted on the slides and incubated at 4°C overnight. Before staining, the slides are washed four times for 10 min, three times for 20 min with TBST, twice for10 min with NTMT and one time with NTMT/ 2 mM Levamisole. The BM purple AP substrate is centrifuged for 5 min at 3000 rpm to remove insoluble particles, 0.1 % Tween-20 and 2 mM Levamisole are added and the slides are incubated in the dark for several days to achieve adequate staining. Finally, the slides are washed twice with NTMT for 15 min, once more with PBS and then embedded in Kaiser's glycerol gelatine.

4.14 Immunofluorescence staining

4.14.1 Indirect immunofluorescence staining of paraffin sections

The slides containing the 5 µm tissue sections are deparaffinized with Xylol for 5 min (2x) and then hydrated with a descending alcohol series from 100 % to 70 % (each step for 3 min). To mask disturbing tissue autofluorescence, the slides are incubated with 2-4 drops of Maxblock™ reagent A for 5 min and washed with 50 % ethanol via dipping. Furthermore, the slides are washed with H_2O for 5 min and PBS for 5 min (3x). The slides are transferred to a coplin jar for antigen retrieval. The coplin jar is filled with freshly prepared 10 mM sodium citrate buffer and incubated in the microwave for 2 min at 1000 W and 25 min at 300-500 W. After a cool down period of 20 min at RT, the slides are washed three times with PBST (PBS + 0.05 % Tween-20) for 5 min and blocked with 3 % BSA in PBST for 1 h. The

primary antibody is diluted 1:200 in 3 % BSA/ PBST (dilution may change depending on the antibody) and each slide is incubated with 200 µl antibody solution in a moist compartment overnight. The following day, the slides are washed three times with PBST and incubated with the secondary antibody (1:200 in 3 % BSA/ PBST) for 1 h. After an additional washing step PBST (3x) and H_2O, the slides are incubated with 2-4 drops of Maxblock™ reagent B for 5 min and then washed three times with H_2O. Staining of the nuclei is achieved by a 5 min incubation with Hoechst (1:10,000 in PBS). After two washing steps with PBST, the slides can be embedded with 2-4 drops of Mowiol. The slides should not be extensively exposed to light and the analysis via fluorescence microscopy should be done within the following two weeks for satisfying staining results.

4.14.2 Whole kidney tissue quantification

Whole embryos at stage E13.5 or kidneys of stage E16.5 embryos are dissected and further processed as stated in the *iDISCO* protocol (Renier et al. 2014). In this work methanol is used for dehydration of whole embryos or whole organs.

Image-stacks of cleared kidney samples are acquired in a home-built scanning light-sheet fluorescence microscope (laser excitation: 488 nm) similar to previous designs (Keller et al. 2008) and controlled by IQ 2.9 software (Andor, UK). Samples are mounted in a square boro-silicate glass capillary (3.0 mm, CM Scientific, United Kingdom) filled with *iDISCO* medium (Renier et al. 2014). The autofluorescence signal of the sample is detected by a 5X/0.15 objective (HCX PL FLUOTAR, Leica, Germany) using a 525/50 emission filter (Brightline HC, Semrock, Rochester, NY , USA) and a sCMOS camera Neo 5.5 (2560 x 2160 pixels, 16.6 mm x 14.0 mm sensor size, 6.5 µm pixel size, Andor). Image Stacks (2560*2160 pixels; Voxel dimensions xyz 1.3*1.3*2 µm) are saved as 16-bit TIFF-file sequence for further processing and analysis.

4.14.3 Image analysis

Kidney structures were derived from light-sheet images by using the pixel classification algorithm of the well-established interactive learning and segmentation toolkit ilastik ver. 1.2.0. (Sommer et al. 2011). Training was performed and output assessed for each sample individually. Four classes were defined: tubular structures, dense tissue, loose tissue, and ductal structures. Classification output was exported from ilastik to Imaris 8.3.1 (Bitplane, Zurich, Switzerland) for segmentation. Iso-surfaces of individual classes were generated, artefacts filtered (by volume, position, shape), statistical parameters extracted and exported from Imaris for further analysis to Microsoft Excel (Microsoft Corporation, Redmond, WA, USA). The image analyses were carried out by Oguzhan Angay (Rudolf Virchow Center, Research Center for Experimental Biomedicine, University of Würzburg, 97078 Würzburg, Germany).

5 Results

The general framework of the results section was structured as followed (Figure 11): First, I created ES cell lines via RMCE (4.9) harboring either an activatable lox-stop-lox shielded transgene for *DROSHA-E1147K* or *SIX1-Q177R*, the two most prevalent mutations, identified by the WT screens (2.3). The correct integration was controlled via PCR (4.9.3) (recombination efficiency: 12.5%) and positive ES cells were injected into C57BL/6 mouse blastocysts. To generate mice with a germline transition, the chimeric mice were mated again with C57BL/6 mice. Germline transition was controlled via PCR (4.10 and Table 10). These transgenic mice were intercrossed with promotor driven cre-expression mouse lines specific for blastemal cells such as Six2-cre and Wt1-cre^{ERT2} (3.8), to achieve a kidney specific activation of the transgenes. For further global activation of SIX1-Q177R, the mice were intercrossed with Zp3 promotor driven cre-recombinase mice. Since the tumor screen proposed a dominant-negative effect for the *DROSHA-E1147K*, I wanted to analyze the effects of a complete knockout of DROSHA in the progress of kidney development. Therefore, mice with a *Drosha* allele, harboring a floxed exon 9 (*Drosha*^{tm1Litt}) (Chong et al. 2008), were used (3.8), to achieve a cre-driven inactivation of *DROSHA*. This inactivation was again driven by the *Six2* and *Wt1* promotors. The three different mouse models were phenotyped at various stages of kidney development. Finally, I created compound mutants of either both transgenes *DROSHA-E1147K* and *SIX1-Q177R* or mice with *Drosha* alleles, harboring a floxed exon 9, and *SIX1-Q177R*. Both mouse lines were intercrossed with Six2-cre mice. With the help of these new compound mutants, the proposed synergetic effect of *DROSHA* and *SIX1* mutations could be investigated.

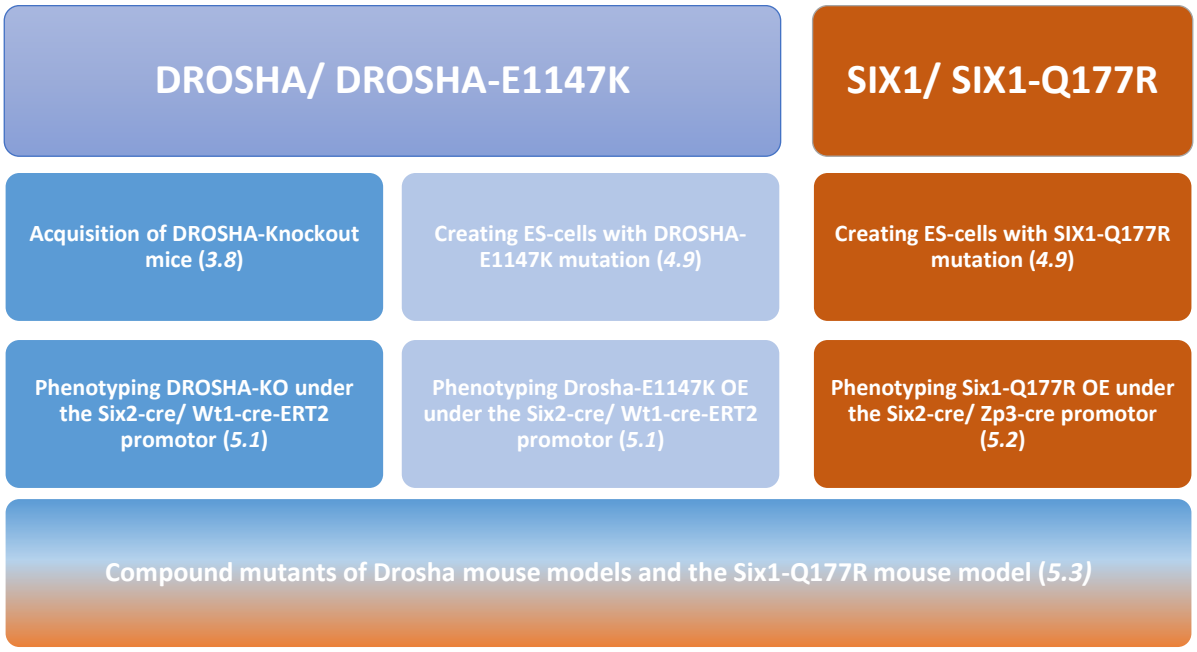

Figure 11: Schematic overview of the results
Corresponding chapters are given in brackets.

5.1 Phenotyping of DROSHA mice models

5.1.1 Expression analysis of conditional *Drosha* knockout in blastemal cells

To test if reduced *Drosha* activity can induce WT, I generated mice with inactivation of one or both alleles of *Drosha* in the condensing metanephric mesenchyme as the origin of most nephron cell types like glomeruli and tubular structures. *Drosha* inactivation was achieved by intercrossing mice with a *Drosha* allele, harboring a floxed exon 9 (*Drosha*^{tm1Litt}), and a *Six2* promoter driven EGFP-cre allele (Six2-cre; *Tg(Six2-EGFP/cre)1Amc/J*). The *Six2* promotor is active in a restricted time window during differentiation of blastemal cells and by that homozygous Drosha$^{\Delta Six2c/\Delta Six2c}$ embryos should show a downregulation of DROSHA protein in condensing metanephric blastema and its derivatives. A clear reduction in *Drosha* expression could be confirmed by immunohistochemistry as well as qRT-PCR (Figure 12 B). The Immunofluorescence staining of DROSHA presented a strong reduction of signal mainly in the blastemal regions of the embryonal kidneys at stage E16.5, but also revealed a remaining expression in tissue that is not derived from the metanephric mesenchyme (Figure 12 B). With this reduction of DROSHA protein, the processing of canonical miRNAs should also be deficient. Therefore, kidneys of mouse embryos at stage E16.5 were analyzed for expression of the canonical miRNAs mir-196a, mir-126 and mir-10b. The expression levels of non-canonical miRNA mir-320 should not be affected by deficiency of the microprocessor complex. Therefore, mir-320 was used to normalize the samples. The expression levels were compared to the expression of littermates with only heterozygous inactivation of *Drosha* (Drosha$^{wt/\Delta Six2c}$). The results of the miRNA expression analysis showed a significant downregulation of all tested canonical miRNAs in Drosha$^{\Delta Six2c/\Delta Six2c}$ kidneys compared to the Drosha$^{wt/\Delta Six2c}$ embryos (Figure 12 A) (2way ANOVA p-values: Interaction: <0.0001 Column factor: <0.0001 Row factor: 0.0001).

Conditional inactivation of only one *Drosha* allele (Drosha$^{\Delta Six2c/wt}$) did not produce obvious alterations, consistent with normal development and fertility of heterozygously deleted mice. The analysis of miRNA levels showed a comparable expression to wild type controls (Figure 12 A). Leading to the conclusion that heterozygous deletion of *Drosha* is phenotypically similar to wild type littermates and heterozygous expression of *Drosha* is sufficient to allow normal microprocessor activity.

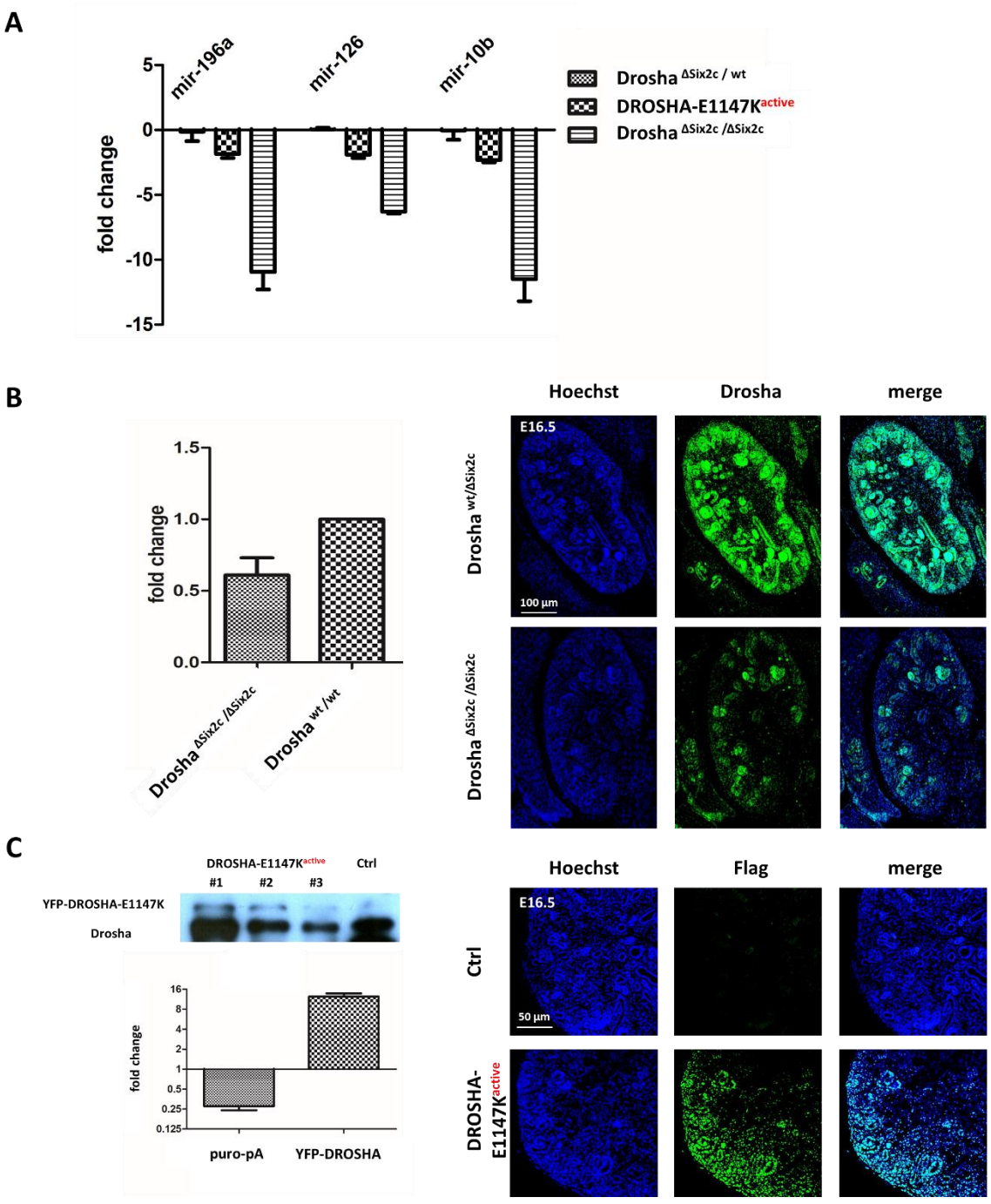

Figure 12: Expression analysis of Drosha$^{\Delta Six2c/\Delta Six2c}$ and DROSHA-E1147K^{active}

(**A**) qPCR of selected canonical miRNAs mir-196a, mir-126 and mir-10b in E16.5 kidneys to show downregulation in Drosha$^{\Delta Six2c/\Delta Six2c}$ and DROSHA-E1147K^{active} mice (5.1.5) and normal processing in Drosha$^{wt/\Delta Six2c}$ mice. The expression levels are normalized to the non-canonical miRNA mir-320 and Drosha$^{wt/\Delta Six2c}$ littermates. (**B**) qPCR to show reduction of Drosha expression in E16.5 in KO kidneys. IF staining against DROSHA to show loss of endogenous DROSHA protein in the metanephric blastema. (**C**) Western Blot and qPCR analysis of DROSHA-E1147K^{active} vs. controls at E16.5. IF staining against flag-tag to show expression of DROSHA-E1147K protein in the metanephric blastema.

5.1.2 Homozygous *Drosha* knockout leads to impairment of nephrogenesis

At embryonic stage E13.5 normal uretic tip branching could be observed and the mesenchymal condensation was comparable between Drosha$^{\Delta Six2c/\Delta Six2c}$ embryos and control littermates (Drosha$^{flox/flox,}$ Drosha$^{wt/flox}$ or Drosha$^{wt/\Delta Six2c}$). Also, renal vesicles in Drosha$^{\Delta Six2c/\Delta Six2c}$ embryos could clearly be identified, histological sectioning revealed a reduction in the number of S-shaped bodies (Figure 13 A).

At E16.5 maturing structures like comma-, S- shaped bodies or mature glomeruli were further reduced in the cortical region and the medulla, while remaining comma- and S- shaped bodies appeared immature and exhibited more densely packed cells compared to controls (Figure 13 B). A quantification of glomeruli numbers of vertically sliced whole E16.5 kidneys showed a significant reduction between Drosha$^{\Delta Six2c/\Delta Six2c}$ and control littermates (6 versus 30.8 glomeruli per mm^2 in controls; p-value < 0.0001) (Figure 13 C).

At stage E18.5 no matured glomeruli were present in Drosha$^{\Delta Six2c/\Delta Six2c}$ kidneys (Figure 13 D). The centrally located glomeruli, which should be more mature, appeared densely packed, respectively clogged and thus likely non-functional.

The newborn Drosha$^{\Delta Six2c/\Delta Six2c}$ mice could easily be distinguished from wild type littermates. They did not react to stimuli and seemed quite lethargic. Further, they showed extensive gasping and suffered from cyanosis. A sign for reduced activity was also the visibly smaller milk spot compared to controls. The Drosha$^{\Delta Six2c/\Delta Six2c}$ mice died within hours after birth with terminal heart failure and pulmonary edema. The kidneys of newborn Drosha$^{\Delta Six2c/\Delta Six2c}$ mice were much smaller (Figure 13 C) and characterized by complete absence of mature glomeruli, reduced tubular structures (black arrow), cystic dilatation of tubuli (arrowheads) and a strong increase in stromal tissue compared to controls.

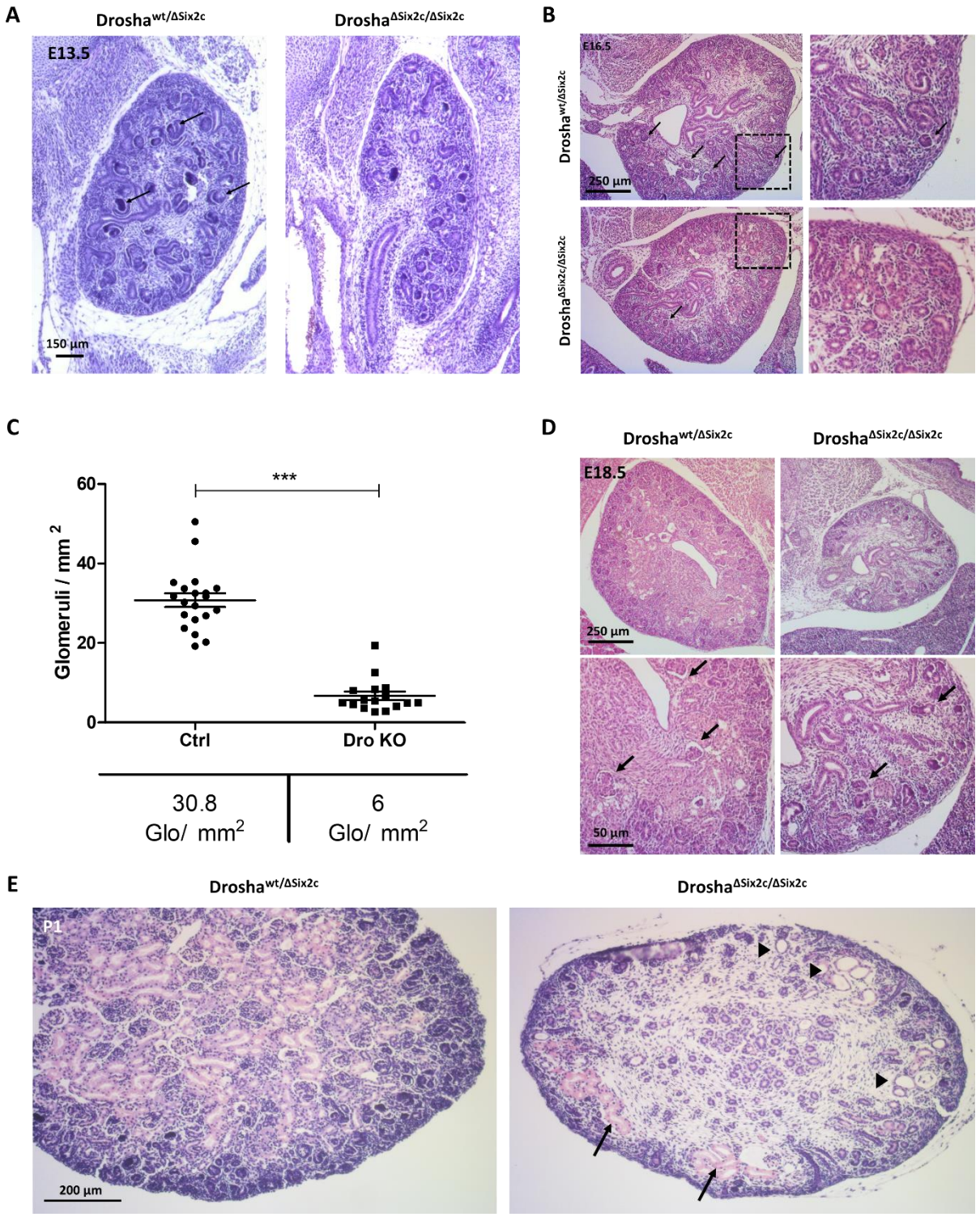

Figure 13: Histological analysis of Drosha KO under the Six2cre-eGFP promotor

(**A**) HE staining of Drosha$^{\Delta Six2c/\Delta Six2c}$ mice at stage E13.5. Arrows indicate S-shaped-bodies Drosha$^{wt/\Delta Six2c}$ mice. (**B**) HE staining of Drosha$^{\Delta Six2c/\Delta Six2c}$ mice at stage E16.5. Arrows mark matured Glomeruli. Arrowhead marks S-shaped-body. (**C**) Quantification of Glomeruli numbers in E16.5 Drosha$^{\Delta Six2c/\Delta Six2c}$ compared to control littermates. (**D**) HE staining of Drosha$^{\Delta Six2c/\Delta Six2c}$ mice at stage E18.5. Arrows indicate location of normal matured glomeruli in Drosha$^{wt/\Delta Six2c}$ mice and malformed glomerular structures in Drosha$^{\Delta Six2c/\Delta Six2c}$ mice. (**E**) HE staining of Drosha$^{\Delta Six2c/\Delta Six2c}$ mice at stage P1. Arrows indicate residual tubular tissue and arrow heads indicate dilated tubules.

5.1.3 Marker analysis of Drosha$^{\Delta Six2c/\Delta Six2c}$ embryos

In situ hybridization of *Cited1*, *Six2* and *Wt1* revealed a correctly established nephrogenic zone with intact cap mesenchyme in E13.5 Drosha$^{\Delta Six2c/\Delta Six2c}$ embryos with expression of all markers in a comparable level and pattern as in control littermates (Figure 14 A). *Wnt4* staining as a marker for epithelization was present, but a stronger *Wt1* staining in the more central glomerular precursors was missing in the Drosha$^{\Delta Six2c/\Delta Six2c}$ kidneys (Figure 14 A, black arrows). Analysis of E16.5 mutant embryos with the same markers revealed an alteration of kidney development on different levels. The nephrogenic zone in the cortex of the kidney with high expression of *Six2* appeared thinner and discontinuous. This effect is yet further evidence of an adequate Six2-cre mediated deletion of *Drosha*. Some blastemal cells of the cortical nephrogenic zone were lacking *Six2* completely. Additionally, *Cited1* expression seemed to be lost completely (Figure 14 A). The epithelialization marker *Wnt4* was infrequently expressed and especially *Wt1* expression was much weaker in the blastemal compartment and limited to fewer regions of maturing glomerular precursors in the center in contrast to controls. Even with these limitations kidney development seemed to proceed, but at a reduced level. Nephrin-positive structures could be found. Yet, their morphology did not resemble glomeruli and their cellular structure seemed to be disarranged (Figure 14 B). GFP positive structures, as a sign for expression of the Six2 driven EGFP/cre transgene, could be found outside the nephrogenic zone in KO kidneys. This might be a hint for incomplete differentiation or reactivation of a progenitor cell program at a later time point.

Drosha$^{Six2c/Six2c}$ kidneys were smaller compared to controls (Figure 13). The cause of this effect could be a reduction of proliferation with depletion of precursors or increased apoptotic cell loss. Staining with the proliferation marker Ki-67 did not show a clear difference in proliferation in mutant and control embryos. Yet, the proliferation zone seemed to be thinner and fewer Ki-67 positive condensed structures like comma- and S-shaped bodies could be found (Figure 14 C, white arrows). To check for increased apoptosis, kidneys were stained for the presence of the apoptotic marker cleaved Caspase 3 (cCasp3) (Figure 14 D). A striking increase in apoptosis could be detected especially in the cortical region along with more central regions that contain mesenchymal and epithelial but not stromal cells. This is a strong sign that along with ongoing differentiation a significant number of cells were lost due to apoptosis. If this apoptosis is too severe, the embryo could suffer from kidney agenesis. Indeed, 36% of the E16.5 Drosha$^{Six2c/Six2c}$ embryos showed loss of at least one kidney (n=11) (Figure 14 E).

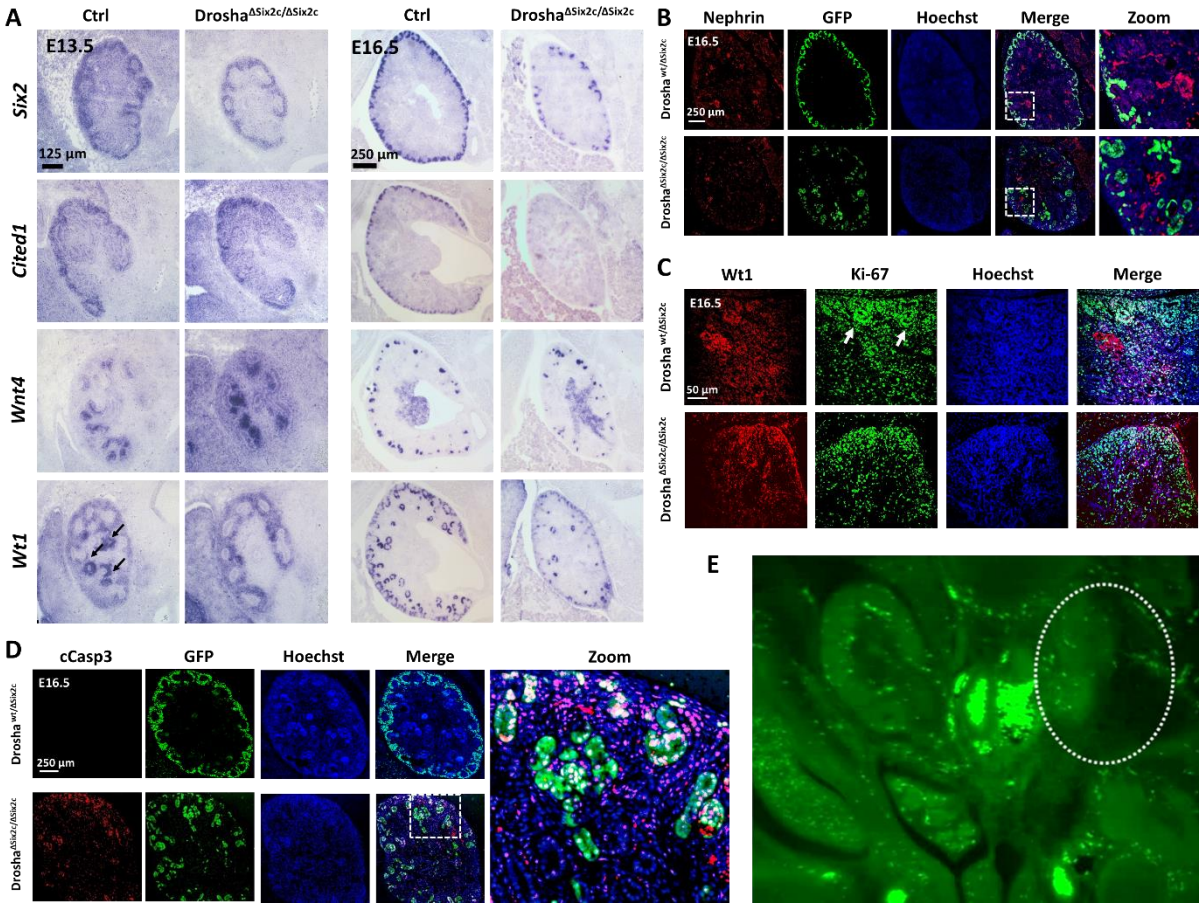

Figure 14: Marker analysis of Drosha$^{\Delta Six2c/\Delta Six2c}$ embryos

(**A**) *in situ* hybridization of E13.5 and E16.5 kidneys with riboprobes to detect progenitor markers: *Six2*, *Cited1*, *Wt1* and *Wnt4*. Arrows indicate *Wt1* staining in central regions of the kidney. (**B**) Immunofluorescent staining against nephrin to label the glomerular structures and GFP to label *Six2* expressing cells of the nephrogenic zone. (**C**) Immunofluorescent staining against the progenitor marker WT1 and the proliferation marker Ki-67. Arrows indicate comma- and S-shaped bodies. (**D**) Immunofluorescent staining against GFP and the apoptosis marker cCasp3. (**E**) Autofluorescence image of Drosha$^{\Delta Six2c/\Delta Six2c}$ mice at stage E16.5 shows unilateral kidney agenesis.

5.1.4 Conditional knockout of *Drosha* in podocyte precursors

Due to the perinatal lethality of Drosha$^{\Delta Six2c/\Delta Six2c}$ mice, the strong reduction of precursor cells, reduced kidney size and partial kidney agenesis, development of WT-like lesion at postnatal stages was not achievable. Hence, a tamoxifen-inducible deletion of *Drosha* in only a fraction of the developing kidney would allow partial kidney development and may lead to WT. The Wt1-driven cre^{ERT2} transgene (*Wt1*$^{tm2(cre/ERT2)Wtp}$) shows weaker activity in uninduced kidney mesenchyme but a stronger expression in glomerular and podocyte precursors. The promotor is tamoxifen inducible and a single prenatal bolus is sufficient for transgene recombination. The fraction of non-recombined cells were expected to rescue kidney function and lead to postnatal survival.

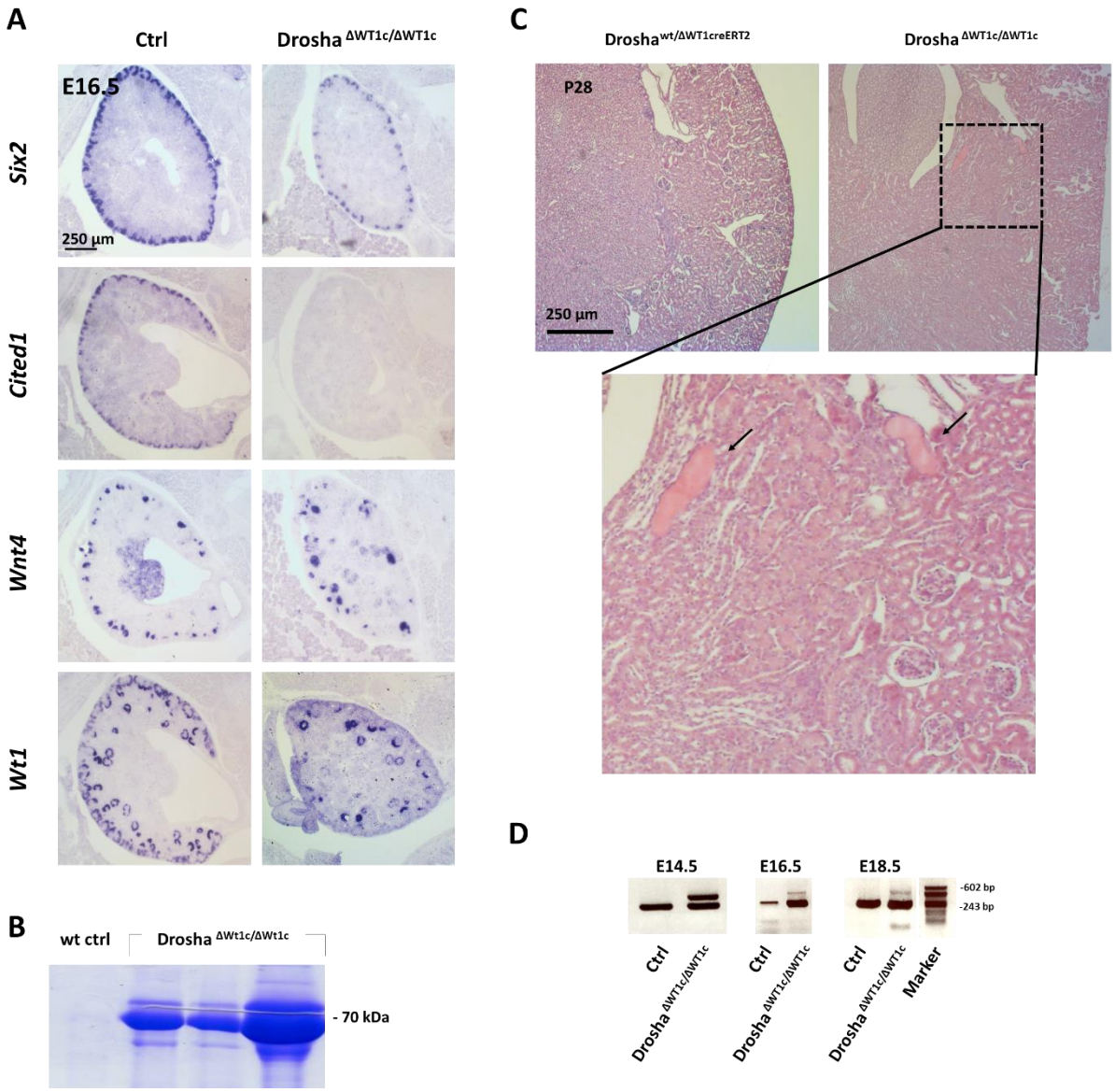

Figure 15: Inducible KO of DROSHA in podocytes precursors

(**A**) *in situ* hybridization of E16.5 kidneys with the same riboprobes. (**B**) SDS-PAGE, stained with Coomassie brilliant blue, of P28 Drosha$^{\Delta WT1c/\Delta WT1c}$ mouse urine shows high albumin content compared to wild type controls. (**C**) HE staining of P28 control and Drosha$^{\Delta WT1c/\Delta WT1c}$ mice. Arrows indicate protein cylinders in collection tubules. (**D**) PCR analysis of tamoxifen treated embryonal kidneys at stage E14.5, E16.5 and E18.5.

After tamoxifen treatment at E12.5, Drosha$^{\Delta Wt1/\Delta Wt1}$ embryos developed the same disruption of the nephrogenic zone compared to Drosha$^{\Delta Six2c/\Delta Six2c}$ embryos, but in a less dramatic manner (Figure 15 A). *Cited1* staining was again missing, but in contrast to Drosha$^{\Delta Six2c/\Delta Six2c}$ *Six2* cap mesenchyme staining showed less reduction. The number of *Wnt4* positive structures as well as fully developed glomeruli at stage E16.5 were higher. Drosha$^{\Delta Wt1/\Delta Wt1}$ mice were in fact viable and developed normal sized kidneys, but suffered from proteinuria starting between day 14 and 28 after birth (stage P14 and P28). As a result of this proteinuria, albumin could be detected in urine by SDS PAGE. HE staining of kidney slides revealed that Drosha$^{\Delta Wt1/\Delta Wt1}$ mice had protein deposits in kidney tubules. The protein deposits were

mainly located in the medulla and the inner cortex (Figure 15 B and C). Nevertheless, this defect seemed to be compensated by the remaining functional kidney tissue, likely derived from non-deleted cells. Accordingly, PCR analysis of tamoxifen treated embryonal kidneys showed that the levels of cells with deletions of Drosha decreased from E13.5 to E18.5 (Figure 15 D). The mice live up to at least 6 months without further impairment or any evidence of kidney tumor formation.

5.1.5 Kidney development is impaired by activation of DROSHA-E1147K

The heterozygous, dominant-negative *DROSHA* alleles seen in human WT likely induce a partial but critical reduction of miRNA species yet did not lead to complete absence as seen in Drosha$^{\Delta Six2c/\Delta Six2c}$ mice. As a way to investigate this predicted dominant effect of the E1147K mutation, I generated a mouse line with an activatable, lox-stop-lox shielded *DROSHA-E1147K* transgene (Figure 16 A). The principal is the same as used in the *Drosha* floxed mouse line, with the difference that this transgene can be switched on by Six2-cre through deletion of the floxed puro-polyA stop cassette with subsequent transcription of the YFP-DROSHA-E1147K fusion protein driven by a CAG promotor (Figure 12 C). Indeed, the predicted reduction of miRNA species in embryonal kidneys could be confirmed with the help of the two-tailed qPCR (Figure 12 A). The level of reduction is still lower than seen in the Drosha$^{\Delta Six2c/\Delta Six2c}$ kidneys, but significantly higher compared to control or Drosha$^{\Delta Six2c/wt}$.

Embryos with activated *DROSHA-E1147K* (DROSHA-E1147K^{active}) developed the same disruption of the nephrogenic zone as Drosha$^{\Delta Six2c/\Delta Six2c}$ mice at E16.5 with reduced and patchy *Six2* expression. Also, the lack of *Cited1* and an early loss of *Wt1* staining in the center of the kidneys were present (Figure 16 B). But none of these deviations were seen at stage E13.5. The degree of impairment seemed to be lower compared to the KO situation since *Wnt4*-positive structures were still present in high numbers at E13.5 but were clearly reduced at stage E16.5. Compared to the control the DROSHA-E1147K^{active} kidneys showed reduced Ki-67 staining. At stage E16.5 it was weaker overall, especially in epithelial cells derived from the nephrogenic zone, but the thickness of the proliferation area in the cortical nephrogenic zone stayed unchanged (Figure 16 C). Analysis of apoptosis by cCasp3 staining revealed apoptosis not only in the nephrogenic zone, but additionally in epithelial cells within the cortex (Figure 16 D). Still, nephrin-positive structures that morphologically resembled functional and intact glomeruli of controls could be detected (Figure 16 E). Nevertheless, like the KO mice, the DROSHA-E1147K^{active} mice also suffered from kidney agenesis. 23% of the E16.5 DROSHA-E1147K^{active} embryos lost at least one kidney at (n=13).

In comparison to Drosha$^{\Delta Six2c/\Delta Six2c}$, mice with an activated *DROSHA-E1147K* transgene were viable. However, they developed proteinuria after birth, similar to Drosha$^{\Delta Wt1c/\Delta Wt1c}$ mice. Yet, the proteinuria was more severe with a higher number of protein deposits throughout the kidneys (Figure 17 A). To check if the activated transgene also had an impact on tubular maturation, *in situ* hybridization for

tubular segment markers like *Uromodulin* and *LAP3* was used. The result was a strong reduction of these markers in P28 kidneys, speaking for loss or reduction of tubular tissue after birth (Figure 17 B).

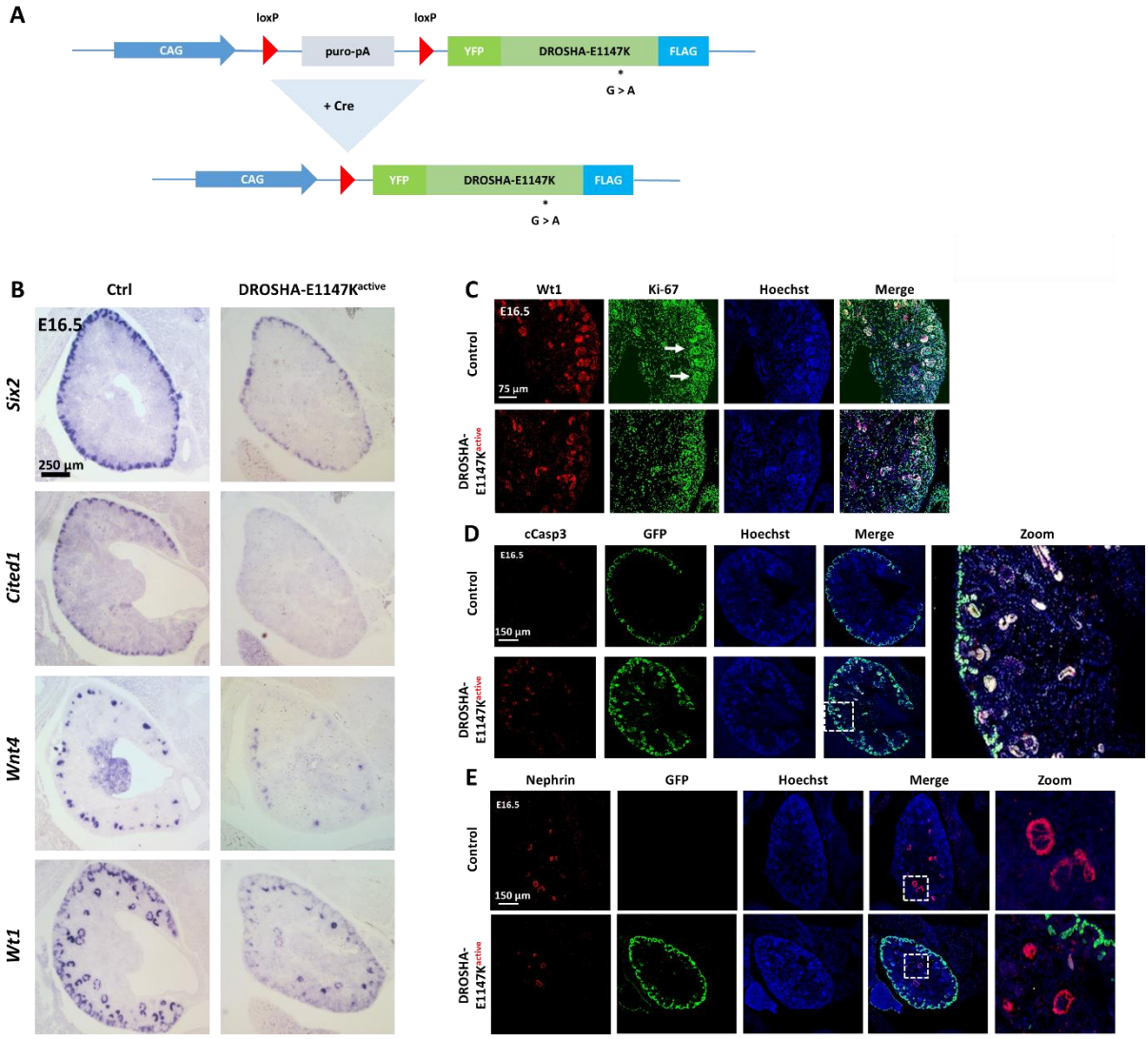

Figure 16: Prenatal development impairments

(**A**) Schematic overview of the DROSHA-E1147K mouse model. (**B**) *in situ* hybridization of E13.5 kidneys with riboprobes to detect progenitor markers: *Six2*, *Cited1*, *Wt1* and *Wnt4* (**C**) Immunofluorescent staining of E16.5 kidneys against WT1 and Ki-67. (**D**) Immunofluorescent staining against GFP and cCasp3 as an apoptotic marker. (**E**) Immunofluorescent staining against GFP and nephrin to label maturing glomeruli.

Apart from the proteinuria phenotype shared with Drosha$^{\Delta Wt1/\Delta Wt1}$ mice, DROSHA-E1147K^{active} mice displayed glomerulosclerosis after birth as a novel phenotype (Figure 17 A2). The number of sclerotic glomeruli increases over time (30% at P14 and >50% at P28; n=4 each). In addition, the sclerotic glomeruli showed positive staining for the fibrosis-marker *Tgfβ* and the blastemal proliferation marker *Six2* (Figure 17 C). Ongoing proliferation could be detected by staining for Ki-67 positive cells at P28, when control kidneys lack Ki-67 positive cells almost completely (Figure 17 D). In DROSHA-E1147K^{active} kidneys, sclerotic glomeruli in particular showed strong Ki-67 staining (Figure 17 D circle). Besides

ongoing proliferation, there was also continuing apoptosis indicated by increased cCasp3 staining (Figure 17 E). While in E16.5 kidneys nephrin staining seemed comparable to the control kidneys, in P28 nephrin staining of the sclerotic glomeruli was weaker and scattered, pointing to functional impairment (Figure 17 F). The glomeruli gave the impression of dilation and disorganization, while cells expressing the *Six2-cre* transgene, which was detected by the fused EGFP protein, were still present. The expression pattern of the *Six2-cre* transgene was highly comparable to the one of the *in situ* hybridization probe shown in Figure 17 C. In control kidneys at stage P28, expressing only the *Six2-cre* transgene but not the *DROSHA-E1147K* transgene, *Six2* expression could not be detected at all.

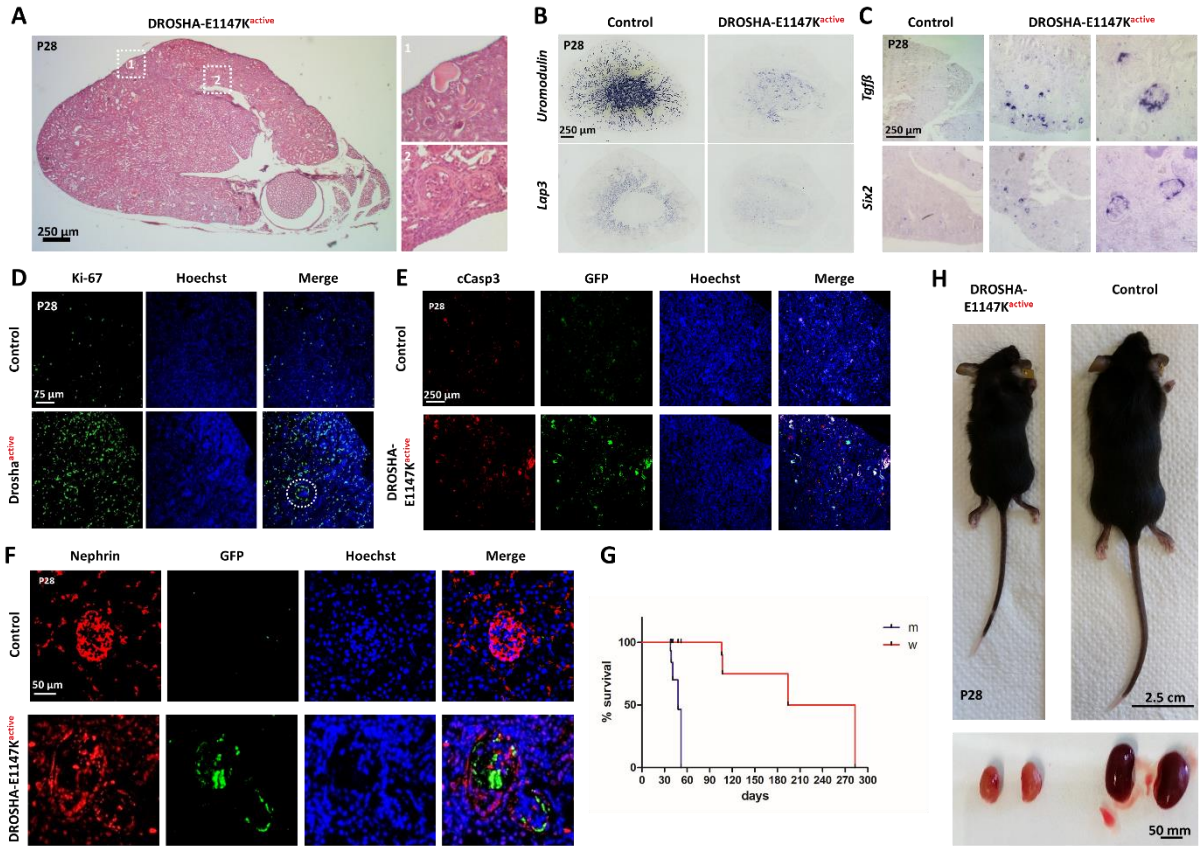

Figure 17: Postnatal developmental impairments

(**A**) HE staining of P28 DROSHA-E1147K^{active} kidneys showing severe proteinuria and glomerulosclerosis (Zoom). (**B**) *in situ* hybridization of P28 DROSHA-E1147K^{active} kidneys with the tubular markers *Uromodulin* and *LAP3*. (**C**) *in situ* hybridization shows expression of fibrosis marker *TGFß* and progenitor marker *Six2* in sclerotic glomeruli of DROSHA-E1147K^{active} kidneys. (**D**) Ki-67 staining shows ongoing proliferation in DROSHA-E1147K^{active} kidneys. (**E**) GFP and cCasp3 staining to reveal *Six2* promoter activity and apoptosis in P28 DROSHA-E1147K^{active} kidneys. (**F**) Immunofluorescent staining against nephrin to label mature glomeruli. DROSHA-E1147K^{active} glomeruli are malformed and still populated with SIX2 expressing (GFP positive) cells. (**G**) Kaplan-Meier curve showing the survival rate of male and female DROSHA-E1147K^{active} mice. (**H**) Growth retardation and reduced kidney size of DROSHA-E1147K^{active} mice in comparison to wild type littermates.

DROSHA-E1147K^{active} life expectancy was reduced and a gender difference could be seen (Figure 17 G). While the monitored male mice had a median survival of 48 days, the female mice had a median survival rate of 238.5 days. The results for DROSHA-E1147K^{active} mice shown in Figure 17 were all based

on male mice. I analyzed female mice in the same way and got exactly the same phenotype, but with a delayed onset. Regardless of gender, DROSHA-E1147K^{active} mice exhibited severe growth retardation and strikingly reduced kidney size (Figure 17 H). However, none of the dissected kidneys showed any tumor formation.

5.1.6 3D analysis of kidney development

Drosha$^{\Delta Six2c/\Delta Six2c}$ kidneys lacked glomeruli and displayed a strong increase of stromal tissue, while the overall kidney volume seemed to be decreased. I investigated how the tissue distribution inside the kidney was affected by impaired miRNA biogenesis in the nephrogenic zone. Furthermore, I wanted to know if the volume reduction and increase of stromal tissue seen in KO kidneys, could also be detected in DROSHA-E1147K^{active} kidneys.

Therefore whole kidneys from E16.5 embryos were dissected and treated according to the *iDisco* clearing protocol. Afterwards, the kidneys were analyzed regarding their tissue composition by light sheet fluorescence microscopy (LSFM) and the autofluorescence data was used to construct 3D images of whole kidneys. This image analysis was carried out by Oguzhan Angay (AG Heinze, RVZ, University of Würzburg, Germany). With the help of *in silico* tissue classification using the image classification and segmentation software *Ilastik*, four different tissue types could be defined: tubular structures, ductal structures, loose tissue and dense tissue (Figure 18). The tubular structures appeared to be predominantly of mesenchymal origin, whereas the ductal structures were connected to the kidney pelvis and likely derived from the uretic bud (UB). The loose tissue component was mostly similar to stromal tissue and the dense tissue to epithelial components.

Tubular structures were completely absent in Drosha$^{\Delta Six2c/\Delta Six2c}$ kidneys and furthermore ductal structures were vastly reduced. In contrast loose tissue was highly enriched and dense tissue including the blastemal cortex was mostly thinner and partly fragmented. As expected from the previous results, DROSHA-E1147K^{active} kidneys displayed an intermediate picture with reduced tubular and ductal structures, while loose tissue was more abundant. The same reduction of tubular tissue with the staining of tubular markers at P28 shown for DROSHA-E1147K^{active} mice had been observed and these results were in line with the previous findings. In addition, I could confirm the already predicted reduction of kidney volume: Total kidney volume was reduced from 1.6 µl in controls to 0.6 µl in Drosha$^{Six2c/Six2c}$ embryos. Loose tissue increased from 8% to 23% of kidney volume. DROSHA-E1147K^{active} kidneys showed no volume reduction, but the same tendency towards increased loose tissue.

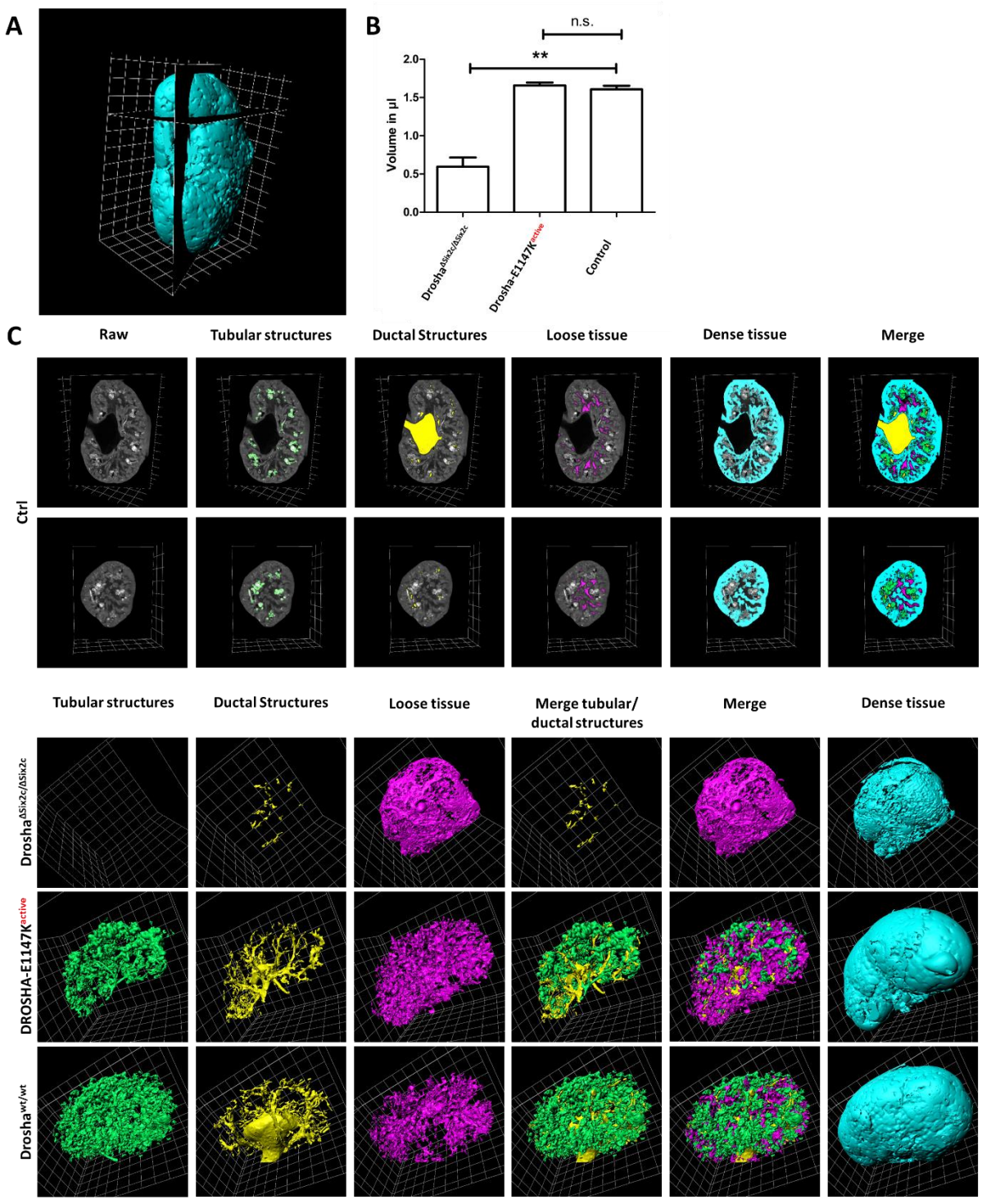

Figure 18: Whole tissue classification of DROSHA KO and DROSHA-E1147K OE kidneys

(**A**) Overview of vertical and horizontal planes of kidney samples. (**B**) Quantification of total kidney volume of Drosha$^{\Delta Six2c/\Delta Six2c}$, DROSHA-E1147K^{active} and controls at stage E16.5. (**C**) Classification results of tissue autofluorescence data analyzed and visualized with Imaris (*grid scale 200µm*). Top two rows: Ortho slice view of image stacks from control kidneys. Class label overlay on raw data. Lower rows: Iso-surface rendering of respective structures.

5.2 Phenotyping of SIX1-Q177R mutant mice

Apart from *Drosha-E1147K*, one of the most frequent somatic changes in WT discovered by the WT screens was the *SIX1-Q177R* mutation. I used a similar approach to *DROSHA-E1147K* as a model for tumorigenesis. Again, I generated mice with an activatable, lox-stop-lox shielded *SIX1-Q177R* transgene (Figure 19 A). As already described for the D*ROSHA-E1147K* transgene, the construct can be switched on by cre-recombinase through deletion of the floxed puro-polyA stop cassette with subsequent translation of SIX1-Q177R protein and an IRES dependent EGFP protein.

5.2.1 Conditional activation of SIX1-Q177R in metanephric blastema

The *Six2* promotor driven cre transgene was used to induce an activation of *SIX1-Q177R* in the condensing metanephric mesenchyme, to investigate if and how *SIX1-Q177R* influences nephrogenesis and kidney development. A successful activation of the transgene and the corresponding loss of puro could be detected via qRT-PCR (Figure 19 B). In contrast to the strong phenotype of *DROSHA-E1147K* mice, I could not detect major aberrations in the phenotype of mice with *SIX1-Q177R* activation.

At stage E16.5 the embryos with activated *SIX1-Q177R* (SIX1-Q177R^{active}) showed no difference in UB tip branching and the mesenchymal condensation seemed to proceed as in control littermates (Figure 19 C). I could clearly detect maturing structures from renal vesicles, comma- and S-shaped bodies to mature glomeruli (Figure 19 B, arrows). The investigation of glomeruli in E16.5 kidneys displayed a normal distribution of 25 – 32 glomeruli/ mm^2 in control and SIX1-Q177R^{active} embryos.

The SIX1-Q177R^{active} mice were viable at birth and had no further impairments in adult stages. At stage P28, I analyzed the kidneys and found fully functional glomeruli (Figure 19 D, arrows), which differed neither in number nor appearance compared to control littermates.

Marker analysis of SIX1-Q177R^{active} at stage E16.5 was in line with the earlier findings. *Six2* and *Cited1* expression displayed a normal condensation of the nephrogenic zone and the epithelialization marked by *Wnt4* was comparable to control littermates. As expected from the histological results, *Wt1* staining presented a normal maturation of glomeruli with staining in the blastemal compartment and in more central regions of the kidney.

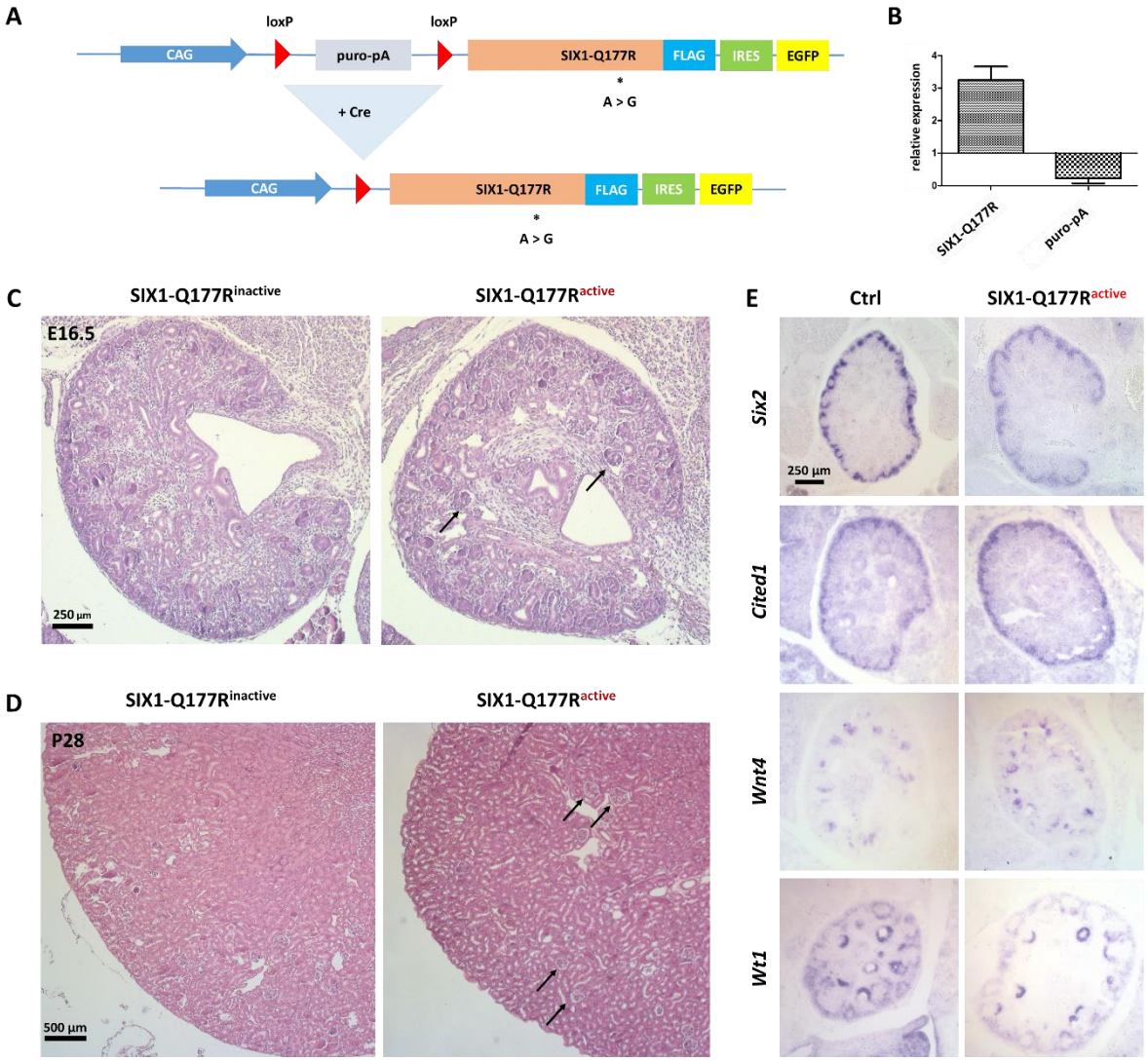

Figure 19: No kidney impairments after SIX1-Q177R activation in metanephric blastema

(**A**) Schematic overview of the SIX1-Q177R mouse model. (**B**) Relative expression of SIX1-Q177R^{active} normalized on control (ctrl = 1) littermates at E16.5. (**C**) HE staining of control and SIX1-Q177R^{active} mice at stage E16.5. Arrows indicate the location of mature glomeruli in SIX1-Q177R^{active} mice. (**D**) HE staining of control and SIX1-Q177R^{active} mice at stage P28. Arrows indicate the location of mature glomeruli in SIX1-Q177R^{active} mice. (**E**) *in situ* hybridization of E16.5 kidneys with riboprobes to detect progenitor markers: *Six2*, *Cited1*, *Wt1* and *Wnt4*.

5.2.2 Global activation of SIX1-Q177R

Because the activation of *SIX1-Q177R* did not have a major impact on kidney development, the mice harboring the *SIX1-Q177R* transgene were intercrossed with the Zp3 promotor driven cre-recombinase mouse line (Zp3-cre; *C57BL/6-Tg(Zp3-cre)93Knw/J*). This leads to an expression of the cre-recombinase in oocytes and a global activation of *SIX1-Q177R* in the embryo respectively. qRT-PCR presented a strong activation of human *SIX1-Q177R* and the associated *EGFP*. Again, downregulation of puro could be detected (Figure 20 A).

At stages E13.5, E16.5 and E18.5 no obvious phenotypic alterations were present. Transition from renal vesicles to mature glomeruli were consistent with normal development, furthermore glomeruli numbers did not change compared to control littermates.

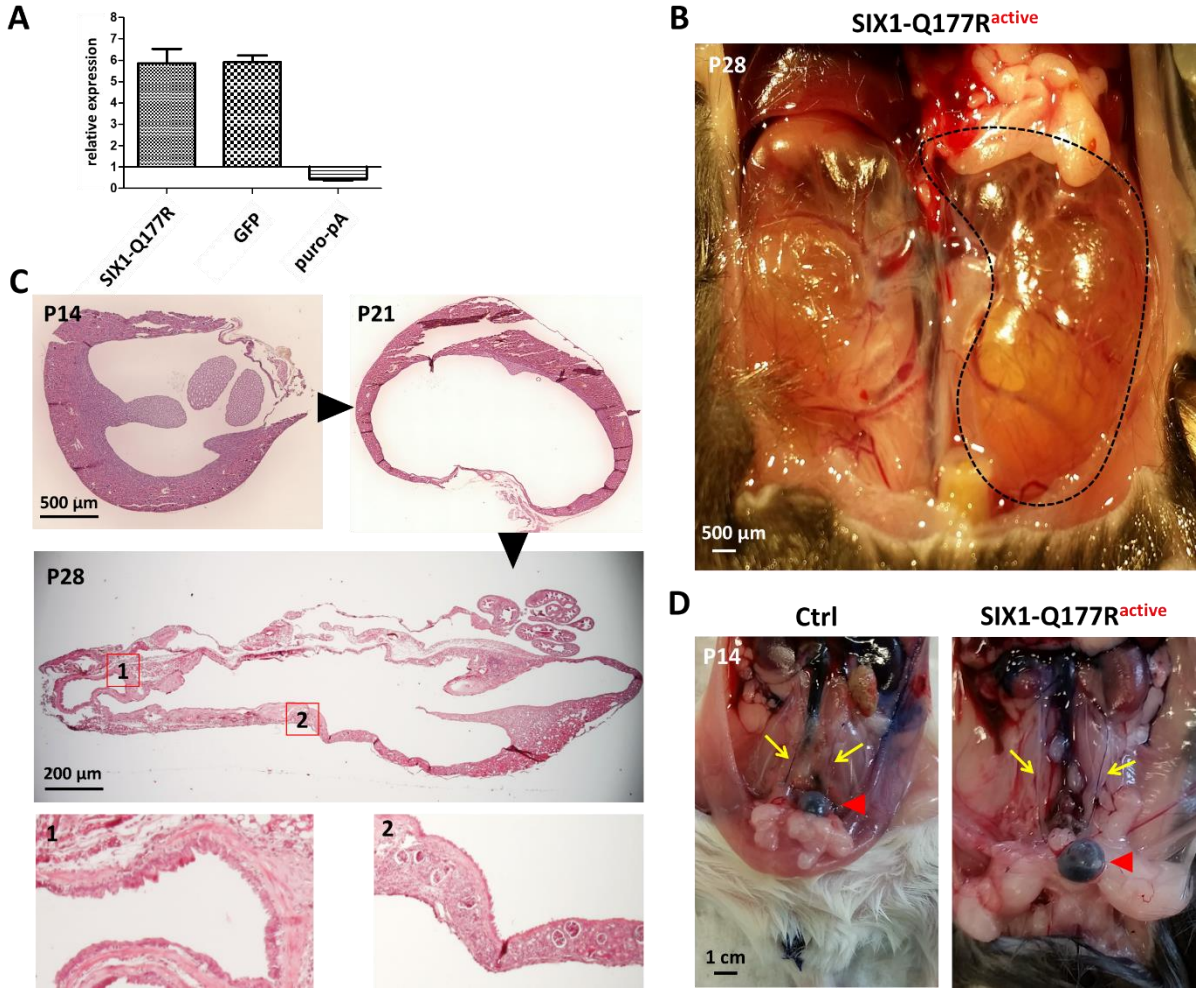

Figure 20: Global activation of SIX1-Q1177R leads to hydronephrosis

(**A**) Relative expression of SIX1-Q177R^{active} normalized on control littermates (ctrl = 1) at E16.5. (**B**) Bilateral hydronephrosis in juvenile mice at stage P28 (**C**) HE staining of SIX1-Q177R^{active} mice from stages P14 to P28. Small pictures show dilated remains of kidney parenchyma (1) and glomeruli (2). (**D**) Ink injection into the pelvis of kidneys stains ureter and bladder and shows correct flux from kidney to bladder.

Newborn SIX1-Q177R^{active} mice were viable and did not show any alterations in behavior or in size. At stage P28 SIX1-Q177R^{active} mice were clearly distinguishable from their wild type littermates due to visible abdominal swelling. These mice developed severe bilateral hydronephrosis, which led to an early death between stages P28-P42 (Figure 20 B).

Histological analysis of different stages revealed that the observed hydronephrosis is an ongoing process starting around stage P14 with distension inside the kidney without overall volume change until the distension is so massive that the whole kidney begins to expand at P21 and finally displays the appearance of a balloon kidney at P28 (Figure 20 C). In this end stage of hydronephrosis, a clear

distension of the renal pelvis could be seen (Figure 20 C1), but intact and probably functional glomeruli in the outer region of the dilated kidney were still present (Figure 20 C2). Since all the tissue at the outline of the dilated areas seemed to be compressed, I wanted to check for a reflux problem based on the clogged ureter, due to possible overproliferation of ureter epithelia, and subsequent accumulation of urine in the kidney. Therefore, I injected ink into the pelvis of both P21 kidneys to label the ureter. The ink labeled each individual ureter (Figure 20 D, yellow arrows) and furthermore the bladder (Figure 20 D, red arrows) in wild type littermates and as well in SIX1-Q177R^{active} mice. A normal flux from the kidneys to the bladder appeared to be possible. The main cause behind the constant appearance of hydronephrosis in mice with global activation of SIX1-Q177R^{active} is likely not to be a complete obstruction of urine flow, but an impaired passage with urine retention and elevated pressure building up.

5.3 Compound mutants

To mimic the possible synergetic effect of *DROSHA-E1147K* and *SIX1-Q177R* seen in WT, I produced compound mutants in two combinations: A homozygous deletion of *Drosha* combined with an activation of *SIX1-Q177R* and in addition a compound mutant with activation of *DROSHA-E1147K* and *SIX1-Q177R*. Both mouse models can be switched on by Six2-cre through deletion of the floxed puro-polyA stop cassette (5.1.5 and 5.2.1) and the homozygous deletion of the floxed exon 9 of the *Drosha* allele (5.1.1).

5.3.1 Deletion of *Drosha* and activation of SIX1-Q177R in blastema derived cells

At embryonic stages E13.5 and E16.5 there was no major difference in histological appearance in Drosha$^{\Delta Six2c/\Delta Six2c}$ / SIX1-Q177R^{active} compared to Drosha$^{wt/\Delta Six2c}$ / SIX1-Q177R^{active} or Drosha$^{wt/wt}$ / SIX1-Q177R^{inactive} littermates. Mature glomeruli could be found at stage E18.5.

Marker analysis underlined this picture of unaltered nephrogenesis with *Wnt4* and *Wt1* positive structures in the cortex and central parts of the kidney (Figure 21 A). Nevertheless, *Six2* staining was weaker compared to the control and *Cited1* showed the already known patchy staining as a sign of a partly disrupted nephrogenic zone.

Drosha$^{\Delta Six2c/\Delta Six2c}$ SIX1-Q177R^{active} mice shared the same lethal phenotype of Drosha$^{\Delta Six2c/\Delta Six2c}$ (5.1.1) and Drosha$^{\Delta Six2c/\Delta Six2c}$ / SIX1-Q177R^{inactive} mice, while the inactivation of only one *Drosha* allele without SIX1-Q177R expression (Drosha$^{wt/\Delta Six2c}$ / SIX1-Q177R^{inactive}) lead to a phenotype comparable to control littermates. Drosha$^{wt/\Delta Six2c}$ / SIX1-Q177R^{active} mice had fully functional glomeruli at stage P21 (Figure 21 B, arrowheads), yet started to develop proteinuria in cortical regions (Figure 21 B, arrows). At stage P28 the kidneys displayed a more dramatic condition with beginning hydronephrosis and dilated tubules in all parts of the kidney (Figure 21 C, overview) and strong proteinuria (Figure 21 C, zoom:

arrows). Also, cells positive for the blastemal marker *Six2* could still be found. Staining against Ki-67 showed ongoing proliferation in the matured kidney, especially in cells surrounding cystic dilated tubules (Figure 21 C, Ki-67: arrowheads). These combined impairments limited the life expectancy of Drosha$^{wt/\Delta Six2c}$ SIX1-Q177R^{active} mice to 6 weeks. The major cause of death is probably due to hydronephrosis and kidney failure.

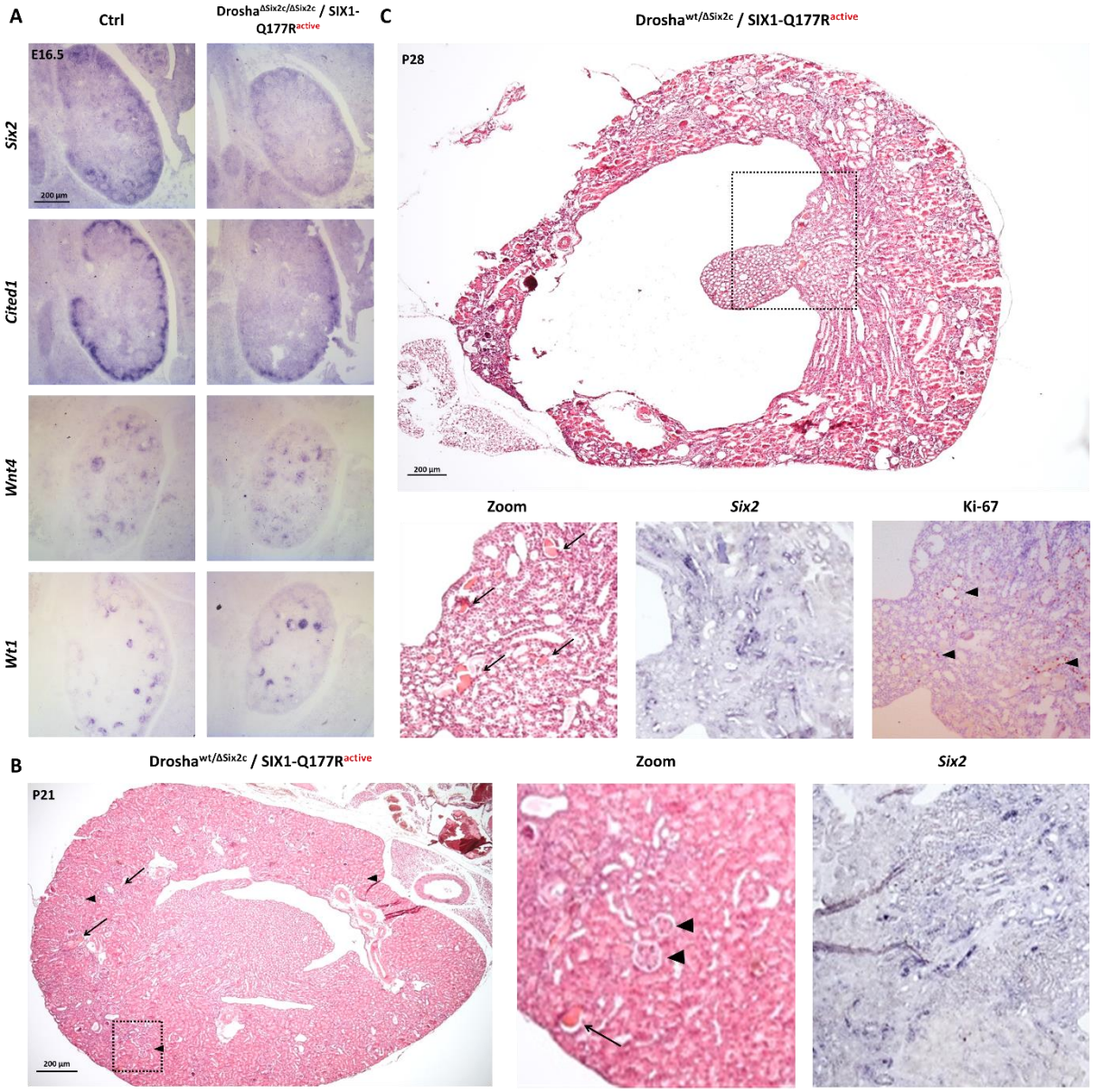

Figure 21: Deletion of DROSHA combined with SIX1-Q177R activation

(**A**) *in situ* hybridization of E16.5 kidneys with riboprobes to detect progenitor markers: *Six2*, *Cited1*, *Wt1* and *Wnt4* (**B**) HE staining of P21 Drosha$^{wt/\Delta Six2c}$ / SIX1-Q177R^{active} kidneys reveals the onset of proteinuria (arrows). *in situ* hybridization displays expression of progenitor marker *Six2* (**C**) HE staining of P28 Drosha$^{wt/\Delta Six2c}$ / SIX1-Q177R^{active} kidneys shows strong proteinuria (Zoom: arrows), *in situ* hybridization displays expression of progenitor marker *Six2* and Ki-67 staining (Ki-67: arrowheads) demonstrates ongoing proliferation.

5.3.2 Co-activation of DROSHA-E1147K and SIX1-Q177R in blastemal cells

DROSHA-E1147K^{active} / SIX1-Q177R^{active} mice developed an even more complex phenotype in mature kidneys compared to the Drosha$^{wt/\Delta Six2c}$ / SIX1-Q177R^{active} mice. At P28 the mice showed strong proteinuria, but in contrast to Drosha$^{wt/\Delta Six2c}$ SIX1-Q177R^{active} mice did not develop hydronephrosis at any stage between P14 and P52 (Figure 22 A). In addition to the proteinuria (Figure 22 A2), the DROSHA-E1147K^{active} / SIX1-Q177R^{active} mice suffered from lesions inside the kidney cortex (Figure 22 A1) and intense glomerulosclerosis (Figure 22 A3). Still, the kidneys had functional glomeruli in the cortical region of the kidney (Figure 22 A).

Analysis of proliferation marker Ki-67 could confirm strikingly increased and ongoing proliferation in Drosha$^{wt/\Delta Six2c}$ / SIX1-Q177R^{active} kidneys at stage P28 in contrast to reduced proliferation in littermate control kidneys (Figure 22 B). In particular, critical structures like glomeruli and dilated tubules presented high numbers of proliferating cells, which are presumably the cause for the sclerotic glomeruli. Furthermore, the lesions were regions of high proliferation activity. This could be caused by inflammation processes.

In spite of these impairments the mice could survive for up to 8 weeks without limitations until the mice had to be sacrificed due to kidney failure.

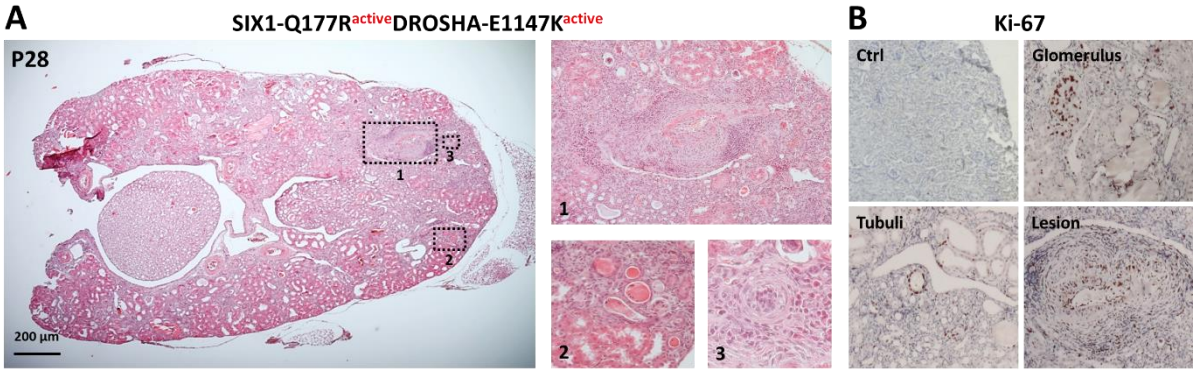

Figure 22: Co-activation of DROSHA-E1147K and SIX1-Q177R in blastemal cells

(**A**) HE staining of P28 DROSHA-E1147K^{active} SIX1-Q177R^{active} kidney showing lesions, proteinuria and glomerulosclerosis (zoomed rectangles 1-3). (**B**) Ki-67 staining shows ongoing proliferation in DROSHA-E1147K^{active} kidneys.

6 Discussion

6.1 DROSHA

Functional processing of miRNA is an essential component of various processes of animal development and homeostasis of different tissue types. Alteration of the microprocessor key players like *Drosha*, *Dgcr8* or *Dicer* shows numerous phenotypes in different organ systems that often share overlapping features (Brandl et al. 2016; Marinaro et al. 2017; Yi et al. 2009; Bartram et al. 2016; Chu et al. 2014). One of the best studied components of the microprocessor complex is *Dicer*. Recent studies have analyzed *Dicer* with global or conditional deletions, yet more limited work has been performed on the microprocessor components *Drosha* and *Dgcr8*. An early or complete loss of either component was often described to be associated with differentiation impairments, proliferation deficit and increase in apoptosis. Nevertheless, a connection to human pathology was still missing, until *DICER* mutations were found to be a leading factor of pleuropulmonary blastema (Hill et al. 2009). Shortly after this finding, *DROSHA* and *DGCR8* mutations were recognized as drivers in WT (Rakheja et al. 2014; Torrezan et al. 2014; Walz et al. 2015; Wegert et al. 2015).

6.1.1 Drosha function is essential in kidney blastema

For a better understanding if and how *Drosha* alterations may contribute to tumor formation, mutant mice with loss or mutant activation of *Drosha* were generated. A previous study had already shown that a podocyte-specific deletion of *Drosha* leads to proteinuria and renal failure (Zhdanova et al. 2011). But this deletion would happen too late as WT is thought to arise in earlier precursor cells. Because of this, I used the Six2-cre and Wt1-cre^{ERT2} transgenes to induce deletion of *Drosha*. This led to an earlier time point of recombination, which clearly affected multiple nephron cell types as validated by DROSHA immunofluorescent staining of Drosha$^{\Delta Six2c/\Delta Six2c}$ embryos. Six2-cre led to a fairly uniform deletion and there were only some DROSHA expressing blastema-derived cells left in mutant kidneys, indicative of a low-level mosaic phenotype. The Wt1-cre^{ERT2} mediated deletion resulted in much weaker effects, consistent with the expectation that a larger fraction of precursor cells may be outside the critical expression window at the time of tamoxifen administration. These cells can then rescue kidney functionality. Both deletion phenotypes shared some overlap when tested by marker analysis, with a reduction in the progenitor cell compartment, reduced proliferation, increased apoptosis and a graded impairment of differentiation. While the Six2-cre mediated deletion was lethal at birth and thus much more severe than the podocyte-limited deletion described by Zhdanova et al. (2011), the Wt1-cre^{ERT2} mediated inducible deletion produced an even milder phenotype, where mice survived with otherwise asymptomatic proteinuria for many weeks without evidence for WT formation.

6.1.2 DROSHA-E1147K is a dominant-negative mutation *in vivo*

The complete loss of *Drosha* in individual cells via Six2-cre or Wt1-cre^{ERT2} mediated recombination which leads to a complete lack of microprocessor activity in descendants may be too harsh to allow for tumor formation. I could show that the expression of the dominant-negative *DROSHA-E1147K* mutant transgene leads to graded reduction in individual canonical miRNAs, while still compatible with normal cell function. This combination offers a chance for malignant transformation. The broad activation of the *DROSHA-E1147K* transgene more closely resembled the Six2-cre mediated loss of *Drosha* activity and not the mosaic Drosha$^{\Delta Wt1/\Delta Wt1}$ situation. The additional occurrence of glomerulosclerosis and ongoing proliferation in postnatal kidneys indicates the development of additional degenerative lesions with advancing life time. Furthermore, the presence of Six2 and GFP positive cells at stage P28 are strong hints that these lesions contain either still incompletely differentiated or subsequently dedifferentiated blastema-like cells since physiological Six2 expression is terminated within the first days after birth (Hartman, Lai, and Patterson 2007). The strong phenotype of mutant DROSHA-E1147K is consistent with the dominant-negative effect already proposed from *in vitro* experiments (Wegert et al. 2015).

6.1.3 All miRNA biogenesis mutations share similar features

As already pointed out, *Drosha* deletions in mouse models have only been induced in a podocyte specific approach (Zhdanova et al. 2011). These mice suffer from late development impairments. Apart from this podocyte specific approach, there are numerous studies for other members of the miRNA biogenesis pathway that show comparable phenotypical alterations. For example kidneys of mice with Pax8-cre mediated *Dgcr8* deletion displayed ongoing proliferation combined with apoptosis in postnatal kidneys, followed by juvenile death (Bartram et al. 2016). This phenotype is comparable to mice with Six2-cre driven activation of DROSHA-E1147K presented in this thesis. Pax8-cre shares a significant overlap in cre driver expression to Six2-cre, even if *Pax8* is activated at a slightly later stage in renal vesicles and additionally in uretic bud derived ducts. The phenotypic similarities are in line with this similar expression pattern. *Dicer* is by far the best studied member of the miRNA biogenesis pathway. Accordingly, several cre driver lines have been crossed with *Dicer* deletion mice and again the offspring share phenotypic similarities. The Six2-cre mediated DICER knockout reported by Nagalakshmi et al. (2011) yielded a picture comparable to the Six2-cre mediated DROSHA KO in this thesis, with a loss of progenitor cells in the nephrogenic zone and around the UB tips and a significant reduction in the number of glomeruli. Interestingly, Chu et al. (2014) had shown that an even earlier loss of the progenitor cell pool due to apoptosis in Pax3-driven DICER KO embryos leads to a stalled nephrogenesis in the metanephros by E14.5. This may underlie the partial loss of kidneys observed in Drosha$^{\Delta Six2c/\Delta Six2c}$ and DROSHA-E1147K^{active} embryos. In regard to the previously characterized *Dicer* and

Dgcr8 deletions as well as my *Drosha* deletion and transgene models, it can be concluded that altered or lost miRNA procession induces not only a depletion of progenitor cells and further apoptosis, but ends up in severe functional kidney impairment to the point of kidney agenesis.

6.1.4 DROSHA-E114K mutation alone is not sufficient to induce Wilms tumors

The deletion or mutant activation of *Drosha* led to strong developmental defects in kidneys, but no changes that pointed in the direction of WT formation could be detected. There are multiple reasons why this may not have happened: The size of the target cell population and the available time window before terminal differentiation may be far too limited when compared to human children. The impairment of differentiation as seen in my mouse model would promote the formation of an embryonal neoplasm. Embryonal neoplasms are thought to be derived from precursor cells that are unable to differentiate beyond the precursor stage. Nevertheless, the observed reduction of proliferation and increase of apoptosis in the embryonic kidney cortex of mutants suggests that additional alterations may be needed. Since SIX2 expression is associated with a proliferative phenotype (Wegert et al. 2015), the synergetic effect of *DROSHA* and *SIX 1/2* mutations points in the direction that a combination miRNA procession impairment together with upregulation of proliferation factors may be the key for WT formation. In agreement with this hypothesis, prototypic mutations of the WT gene *Wt1* did not promote tumor formation without a complex assortment of *Wt1* and *Igf2* alterations (Hu et al. 2011).

6.2 SIX1

The importance of *SIX1* for kidney development and the found *SIX1* alterations in WT may represent a promising strategy to model malignant transformation leading to WT in the mouse. Therefore, I generated mice with the activation of the SIX1-Q117R mutant. *SIX1* and *SIX2* are known as blastemal markers for WT and as influencing cellular proliferation, but there were so far no signs for *SIX1/2* to be tumorigenic drivers (Sehic et al. 2012; Senanayake et al. 2013). Nevertheless, Wegert et al. (2015) could identify a sub group of WT that showed strong expression of *SIX* and *SALL* family members as well as *SIX* cofactor *EYA1*. In addition, these tumors showed expression of other kidney development genes like *CITED1*, *NCAM1*, *GDNF*, *REST* and *MYCN*, suggesting a progenitor cell state. Binding motif analysis proposed that the preferred binding site of the *SIX1* mutant changes with the slightly altered binding specificity compared to tumors with wild type *SIX1* (Wegert et al. 2015). However, the functional impact is still unknown.

6.2.1 SIX1 mutant expression in blastemal cells has no impact on kidney development

The activation of SIX1-Q177R in nephron progenitor cells of mouse kidneys did not exhibit a phenotypic alteration that could be easily detected. Even with high expression levels of the mutant SIX1 protein,

embryonic nephrogenesis seems to be unaltered and the mice are able to maintain normal kidney function leading to a life span comparable to wild type mice. I could not find any *Six2* expressing cells acting in a blastemal like manner in the adult kidney as I could in the DROSHA-E1147K^{active} mice. The termination of physiological *Six2* expression within the first days after birth, shown in earlier studies (Hartman, Lai, and Patterson 2007), could be observed. It seems that even if the blastemal cell compartment has a changed proliferation pattern, which could not be detected by Ki-67 staining, nephrogenesis goes on and mature glomeruli are formed. Therefore, activation of *SIX1-Q177R* in blastemal cells leads to a either a subtle or an unaltered phenotype, indicating that the mutation has no effect or the induced alterations may be compensated by genetic regulatory networks.

6.2.2 Global activation of *SIX1-Q177R* leads to hydronephrosis and early death

In contrast to the mice with activated *SIX1-Q177R* in blastemal cells, a global expression of *SIX1-Q177R* exhibits a far stronger phenotype with juvenile hydronephrosis and early death after birth. The fact that I could not find alterations in the prenatal kidney development led me to the conclusion that this hydronephrosis may be a product of defective flux from kidney to bladder. But with the ink staining it could be confirmed that liquid can pass through each individual ureter and reach the bladder. The real cause of the hydronephrosis, even with its recurring character, is still to be found. Because *SIX1* plays an important role in ureteral smooth muscle formation (Nie et al. 2010), a possible explanation could be that proliferation alterations in the ureter smooth muscle cells disturb the peristaltic motion and lead to reflux into the kidney,. Nevertheless, the global activation of *SIX1-Q177R* mutant can affect various parts of the urinary system of the mice, which makes the search for the leading cause of hydronephrosis a difficult task. Yet, the recurring hydronephrosis could be an interesting model for hydronephrosis in mice.

6.3 Synergetic effect of DROSHA and SIX1 mutants

6.3.1 SIX1-Q177R expression and heterozygous deletion of *Drosha* are sufficient to induce kidney impairment

One of my two approaches to mimic the synergetic effect seen in WT was activation of SIX1-Q177R along with a homo- and heterozygous knockout of Drosha in blastemal cells. I could detect that the Drosha$^{\Delta Six2c/\Delta Six2c}$ / SIX1-Q177R^{active} mice died at P1 comparable to the mice with Six2-cre driven homozygous deletion of *Drosha*. The Drosha$^{\Delta Six2c/\Delta Six2c}$ / SIX1-Q177R^{active} mice showed the typical disrupted nephrogenic zone, but did not suffer from complete depletion of glomeruli precursors leading to maturing glomeruli in the central regions of the kidney. I concluded that a presumed benefit gained from activated SIX1-Q177R enables precursor cells to make the transition into a more differentiated cell state instead of an apoptotic cell fate seen in Drosha$^{\Delta Six2c/\Delta Six2c}$ mice. Yet, it seems

that these cells, even if able to form mature glomeruli, could not compensate the loss of progenitor cells and prevent a lethal phenotype.

The heterozygous deletion of *Drosha* combined with activation of the *SIX1-Q177R* transgene resulted in a viable phenotype. Interestingly, the mice still expressed *Six2* in the kidney at stage P24, where *Six2* staining should already be terminated (Hartman, Lai, and Patterson 2007). With these undifferentiated and possibly proliferating cells still inside the mature kidney the possibility for WT formation was given. Since the Drosha$^{wt/\Delta Six2c}$ mice were close to the wild type in their phenotypic appearance, it was surprising that heterozygous deletion of *Drosha* with activation of the *SIX1-Q177R* transgene was sufficient to induce a new composition of kidney impairments. The mice exhibited severe proteinuria and beginning hydronephrosis, which in combination leads to an early death around P28, a time point probably too early to allow successful formation of WT. Yet, this results are a strong hint for a synergetic effect of SIX1-Q177R activation and heterozygous deletion *Drosha* with a new phenotype and numerous progenitor cells inside the matured kidneys.

6.3.2 SIX1-Q177R and DROSHA-E1147K display a synergistic effect and new phenotype

The overexpression of DROSHA-E1147K showed a dominant-negative effect, but a miRNA processing alteration that lay in between the KO and wild type situation could be seen. Furthermore, DROSHA-E1147K^{active} offspring were viable. A combination of SIX1-Q177R and DROSHA-E1147K activation in blastemal cells was therefore one of the most promising approaches to allow for WT formation in mice kidneys. Indeed, the mice were viable after birth and displayed a phenotype that was again partly a combination of already known alterations like proteinuria and glomerulosclerosis, and the mice suffered from early death within the first 2 months. A new feature that had not be experienced so far was the formation of lesions inside the kidneys. This lesions displayed strong proliferation staining. Furthermore, proliferation hotspots in various areas of the kidney including glomeruli and dilated tubuli were found. The results suggest that also in SIX1-Q177R^{active} / DROSHA-E1147K^{active} kidneys precursor cells with the ability to proliferate are present.

It seems that in both compound mutants, cells were able to maintain their progenitor cell status even after nephrogenesis had finished. The expression of SIX1-Q177R could prevent the progenitor cells from complete depletion and benefits the formation of glomeruli at prenatal stages, seen in the Drosha$^{\Delta Six2c/\Delta Six2c}$ / SIX1-Q177R^{active} mice, but seems to be a driving force behind the transition of still active and proliferating progenitor cells into postnatal stages resulting in the correlated severe kidney alterations. Kidney injuries could promote the activation of progenitor cell program even further. Interestingly, the expression of SIX1-Q177R is sufficient to induce a severe phenotype with only heterozygous *Drosha* deletion which would be comparable to wild type littermates without SIX1 mutations, leading to the conclusion that even a subtle alterations of miRNA processing can have a

severe outcome if *SIX1* mutations are present. In line with these findings, the severe phenotype of Six2-cre driven DROSHA-E1147K activation was worse in SIX1-Q177R^{active} / DROSHA-E1147K^{active} mice under the same promotor.

In summary, I could not observe Wilms tumor formation in kidneys of the mouse models newly established in this thesis. Nonetheless, the results show the importance of DROSHA and SIX1 for kidney development. The DROSHA mutations seen in Wilms tumors are dominant-negative alterations *in vivo* that strongly impair kidney development leading to kidney failure. Furthermore, global activation of SIX1 mutations can be a new approach to model hydronephrosis in the mouse. I could clearly confirm the synergetic effect of alteration in the *SIX-SALL* pathway and the microprocessor complex proposed by the Wilms tumor screens. The compound mutants show new combinations of kidney impairments with kidney failure as a terminal end point. Yet, additional genetic alterations seems to be needed to fully recapitulate WT formation in the mouse. In the future, another promising approach to allow WT formation would be the combination of my compound mutants with different cre driver mouse lines to induce SIX1 and DROSHA mutant expression at different time points of nephrogenesis and to target different cell types of the developing kidney. This could prevent apoptotic loss of progenitor cells and promote tumorigenesis.

7 References

Al-Awqati, Q., and X. B. Gao. 2011. 'Differentiation of intercalated cells in the kidney', *Physiology (Bethesda)*, 26: 266-72.

Androvic, P., L. Valihrach, J. Elling, R. Sjoback, and M. Kubista. 2017. 'Two-tailed RT-qPCR: a novel method for highly accurate miRNA quantification', *Nucleic Acids Res*, 45: e144.

Babyn, P., C. Owens, M. Gyepes, and G. J. D'Angio. 1995. 'Imaging patients with Wilms tumor', *Hematol Oncol Clin North Am*, 9: 1217-52.

Barker, N., M. B. Rookmaaker, P. Kujala, A. Ng, M. Leushacke, H. Snippert, M. van de Wetering, S. Tan, J. H. Van Es, M. Huch, R. Poulsom, M. C. Verhaar, P. J. Peters, and H. Clevers. 2012. 'Lgr5(+ve) stem/progenitor cells contribute to nephron formation during kidney development', *Cell Rep*, 2: 540-52.

Bartram, M. P., E. Amendola, T. Benzing, B. Schermer, G. de Vita, and R. U. Muller. 2016. 'Mice lacking microRNAs in Pax8-expressing cells develop hypothyroidism and end-stage renal failure', *BMC Mol Biol*, 17: 11.

Behbakht, K., L. Qamar, C. S. Aldridge, R. D. Coletta, S. A. Davidson, A. Thorburn, and H. L. Ford. 2007. 'Six1 overexpression in ovarian carcinoma causes resistance to TRAIL-mediated apoptosis and is associated with poor survival', *Cancer Res*, 67: 3036-42.

Bell, P. D., J. Y. Lapointe, and J. Peti-Peterdi. 2003. 'Macula densa cell signaling', *Annu Rev Physiol*, 65: 481-500.

Bouchard, M., A. Souabni, M. Mandler, A. Neubuser, and M. Busslinger. 2002. 'Nephric lineage specification by Pax2 and Pax8', *Genes Dev*, 16: 2958-70.

Boyle, S., A. Misfeldt, K. J. Chandler, K. K. Deal, E. M. Southard-Smith, D. P. Mortlock, H. S. Baldwin, and M. de Caestecker. 2008. 'Fate mapping using Cited1-CreERT2 mice demonstrates that the cap mesenchyme contains self-renewing progenitor cells and gives rise exclusively to nephronic epithelia', *Dev Biol*, 313: 234-45.

Boyle, S., T. Shioda, A. O. Perantoni, and M. de Caestecker. 2007. 'Cited1 and Cited2 are differentially expressed in the developing kidney but are not required for nephrogenesis', *Dev Dyn*, 236: 2321-30.

Brandl, A., P. Daum, S. Brenner, S. R. Schulz, D. Y. Yap, M. R. Bosl, J. Wittmann, W. Schuh, and H. M. Jack. 2016. 'The microprocessor component, DGCR8, is essential for early B-cell development in mice', *Eur J Immunol*, 46: 2710-18.

Breslow, N., A. Olshan, J. B. Beckwith, and D. M. Green. 1993. 'Epidemiology of Wilms tumor', *Med Pediatr Oncol*, 21: 172-81.

Cebrian, C., N. Asai, V. D'Agati, and F. Costantini. 2014. 'The number of fetal nephron progenitor cells limits ureteric branching and adult nephron endowment', *Cell Rep*, 7: 127-37.

Chai, L., J. Yang, C. Di, W. Cui, K. Kawakami, R. Lai, and Y. Ma. 2006. 'Transcriptional activation of the SALL1 by the human SIX1 homeodomain during kidney development', *J Biol Chem*, 281: 18918-26.

Chong, Mark M.W., Jeffrey P. Rasmussen, Alexander Y. Rudensky, and Dan R. Littman. 2008. 'The RNAseIII enzyme Drosha is critical in T cells for preventing lethal inflammatory disease', *The Journal of Experimental Medicine*, 205: 2005-17.

Chu, J. Y., S. Sims-Lucas, D. S. Bushnell, A. J. Bodnar, J. A. Kreidberg, and J. Ho. 2014. 'Dicer function is required in the metanephric mesenchyme for early kidney development', *Am J Physiol Renal Physiol*, 306: F764-72.

Coletta, R. D., P. Jedlicka, A. Gutierrez-Hartmann, and H. L. Ford. 2004. 'Transcriptional control of the cell cycle in mammary gland development and tumorigenesis', *J Mammary Gland Biol Neoplasia*, 9: 39-53.

Combes, A. N., J. A. Davies, and M. H. Little. 2015. 'Cell-cell interactions driving kidney morphogenesis', *Curr Top Dev Biol*, 112: 467-508.

Coppes-Zantinga, A. R., and M. J. Coppes. 1999. 'The eponym "Wilms": a reminder of a surgeon's lifelong contributions to medicine', *Med Pediatr Oncol*, 32: 438-9.

Costantini, F. 2006. 'Renal branching morphogenesis: concepts, questions, and recent advances', *Differentiation*, 74: 402-21.

Costantini, F., and R. Kopan. 2010. 'Patterning a complex organ: branching morphogenesis and nephron segmentation in kidney development', *Dev Cell*, 18: 698-712.

Davidoff, A. M. 2012. 'Wilms tumor', *Adv Pediatr*, 59: 247-67.

Dome, J. S., C. V. Fernandez, E. A. Mullen, J. A. Kalapurakal, J. I. Geller, V. Huff, E. J. Gratias, D. B. Dix, P. F. Ehrlich, G. Khanna, M. H. Malogolowkin, J. R. Anderson, A. Naranjo, E. J. Perlman, and C. O. G. Renal Tumors Committee. 2013. 'Children's Oncology Group's 2013 blueprint for research: renal tumors', *Pediatr Blood Cancer*, 60: 994-1000.

Ford, H. L., E. N. Kabingu, E. A. Bump, G. L. Mutter, and A. B. Pardee. 1998. 'Abrogation of the G2 cell cycle checkpoint associated with overexpression of HSIX1: a possible mechanism of breast carcinogenesis', *Proc Natl Acad Sci U S A*, 95: 12608-13.

Fukunaga, R., B. W. Han, J. H. Hung, J. Xu, Z. Weng, and P. D. Zamore. 2012. 'Dicer partner proteins tune the length of mature miRNAs in flies and mammals', *Cell*, 151: 533-46.

Gan, J., J. E. Tropea, B. P. Austin, D. L. Court, D. S. Waugh, and X. Ji. 2006. 'Structural insight into the mechanism of double-stranded RNA processing by ribonuclease III', *Cell*, 124: 355-66.

Georgas, K., B. Rumballe, M. T. Valerius, H. S. Chiu, R. D. Thiagarajan, E. Lesieur, B. J. Aronow, E. W. Brunskill, A. N. Combes, D. Tang, D. Taylor, S. M. Grimmond, S. S. Potter, A. P. McMahon, and M. H. Little. 2009. 'Analysis of early nephron patterning reveals a role for distal RV proliferation in fusion to the ureteric tip via a cap mesenchyme-derived connecting segment', *Dev Biol*, 332: 273-86.

Gregory, R. I., K. P. Yan, G. Amuthan, T. Chendrimada, B. Doratotaj, N. Cooch, and R. Shiekhattar. 2004. 'The Microprocessor complex mediates the genesis of microRNAs', *Nature*, 432: 235-40.

Han, J., Y. Lee, K. H. Yeom, Y. K. Kim, H. Jin, and V. N. Kim. 2004. 'The Drosha-DGCR8 complex in primary microRNA processing', *Genes Dev*, 18: 3016-27.

Han, J., Y. Lee, K. H. Yeom, J. W. Nam, I. Heo, J. K. Rhee, S. Y. Sohn, Y. Cho, B. T. Zhang, and V. N. Kim. 2006. 'Molecular basis for the recognition of primary microRNAs by the Drosha-DGCR8 complex', *Cell*, 125: 887-901.

Harding, S. D., C. Armit, J. Armstrong, J. Brennan, Y. Cheng, B. Haggarty, D. Houghton, S. Lloyd-MacGilp, X. Pi, Y. Roochun, M. Sharghi, C. Tindal, A. P. McMahon, B. Gottesman, M. H. Little, K. Georgas, B. J. Aronow, S. S. Potter, E. W. Brunskill, E. M. Southard-Smith, C. Mendelsohn, R. A. Baldock, J. A. Davies, and D. Davidson. 2011. 'The GUDMAP database--an online resource for genitourinary research', *Development*, 138: 2845-53.

Hartman, H. A., H. L. Lai, and L. T. Patterson. 2007. 'Cessation of renal morphogenesis in mice', *Dev Biol*, 310: 379-87.

Hill, D. A., J. Ivanovich, J. R. Priest, C. A. Gurnett, L. P. Dehner, D. Desruisseau, J. A. Jarzembowski, K. A. Wikenheiser-Brokamp, B. K. Suarez, A. J. Whelan, G. Williams, D. Bracamontes, Y. Messinger, and P. J. Goodfellow. 2009. 'DICER1 mutations in familial pleuropulmonary blastoma', *Science*, 325: 965.

Hinchliffe, S. A., P. H. Sargent, C. V. Howard, Y. F. Chan, and D. van Velzen. 1991. 'Human intrauterine renal growth expressed in absolute number of glomeruli assessed by the disector method and Cavalieri principle', *Lab Invest*, 64: 777-84.

Hitz, C., W. Wurst, and R. Kuhn. 2007. 'Conditional brain-specific knockdown of MAPK using Cre/loxP regulated RNA interference', *Nucleic Acids Res*, 35: e90.

Horner, M.J., LAG. Ries, M. Krapcho, N. Neyman, R. Aminou, N. Howlader, SF. Altekruse, E.J. Feuer, L. Huang, A. Mariotto, B.A. Miller, D.R. Lewis, M.P. Eisner, D.G. Stinchcomb, and B.K. Edwards. 2009. "SEER Cancer Statistics Review, 1975-2006." In. National Cancer Institute. Bethesda, MD, http://seer.cancer.gov/csr/1975_2006/, based on November 2008 SEER data submission, posted to the SEER web site, 2009.

Houghton, P. J., C. L. Morton, C. Tucker, D. Payne, E. Favours, C. Cole, R. Gorlick, E. A. Kolb, W. Zhang, R. Lock, H. Carol, M. Tajbakhsh, C. P. Reynolds, J. M. Maris, J. Courtright, S. T. Keir, H. S. Friedman, C. Stopford, J. Zeidner, J. Wu, T. Liu, C. A. Billups, J. Khan, S. Ansher, J. Zhang, and

M. A. Smith. 2007. 'The pediatric preclinical testing program: description of models and early testing results', *Pediatr Blood Cancer*, 49: 928-40.

Hu, Q., F. Gao, W. Tian, E. C. Ruteshouser, Y. Wang, A. Lazar, J. Stewart, L. C. Strong, R. R. Behringer, and V. Huff. 2011. 'Wt1 ablation and Igf2 upregulation in mice result in Wilms tumors with elevated ERK1/2 phosphorylation', *J Clin Invest*, 121: 174-83.

Huang, L., S. Mokkapati, Q. Hu, E. C. Ruteshouser, M. J. Hicks, and V. Huff. 2016. 'Nephron Progenitor But Not Stromal Progenitor Cells Give Rise to Wilms Tumors in Mouse Models with beta-Catenin Activation or Wt1 Ablation and Igf2 Upregulation', *Neoplasia*, 18: 71-81.

Huff, V. 1998. 'Wilms tumor genetics', *Am J Med Genet*, 79: 260-7.

Hughson, M., A. B. Farris, 3rd, R. Douglas-Denton, W. E. Hoy, and J. F. Bertram. 2003. 'Glomerular number and size in autopsy kidneys: the relationship to birth weight', *Kidney Int*, 63: 2113-22.

Huntzinger, E., and E. Izaurralde. 2011. 'Gene silencing by microRNAs: contributions of translational repression and mRNA decay', *Nat Rev Genet*, 12: 99-110.

Kao, R. M., A. Vasilyev, A. Miyawaki, I. A. Drummond, and A. P. McMahon. 2012. 'Invasion of distal nephron precursors associates with tubular interconnection during nephrogenesis', *J Am Soc Nephrol*, 23: 1682-90.

Kawakami, K., S. Sato, H. Ozaki, and K. Ikeda. 2000. 'Six family genes--structure and function as transcription factors and their roles in development', *Bioessays*, 22: 616-26.

Keller, P. J., A. D. Schmidt, J. Wittbrodt, and E. H. Stelzer. 2008. 'Reconstruction of zebrafish early embryonic development by scanned light sheet microscopy', *Science*, 322: 1065-9.

Kobayashi, A., M. T. Valerius, J. W. Mugford, T. J. Carroll, M. Self, G. Oliver, and A. P. McMahon. 2008. 'Six2 defines and regulates a multipotent self-renewing nephron progenitor population throughout mammalian kidney development', *Cell Stem Cell*, 3: 169-81.

Kumar, J. P. 2009. 'The sine oculis homeobox (SIX) family of transcription factors as regulators of development and disease', *Cell Mol Life Sci*, 66: 565-83.

Lahoti, C., P. Thorner, D. Malkin, and H. Yeger. 1996. 'Immunohistochemical detection of p53 in Wilms' tumors correlates with unfavorable outcome', *Am J Pathol*, 148: 1577-89.

Landthaler, M., A. Yalcin, and T. Tuschl. 2004. 'The human DiGeorge syndrome critical region gene 8 and Its D. melanogaster homolog are required for miRNA biogenesis', *Curr Biol*, 14: 2162-7.

Levitt, G. , G. Hamard, and J. Demignon. 2012. 'Renal tumours: long-term outcome', *Pediatr Nephrol*, 27: 911-6.

Little, M. H., and A. P. McMahon. 2012. 'Mammalian kidney development: principles, progress, and projections', *Cold Spring Harb Perspect Biol*, 4.

Macias, S., R. A. Cordiner, and J. F. Caceres. 2013. 'Cellular functions of the microprocessor', *Biochem Soc Trans*, 41: 838-43.

Marinaro, F., M. J. Marzi, N. Hoffmann, H. Amin, R. Pelizzoli, F. Niola, F. Nicassio, and D. De Pietri Tonelli. 2017. 'MicroRNA-independent functions of DGCR8 are essential for neocortical development and TBR1 expression', *EMBO Rep*, 18: 603-18.

Markham, N. R., and M. Zuker. 2008. 'UNAFold: software for nucleic acid folding and hybridization', *Methods Mol Biol*, 453: 3-31.

Matsunaga, E. 1981. 'Genetics of Wilms' tumor', *Hum Genet*, 57: 231-46.

McMahon, A. P. 2016. 'Development of the Mammalian Kidney', *Curr Top Dev Biol*, 117: 31-64.

Micalizzi, D. S., K. L. Christensen, P. Jedlicka, R. D. Coletta, A. E. Baron, J. C. Harrell, K. B. Horwitz, D. Billheimer, K. A. Heichman, A. L. Welm, W. P. Schiemann, and H. L. Ford. 2009. 'The Six1 homeoprotein induces human mammary carcinoma cells to undergo epithelial-mesenchymal transition and metastasis in mice through increasing TGF-beta signaling', *J Clin Invest*, 119: 2678-90.

Micalizzi, D. S., C. A. Wang, S. M. Farabaugh, W. P. Schiemann, and H. L. Ford. 2010. 'Homeoprotein Six1 increases TGF-beta type I receptor and converts TGF-beta signaling from suppressive to supportive for tumor growth', *Cancer Res*, 70: 10371-80.

Miner, J. H. 2011. 'Organogenesis of the kidney glomerulus: focus on the glomerular basement membrane', *Organogenesis*, 7: 75-82.

Mugford, J. W., J. Yu, A. Kobayashi, and A. P. McMahon. 2009. 'High-resolution gene expression analysis of the developing mouse kidney defines novel cellular compartments within the nephron progenitor population', *Dev Biol*, 333: 312-23.

Mundlos, S., J. Pelletier, A. Darveau, M. Bachmann, A. Winterpacht, and B. Zabel. 1993. 'Nuclear localization of the protein encoded by the Wilms' tumor gene WT1 in embryonic and adult tissues', *Development*, 119: 1329-41.

Nagalakshmi, V. K., Q. Ren, M. M. Pugh, M. T. Valerius, A. P. McMahon, and J. Yu. 2011. 'Dicer regulates the development of nephrogenic and ureteric compartments in the mammalian kidney', *Kidney Int*, 79: 317-30.

Ng, K. T., T. K. Lee, Q. Cheng, J. Y. Wo, C. K. Sun, D. Y. Guo, Z. X. Lim, C. M. Lo, R. T. Poon, S. T. Fan, and K. Man. 2010. 'Suppression of tumorigenesis and metastasis of hepatocellular carcinoma by shRNA interference targeting on homeoprotein Six1', *Int J Cancer*, 127: 859-72.

Ng, K. T., K. Man, C. K. Sun, T. K. Lee, R. T. Poon, C. M. Lo, and S. T. Fan. 2006. 'Clinicopathological significance of homeoprotein Six1 in hepatocellular carcinoma', *Br J Cancer*, 95: 1050-5.

Nie, X., J. Sun, R. E. Gordon, C. L. Cai, and P. X. Xu. 2010. 'SIX1 acts synergistically with TBX18 in mediating ureteral smooth muscle formation', *Development*, 137: 755-65.

Nishinakamura, R., Y. Matsumoto, K. Nakao, K. Nakamura, A. Sato, N. G. Copeland, D. J. Gilbert, N. A. Jenkins, S. Scully, D. L. Lacey, M. Katsuki, M. Asashima, and T. Yokota. 2001. 'Murine homolog of SALL1 is essential for ureteric bud invasion in kidney development', *Development*, 128: 3105-15.

O'Brien, L. L., and A. P. McMahon. 2013. 'Progenitor programming in mammalian nephrogenesis', *Nephrology (Carlton)*, 18: 177-9.

Ohto, H., S. Kamada, K. Tago, S. I. Tominaga, H. Ozaki, S. Sato, and K. Kawakami. 1999. 'Cooperation of six and eya in activation of their target genes through nuclear translocation of Eya', *Mol Cell Biol*, 19: 6815-24.

Park, J. S., W. Ma, L. L. O'Brien, E. Chung, J. J. Guo, J. G. Cheng, M. T. Valerius, J. A. McMahon, W. H. Wong, and A. P. McMahon. 2012. 'Six2 and Wnt regulate self-renewal and commitment of nephron progenitors through shared gene regulatory networks', *Dev Cell*, 23: 637-51.

Pearce, D., R. Soundararajan, C. Trimpert, O. B. Kashlan, P. M. Deen, and D. E. Kohan. 2015. 'Collecting duct principal cell transport processes and their regulation', *Clin J Am Soc Nephrol*, 10: 135-46.

Peters, L., and G. Meister. 2007. 'Argonaute proteins: mediators of RNA silencing', *Mol Cell*, 26: 611-23.

Radisky, D. C. 2009. 'Defining a role for the homeoprotein Six1 in EMT and mammary tumorigenesis', *J Clin Invest*, 119: 2528-31.

Rakheja, D., K. S. Chen, Y. Liu, A. A. Shukla, V. Schmid, T. C. Chang, S. Khokhar, J. E. Wickiser, N. J. Karandikar, J. S. Malter, J. T. Mendell, and J. F. Amatruda. 2014. 'Somatic mutations in DROSHA and DICER1 impair microRNA biogenesis through distinct mechanisms in Wilms tumours', *Nat Commun*, 2: 4802.

Reichenberger, K. J., R. D. Coletta, A. P. Schulte, M. Varella-Garcia, and H. L. Ford. 2005. 'Gene amplification is a mechanism of Six1 overexpression in breast cancer', *Cancer Res*, 65: 2668-75.

Renier, N., Z. Wu, D. J. Simon, J. Yang, P. Ariel, and M. Tessier-Lavigne. 2014. 'iDISCO: a simple, rapid method to immunolabel large tissue samples for volume imaging', *Cell*, 159: 896-910.

Rose, S. R., V. E. Horne, J. Howell, S. A. Lawson, M. M. Rutter, G. E. Trotman, and S. D. Corathers. 2016. 'Late endocrine effects of childhood cancer', *Nat Rev Endocrinol*, 12: 319-36.

Ruteshouser, E. C., S. M. Robinson, and V. Huff. 2008. 'Wilms tumor genetics: mutations in WT1, WTX, and CTNNB1 account for only about one-third of tumors', *Genes Chromosomes Cancer*, 47: 461-70.

Scott, R. P., and S. E. Quaggin. 2015. 'Review series: The cell biology of renal filtration', *J Cell Biol*, 209: 199-210.

Sehic, D., C. D. Ciornei, and D. Gisselsson. 2014. 'Evaluation of CITED1, SIX1, and CD56 protein expression for identification of blastemal elements in Wilms tumor', *Am J Clin Pathol*, 141: 828-33.

Sehic, D., J. Karlsson, B. Sandstedt, and D. Gisselsson. 2012. 'SIX1 protein expression selectively identifies blastemal elements in Wilms tumor', *Pediatr Blood Cancer*, 59: 62-8.

Self, M., O. V. Lagutin, B. Bowling, J. Hendrix, Y. Cai, G. R. Dressler, and G. Oliver. 2006. 'Six2 is required for suppression of nephrogenesis and progenitor renewal in the developing kidney', *EMBO J*, 25: 5214-28.

Senanayake, U., K. Koller, M. Pichler, I. Leuschner, H. Strohmaier, U. Hadler, S. Das, G. Hoefler, and B. Guertl. 2013. 'The pluripotent renal stem cell regulator SIX2 is activated in renal neoplasms and influences cellular proliferation and migration', *Hum Pathol*, 44: 336-45.

Short, K. M., A. N. Combes, J. Lefevre, A. L. Ju, K. M. Georgas, T. Lamberton, O. Cairncross, B. A. Rumballe, A. P. McMahon, N. A. Hamilton, I. M. Smyth, and M. H. Little. 2014. 'Global quantification of tissue dynamics in the developing mouse kidney', *Dev Cell*, 29: 188-202.

Siomi, H., and M. C. Siomi. 2010. 'Posttranscriptional regulation of microRNA biogenesis in animals', *Mol Cell*, 38: 323-32.

Sommer, C., C. Straehle, U. Köthe, and FA. Hamprecht. 2011. ' ilastik: Interactive learning and segmentation toolkit', *Eighth IEEE International Symposium on Biomedical Imaging (ISBI)*, Proceedings, (2011).

Sonn, G., and L. M. Shortliffe. 2008. 'Management of Wilms tumor: current standard of care', *Nat Clin Pract Urol*, 5: 551-60.

Subramanya, A. R., and D. H. Ellison. 2014. 'Distal convoluted tubule', *Clin J Am Soc Nephrol*, 9: 2147-63.

Suh, J. H., and J. H. Miner. 2013. 'The glomerular basement membrane as a barrier to albumin', *Nat Rev Nephrol*, 9: 470-7.

Taguchi, A., Y. Kaku, T. Ohmori, S. Sharmin, M. Ogawa, H. Sasaki, and R. Nishinakamura. 2014. 'Redefining the in vivo origin of metanephric nephron progenitors enables generation of complex kidney structures from pluripotent stem cells', *Cell Stem Cell*, 14: 53-67.

Takasato, M., and M. H. Little. 2015. 'The origin of the mammalian kidney: implications for recreating the kidney in vitro', *Development*, 142: 1937-47.

Taylor, A. J., D. L. Winter, K. Pritchard-Jones, C. A. Stiller, C. Frobisher, E. R. Lancashire, R. C. Reulen, M. M. Hawkins, and Study British Childhood Cancer Survivor. 2008. 'Second primary neoplasms in survivors of Wilms' tumour--a population-based cohort study from the British Childhood Cancer Survivor Study', *Int J Cancer*, 122: 2085-93.

Torrezan, G. T., E. N. Ferreira, A. M. Nakahata, B. D. Barros, M. T. Castro, B. R. Correa, A. C. Krepischi, E. H. Olivieri, I. W. Cunha, U. Tabori, P. E. Grundy, C. M. Costa, B. de Camargo, P. A. Galante, and D. M. Carraro. 2014. 'Recurrent somatic mutation in DROSHA induces microRNA profile changes in Wilms tumour', *Nat Commun*, 5: 4039.

Vujanic, G. M., and B. Sandstedt. 2010. 'The pathology of Wilms' tumour (nephroblastoma): the International Society of Paediatric Oncology approach', *J Clin Pathol*, 63: 102-9.

Vujanic, G. M., B. Sandstedt, D. Harms, A. Kelsey, I. Leuschner, J. de Kraker, and Siop Nephroblastoma Scientific Committee. 2002. 'Revised International Society of Paediatric Oncology (SIOP) working classification of renal tumors of childhood', *Med Pediatr Oncol*, 38: 79-82.

Walz, A. L., A. Ooms, S. Gadd, D. S. Gerhard, M. A. Smith, J. M. Guidry Auvil, D. Meerzaman, Q. R. Chen, C. H. Hsu, C. Yan, C. Nguyen, Y. Hu, R. Bowlby, D. Brooks, Y. Ma, A. J. Mungall, R. A. Moore, J. Schein, M. A. Marra, V. Huff, J. S. Dome, Y. Y. Chi, C. G. Mullighan, J. Ma, D. A. Wheeler, O. A. Hampton, N. Jafari, N. Ross, J. M. Gastier-Foster, and E. J. Perlman. 2015. 'Recurrent DGCR8, DROSHA, and SIX homeodomain mutations in favorable histology Wilms tumors', *Cancer Cell*, 27: 286-97.

Wan, F., X. Miao, I. Quraishi, V. Kennedy, K. E. Creek, and L. Pirisi. 2008. 'Gene expression changes during HPV-mediated carcinogenesis: a comparison between an in vitro cell model and cervical cancer', *Int J Cancer*, 123: 32-40.

Wang, C. A., P. Jedlicka, A. N. Patrick, D. S. Micalizzi, K. C. Lemmer, E. Deitsch, M. Casas-Selves, J. C. Harrell, and H. L. Ford. 2012. 'SIX1 induces lymphangiogenesis and metastasis via upregulation of VEGF-C in mouse models of breast cancer', *J Clin Invest*, 122: 1895-906.

Wegert, J., N. Ishaque, R. Vardapour, C. Georg, Z. Gu, M. Bieg, B. Ziegler, S. Bausenwein, N. Nourkami, N. Ludwig, A. Keller, C. Grimm, S. Kneitz, R. D. Williams, T. Chagtai, K. Pritchard-Jones, P. van Sluis, R. Volckmann, J. Koster, R. Versteeg, T. Acha, M. J. O'Sullivan, P. K. Bode, F. Niggli, G. A. Tytgat, H. van Tinteren, M. M. van den Heuvel-Eibrink, E. Meese, C. Vokuhl, I. Leuschner, N. Graf, R. Eils, S. M. Pfister, M. Kool, and M. Gessler. 2015. 'Mutations in the SIX1/2 pathway and the DROSHA/DGCR8 miRNA microprocessor complex underlie high-risk blastemal type Wilms tumors', *Cancer Cell*, 27: 298-311.

Weirich, A., I. Leuschner, D. Harms, G. M. Vujanic, J. Troger, U. Abel, N. Graf, D. Schmidt, R. Ludwig, and P. A. Voute. 2001. 'Clinical impact of histologic subtypes in localized non-anaplastic nephroblastoma treated according to the trial and study SIOP-9/GPOH', *Ann Oncol*, 12: 311-9.

Weirich, A., R. Ludwig, N. Graf, U. Abel, I. Leuschner, G. M. Vujanic, O. Mehls, J. Boos, J. Beck, B. Royer-Pokora, and P. A. Voute. 2004. 'Survival in nephroblastoma treated according to the trial and study SIOP-9/GPOH with respect to relapse and morbidity', *Ann Oncol*, 15: 808-20.

Wright, K. D., D. M. Green, and N. C. Daw. 2009. 'Late effects of treatment for wilms tumor', *Pediatr Hematol Oncol*, 26: 407-13.

Wu, Wangjun, Zhuqing Ren, Pinghua Li, Debing Yu, Jie Chen, Ruihua Huang, and Honglin Liu. 2015. 'Six1: A critical transcription factor in tumorigenesis', *International Journal of Cancer*, 136: 1245-53.

Xu, P. X., J. Adams, H. Peters, M. C. Brown, S. Heaney, and R. Maas. 1999. 'Eya1-deficient mice lack ears and kidneys and show abnormal apoptosis of organ primordia', *Nat Genet*, 23: 113-7.

Xu, P. X., W. Zheng, L. Huang, P. Maire, C. Laclef, and D. Silvius. 2003. 'Six1 is required for the early organogenesis of mammalian kidney', *Development*, 130: 3085-94.

Yang, J. S., and E. C. Lai. 2011. 'Alternative miRNA biogenesis pathways and the interpretation of core miRNA pathway mutants', *Mol Cell*, 43: 892-903.

Yeger, H., R. Baumal, G. Pawlin, and M. J. Phillips. 1985. 'Relationship of histology of Wilms' tumor to growth characteristics of nude mouse heterotransplants', *Cancer Res*, 45: 2340-9.

Yi, R., H. A. Pasolli, M. Landthaler, M. Hafner, T. Ojo, R. Sheridan, C. Sander, D. O'Carroll, M. Stoffel, T. Tuschl, and E. Fuchs. 2009. 'DGCR8-dependent microRNA biogenesis is essential for skin development', *Proc Natl Acad Sci U S A*, 106: 498-502.

Yu, Y., E. Davicioni, T. J. Triche, and G. Merlino. 2006. 'The homeoprotein six1 transcriptionally activates multiple protumorigenic genes but requires ezrin to promote metastasis', *Cancer Res*, 66: 1982-9.

Yu, Y., J. Khan, C. Khanna, L. Helman, P. S. Meltzer, and G. Merlino. 2004. 'Expression profiling identifies the cytoskeletal organizer ezrin and the developmental homeoprotein Six-1 as key metastatic regulators', *Nat Med*, 10: 175-81.

Zhdanova, O., S. Srivastava, L. Di, Z. Li, L. Tchelebi, S. Dworkin, D. B. Johnstone, J. Zavadil, M. M. Chong, D. R. Littman, L. B. Holzman, L. Barisoni, and E. Y. Skolnik. 2011. 'The inducible deletion of Drosha and microRNAs in mature podocytes results in a collapsing glomerulopathy', *Kidney Int*, 80: 719-30.

8 Abbreviations

A	
aa	amino acid
ALP mix	Aprotinin, Leupeptin, Pepstatin mix
B	
bp	base pair
BSA	bovine serum albumin
C	
cDNA	complementary DNA
ct-value	cycle threshold value
D	
DAB	3,3'-Diaminobenzidine
DEPC	diethylpyrocarbonate
DMEM	Dulbecco's Modified Eagle Medium
dNTP	deoxynucleoside-triphosphate
E	
EDTA	ethylenediaminetetraacetic acid
EMT	epithelial mesenchymal transition
ESC	embryonic stem cells
F	
FCS	fetal calve serum
G	
eGFP	enhanced green fluorescent protein
GFP	green fluorescent protein
GOI	gene of interest
H	
HE	hematoxylin and eosin
I	
IRES	internal ribosome entry site
K	
kb	kilobase
KO	knockout
L	
LIF	leukemia inhibitory factor
LSFM	light sheet fluorescence microscopy
M	
mES	mouse embryonic stem cells
MOPS	3-(N-morpholino) propane sulfonic acid
N	
NEAA	non-essential amino acids
P	
PAGE	poly acrylamide gel electrophoresis
PBS	phosphate buffered saline
PFA	paraformaldehyde
PCR	polymerase chain reaction
Q	
qRT-PCR	quantitative realtime PCR
R	
RT	room temperature
S	
SDS	sodium dodecyl sulfate
SSC	saline sodium citrate
W	
WT	Wilms tumor
U	
UB	Ureteric bud
Y	
YFP	yellow fluorescence protein

9 Supplement

9.1 Primer tables

Table 9: Mouse oligonucleotides for RMCE

bGHpA-for	CCTTCTAGTTGCCAGCCATC
Flag-tag-for	GGATTACAAGGATGACGACGAT
FRTneo2	GCGAAGCTTGATATCGAATTCCGAAGTTCCTATTCTCTA
GFP-real-for	ACGTAAACGGCCACAAGTTC
GFP-real-rev	AAGTCGTGCTGCTTCATGTG
hDrosha-for1	CGACAACTTATTGAAACTTCTCCAGT
hDrosha-rev1	GAAGCTGGGATTTGGGGTCA
hes1-kO2_bgh	GGGAGGATTGGGAAGACAAT
hSIX1-f	GCGGAGGCCAAGGAAAGGGAGAAC
hSIX1-r	GCTTGCCCCCTTCCAGAGGAGA
hygro5'out	CACGCCCTCCTACATCGAAG
neo-rev	GAAGAACTCGTCAAGAAGGC
Neotest1	CGTGCAATCCATCTTGTTCA
PGK-forw	CATTCTGCACGCTTCAAAAG
R523	GGAGCGGGAGAAATGGATATG
reverse	AGCGGATAACAATTTCACACAGGA
Rosa-rev	CTTTAAGCCTGCCCAGAAGA
T3-69	GCGCGCAATTAACCCTCACTAAAGG

Table 10: Mouse oligonucleotides for mouse genotyping

Drosha Deletion:	
mDrosha-flox1	AGTACCGGTGTATTGCCAGC
mDrosha-flox2	AAACCAGAAAAAGACAGAGTTCCT
mDrosha-flox4	ACACTGAAAACTTAATTCTAAGGCA
SIX1-Q177R/ DROSHA-E1147K het/hom:	
R26F2	CCAAAGTCGCTCTGAGTTGTTAT
TK1	CTAAAGCGCATGCTCCAGAC
PGK-forw	CATTCTGCACGCTTCAAAAG

SIX1-Q177R/ DROSHA-E1147K activation:	
AG3	CTGCTAACCATGTTCATGCC
Q177-rev2	TTGGCCTTGAGTACGCTCTC
Q177-for1	CTCCCCCTGAACCTGAAACATA
AG3	CTGCTAACCATGTTCATGCC
GFP-real-rev	AAGTCGTGCTGCTTCATGTG
Q177-for1	CTCCCCCTGAACCTGAAACATA
Six2-cre:	
mCitrine-3'out	ACATGGTCCTGCTGGAGTTC
ROSA26-creER	ACGGACAGAAGCATTTTCCA
Wt1-cre	
Wt1-creERT2-for	ATCGCAGGAGCGGAGAAC
Wt1-creERT2-TG	GCAAACGGACAGAAGCATTT
Zp3-cre:	
mCitrine-3'out	ACATGGTCCTGCTGGAGTTC
SM22-3'-cre	ACGGACAGAAGCATTTTCCA

Table 11: Mouse oligonucleotides for qPCR

GFPreal-for	ACGTAAACGGCCACAAGTTC
GFP-real-rev	AAGTCGTGCTGCTTCATGTG
hDrosha_real-for	TCAGAGAATGAAATTCCTAGGTGACTCCA
hDrosha_real-rev	CTCCATGTCCTCCTCGTCCT
hSix2-q1	CACAGGTCAGCAACTGGTTCA
hSix2-q2	CAGCGGGTTGTGGCTGTTA
mHPRT-real-ex8	TGTTGTTGGATATGCCCTTG
mHPRT-real-ex9	ACTGGCAACATCAACAGGACT

Table 12: Mouse oligonucleotides for two-tailed PCR

Two-tailed primer:	
mmu-miR-196a	ACTACCTACAACGACCAGAGCTAGAGAACCTAGCTCACCCACTACCCCAA
mmu-miR-126	GGTACGATCAAGCTCTCCAGGTACAGTTGGTACCTGACTCCACGCCGCAT
mmu-miR-10b	ACAGGGTACGACGAATACTGCTAGAGTTGCTAGCAGAGCCCTTAACACAA
mmu-miR-320	TCTCAACCCGCTAGCTATGCAGGTACAGTTGGTACCTGACTCTTGTTTCGCC
qRT-PCR primer forward:	
mmu-miR-196a	CGACTACCTACAACGACCAGAG
mmu-miR-126	GGTACGATCAAGCTCTCCAGG
mmu-miR-10b	ACAGGGTACGACGAATACTGC
mmu-miR-320	TCTCAACCCGCTAGCTATGCAG
qRT-PCR primer reverse:	
mmu-miR-196a	GGGCTAGGTAGTTTCATGTTGTT
mmu-miR-126	GGGCTCGTACCGTGAGTAATAA
mmu-miR-10b	GGCTACCCTGTAGAACCGAAT
mmu-miR-320	CGGAAAAGCTGGGTTGAGAG

9.2 Figure index

9.3 Table index

9.4 Oral presentations and Posters

05/2014 Eureka 9th International GSLS Students symposium

Poster: “Functional analysis of *Drosha* knockout in kidney development”

03/2015 AEK 18th International Cancer congress

Poster: “Functional analysis of *DROSHA* and *DGCR8* mutations in Wilms tumor”

04/2016 2nd PCCC-Kloster Seeon Meeting on Mouse Models of Human Cancer

Poster: “Functional analysis of *DROSHA* and *SIX1/2* mutations”

06/2016 6th International Tübingen-Symposium on Pediatric Solid Tumors

Oral presentation: “Functional analysis of *DROSHA* mutations in Wilms tumor”

9.5 Curriculum vitae

9.6 Affidavit

I hereby confirm that my thesis entitled “Functional analysis of *DROSHA* and *SIX1* mutations in kidney development and Wilms tumor” is the result of my own work. I did not receive any help or support from commercial consultants. All sources and / or materials applied are listed and specified in the thesis.

Furthermore, I confirm that this thesis has not yet been submitted as part of another examination process neither in identical nor in similar form.

Place, Date Signature

Eidesstattliche Erklärung

Hiermit erkläre ich an Eides statt, die Dissertation „Funktionelle Analysen von *DROSHA* und *SIX1* Mutationen in der Nierenentwicklung und dem Wilms-Tumor“ eigenständig, d.h. insbesondere selbständig und ohne Hilfe eines kommerziellen Promotionsberaters, angefertigt und keine anderen als die von mir angegebenen Quellen und Hilfsmittel verwendet zu haben.

Ich erkläre außerdem, dass die Dissertation weder in gleicher noch in ähnlicher Form bereits in einem anderen Prüfungsverfahren vorgelegen hat.

Ort, Datum Unterschrift

9.7 Copy right agreements

Copyright Clearance Center RightsLink®

Account Info | Help

ELSEVIER

Chapter: Chapter Three Development of the Mammalian Kidney
Book: Current Topics in Developmental Biology
Author: Andrew P. McMahon
Publisher: Elsevier
Date: Jan 1, 2016

Logged in as:
Philip Kruber
Developmental Biochemistry
Account #:
3001181448
LOGOUT

Order Completed

Thank you for your order.

This Agreement between Philip Kruber ("You") and Elsevier ("Elsevier") consists of your order details and the terms and conditions provided by Elsevier and Copyright Clearance Center.

License number	Reference confirmation email for license number
License date	Aug, 22 2017
Licensed Content Publisher	Elsevier
Licensed Content Publication	Elsevier Books
Licensed Content Title	Current Topics in Developmental Biology
Licensed Content Author	Andrew P. McMahon
Licensed Content Date	2016
Licensed Content Volume	117
Licensed Content Issue	n/a
Licensed Content Pages	34
Type of Use	reuse in a thesis/dissertation
Portion	figures/tables/illustrations
Number of figures/tables/illustrations	3
Format	both print and electronic
Are you the author of this Elsevier chapter?	No
Will you be translating?	No
Original figure numbers	figure 1,2,3
Title of your thesis/dissertation	DROSHA mutations in Wilms tumor
Expected completion date	Mar 2018
Estimated size (number of pages)	150
Requestor Location	Developmental Biochemistry Biocenter Am Hubland Würzburg, Bavaria 97074 Germany Attn: Developmental Biochemistry
Publisher Tax ID	GB 494 6272 12
Billing Type	Invoice
Billing address	Developmental Biochemistry Biocenter Am Hubland Würzburg, Germany 97074 Attn: Developmental Biochemistry
Total	0.00 USD

CLOSE WINDOW

10 Acknowledgment

An erster Stelle möchte ich mich ganz herzlich bei meinem Doktorvater Prof. Dr. Manfred Gessler für die Bereitstellung dieses Projekts und für die freundliche Betreuung bedanken. Besonders seine immer offene Tür und die konstruktiven Anregungen haben in besonderem Maße zum Gelingen dieser Arbeit beigetragen. Des Weiteren möchte ich mich bei Prof. Dr. Ricardo Benavente und Prof. Dr. Svenja Meierjohann dafür bedanken, dass Sie, als Teil meines Prüfungskomitees, diese Arbeit über die Jahre begleitet haben und mir immer mit gutem Rat zur Seite standen.

Prof. Dr. Alexander Buchberger danke ich für die Übernahme des Prüfungsvorsitzes.

Ein ganz besonderen Dank gilt Anja für die Klonierung der Vektoren, die Erzeugung der SIX1-Q177R ES Zellen, die Genotypisierung der Mäuse und ihrer Bereitschaft mir bei jeder Frage Rede und Antwort zu stehen. Bei Christian möchte ich mich für die vielen Gespräche während der gemeinsamen Kaffeepausen und seiner grundsätzlichen hilfsbereiten und offenen Art bedanken. Des Weiteren gilt mein Dank allen Mitarbeitern der EBCh und der PC1 für eine nette Atmosphäre während der Doktorarbeit und dass Sie meine spontanen Gesangseinlagen über die letzten Jahre stoisch erduldet haben. Ein großer Dank gilt auch Steffi und dem Tierstall für die Pflege der Mäuse.

Ich bedanke mich bei meinen Mitdoktoranden Romina und Ovidio für die vielen Gespräche und Anregungen im Denkraum. Insbesondere, Romina danke ich ganz herzlich für die vielen Unternehmungen abseits der Arbeit und ihrer Mithilfe bei der Leitung des Eureka Komitees. Ein besonderer Dank gilt auch Mateus für den täglichen Gang zu Mensa, die vielen interessanten Gespräche und der Gitarrenbegeleitung bei so manchem Konzert.

Ein großer Dank geht an meine Freunde Martin, Hans, Christoph, Ralf und Till dafür, dass Sie keine Gelegenheit ungenutzt gelassen haben, mich zu besuchen und ich mich immer blind auf Sie verlassen kann. Auch danke ich der SBS Kleinrinderfeld, die mir eine musikalische Heimat in Franken gegeben und mich von der ersten Minute freundlich aufgenommen hat. Ebenfalls großer Dank geht an Andreas und die Jungs vom ASW Würzburg, die für die nötige sportliche und soziale Ablenkung gesorgt haben.

Ich kann Nadine gar nicht genug danken, dass Sie jeder Zeit für mich da war und so manche Entbehrung in Kauf genommen hat ohne sich einmal darüber zu beklagen. Danke für die Kraft, die du mir gibst.

Ich danke meiner Mutter, ohne die meine Ausbildung und damit auch diese Arbeit nicht möglich gewesen wäre, für ihre bedingungslose Unterstützung und den Rückhalt den Sie mir gibt. Ich danke meinem Vater, da er für mich immer moralischer Kompass, Motivation und Vorbild sein wird.

Vielen Dank, euch allen!